UNIVERSITY OF BAHRAIN

College of Science **Department of Chemistry**

Preparation and Characterization of Polymer-coated Magnetic Nanoparticles: Assessment of Heating Ability and Pollutants Remediation Efficiency

A Thesis Submitted in Partial Fulfilment of the Requirements for

M.Sc. Degree in Environmental Chemistry

Submitted by

Hawraa Ahmed Mohammed

20176829

Supervised by

Dr. Kheireddine El-Boubbou

Associate Professor

November 2025

UNIVERSITY OF BAHRAIN
Deanship of Graduate Studies & Scientific Research

جامعة البحرين
عمادة الدراسات العليا والبحث العلمي

Thesis Discussion Committee Decision

Form Code: UDNGS013

Student Name:	Hawra Ahmed Mohammed
Student ID. No.	20176829
Department:	Chemistry
College:	Science
Program:	M.Sc. in Environmental Chemistry
Student GPA:	4.00
Thesis Title:	Preparation and Characterization of Different Polymer-Coated Magnetic Nanoparticles: Assessment of Heating Ability and Pollutants Remediation Efficiency.

The Discussion Committee met on November 20, 2025 **in** S41-0044 **upon discussing the student whose details are stated above in public. The discussion committee recommends the following:**

The student is awarded the grade PASS **in the thesis course** CHEMY622 **.**

☐ **Without making any changes to the thesis.**

☑ **After making the modifications attached with this decision.**

Discussion Committee Members Approval:

1.	**Supervisor Name:**	Dr. Kheireddine El-Boubbou	**Sign.:**	
2.	**Internal Examiner:**	Dr. Javed Iqbal	**Sign.:**	
3.	**External Examiner:**	Prof. Dr. Mazen Al-Ghoul	**Sign.:**	

ACKNOWLEDGMENT

First and foremost, I would like to express my sincere gratitude to my supervisor, Dr. Kheireddine El-Boubou, whose guidance, mentorship, and continuous support have been instrumental in the completion of this research. His generous sharing of expertise, thoughtful feedback, and unwavering encouragement have not only shaped the direction of this study but also enriched my academic and personal growth. This work would not have been possible without his dedicated supervision.

I would also like to extend my heartfelt thanks to Mr. Jassim Al-Sadadi, Mr. Hussain Ali, and Mr. Hussain Ibrahim for their invaluable assistance in the laboratory. Their support in providing the essential chemicals and equipment played a vital role in the successful execution of my experiments. A special thanks to Ms. Alia Mustafa and Dr. Basma Al-Najar from the Physics department at UOB, Prof. Mohamed Lemine and Dr. Nawal Madkhali from Imam Mohammed Ibn Saud Islamic University (IMSIU).

A special note of appreciation goes to Mrs. Amal Al-Wadi from ALBA for her kind support and help, as well as to the ALBA management for their continued encouragement and support in allowing me to pursue my higher studies.

On a personal level, I am deeply grateful to my family for their unwavering love and support throughout this journey. Their help in caring for my son and their constant encouragement made this achievement possible.

I am deeply grateful to my parents, whose unconditional love, prayers, and endless support have been the foundation of all my achievements. Their belief in me has been a constant source of motivation and strength. I also extend my warmest thanks to my spouse, for his unwavering encouragement, patience, and selfless sacrifices. Your support has meant the world to me throughout this journey.

Finally, to my beloved son, Sayed Ahmed, my little source of sunshine and strength. Thank you for your patience and understanding far beyond your years. Your smiles and hugs gave me the energy to keep going, even on the hardest days. This accomplishment is dedicated to you, with all my love.

ABSTRACT

Chlorophenols (CPs) are hazardous compounds widely used in industries including plastic, papers, textiles, steel, pharmaceuticals, dyes, pesticides, insecticides, and herbicides. However, their environmental persistence leads to their accumulation in soil and water, thereby posing significant risks to ecosystems and human health. In this work, we synthesized various types of iron oxide magnetic nanoparticles (MNPs), either coated with polymers (i.e. PVP, Chitosan, Starch) or doped with metal ions (i.e. Co^{2+}, Ni^{2+}, Zn^{2+}) and studied their catalytic efficiency in degrading two common organic CP contaminants: 4-Chlorophenol (4-CP) and 2-Chlorophenol (2-CP). All MNPs were thoroughly characterized using XRD, FTIR, VSM, TEM, and SEM-EDX. These characterization techniques confirmed the formation of uniform nanosized particles (~ 8-15 nm), highly crystalline cubic spinel structures, and superparamagnetic behavior. The CPs degradation studies showed that both polymer-coated MNPs (PMNPs) and metal-doped MNPs (MMNPs) were effective at eliminating CPs albeit at different efficiencies. Interestingly, the metal-doped MNPs, especially CoF_2O_4, exhibited outstanding performance, achieving complete degradation of 50 ppm 4-CP and 2-CP within 15 and 80 seconds, respectively. These enhancements are attributed to the spinel ferrite structure, intrinsic peroxidase-like activity, stability of the redox pair in octahedral sites, and reduced particle sizes. Additional factors such as pH, catalyst dosage, pollutant concentration, H_2O_2 levels, and temperature were also tested and were found to influence degradation. Reusability studies demonstrated that the different as-synthesized NPs could be reused for six consecutive cycles without significant loss of activity (~ 99% for $CoFe_2O_4$, 91.1% for PVP-coated MNPs, and 76.97% for bare Fe_3O_4). Interestingly, the application of an alternating magnetic field (AMF) generating heat dissipation from MNPs significantly accelerated the degradation process compared to mechanical stirring. For instance, 100% degradation for 50 ppm 4-CP was reached within 10 minutes under AMF, while within the same time-fame, and without mechanical shaking nor, AMF, only 4% degradation was achieved. According to our knowledge, these promising results utilizing AMF to degrade CPs are presented for the first time. This underscores the promise of such metal-doped MNPs as fast, efficient, and reusable nanocatalysts for potential industrial wastewater treatment involving chlorophenol contaminants.

TABLE OF CONTENTS

Defense Committee's Approval…… B

Acknowledgements……C

Abstract……D

Table of Contents……E

List of Tables……F

List of Figures……G

Chapter 1. Introduction 9

1.1. Research Problem 11

1.2. Research Question 11

1.3. Research Objectives 12

1.4. Research Significance 12

1.5. The Study's Setting 14

Chapter 2. Literature Review 15

2.1. MNPs and Environmental Applications 15

2.2. MNP Synthetic Methods 17

2.3. MNPs Characterization Techniques 21

2.4. Chlorophenol Remediation using MNPs 22

2.5. Fenton and Fenton-like Reactions 26

2.6. Advanced Physicochemical Insights and Emerging Catalytic Mechanisms 29

Chapter 3. Research Methodology 30

3.1. Materials and Methods 30

3.2. Characterization 30

3.3. Preparation of PMNPs and metal-doped MNPs 31

3.4. Catalytic Degradation of Chlorophenols 34

3.5. Catalytic Degradation of Chlorophenols under AMF 35

Chapter 4. Results and Discussion 37

4.1. Preparation and Characterization of various MNPs 37

4.2 Catalytic Degradation of Chlorophenols 53

4.3 Catalytic Degradation of Chlorophenols under AMF 81

Chapter 5. Conclusion and Future Work 83

5.1. Conclusion 83

5.2. Future Work 85

List of Tables

Table 1. Structural cation distribution in different types of spinel ferrites. 16
Table 2. Summary of MNPs' synthetic methods and main advantages of each. 20
Table 3. Various MNPs and ferrites used for removal of organic dyes and CPs from wastewater. ... 25
Table 4. Rietveld analysis of the different polymer-coated and metal-doped MNPs. 43
Table 5. Magnetic parameters obtained from M–H curves and law of approach to saturation (LAS) for polymer-coated 48
Table 6. Heating properties of metal-doped MNPs at different concentrations (field = 160 Oe, frequency = 472 kHz). 49
Table 7. Heating properties of metal-doped MNPs at different concentrations (field = 160 Oe, frequency = 472 kHz). 50

List of Figures

Figure 1. Spinel ferrite crystal structure. Reproduced with permission from (Hwang, Choi, Shin, Ju, & Chun, 2020). 16
Figure 2. Overview of the synthetic methods used to prepare MNPs. 18
Figure 3. Schematic illustration of the KHB synthetic methodology utilized to prepare PMNPs. 32
Figure 4. Schematic illustration of the KHB synthetic method used to prepare metal-doped MNPs 33
Figure 5. Schematic illustration of the experimental setup for the catalytic degradation of chlorophenols. 35
Figure 6. Schematic illustration for the experimental setup for the catalytic degradation of chlorophenols under AMF. 36
Figure 7. a) TEM images of the various polymer-coated MNPs showing sizes ~ 10 – 15 nm, b) corresponding size distributions. 38
Figure 8. Powder XRD patterns of the as-synthesized a) polymer-coated MNPs and b) metal-doped ferrites. 38
Figure 9. SEM-EDX elemental analysis of the various metal-doped ferrites. 40
Figure 10. FTIR spectra of the as-synthesized a) polymer-coated-MNPs and b) metal-doped ferrites. 42
Figure 11. Field-dependent magnetization hysteresis loops at room temperature for a) polymer-coated MNPs, and b) law of saturation *(LAS)*; c) metal-doped MNPs and d) LAS fitting. 47
Figure 12. Heating efficiencies of (a-b) Fe_3O_4-MNPs, (c-d) PVP-MNPs, (e-f) Chitosan-MNPs, (g-h) Starch-MNP at H_0 = 160 Oe, f = 472 kHz. 51
Figure 13. Heating efficiencies of the different MNPs at different concentrations (a-b) 2.5 mg/mL, (c-d) 5 mg/mL, (e-f) 7.5 mg/mL, (g-h)10 mg/mL at H_0 = 160 Oe, f = 472 kHz. 52
Figure 14. Control degradation experiments for 4-CP & 2-CP in the presence of either 1% H_2O_2 only or Fe_3O_4 NPs (10 mg/mL) only. 53
Figure 15. Effect of polymer coatings on the catalytic degradation of 4-CP for a) 10 mg/mL catalysts dosage + 50 ppm 4-CP (PMNPs control experiments), and b) 10 mg/mL catalysts dosage + 50 ppm 4-CP + 1% H_2O_2. 55
Figure 16. Effect of polymer coatings on the catalytic degradation of 2-CP for a) 10 mg/mL catalysts dosage + 50 ppm 2-CP (PMNPs control experiments), and b) 10 mg/mL catalysts dosage + 50 ppm 2-CP + 1% H_2O_2. 55
Figure 17. Mechanistic sketch of the catalytic oxidation of 2-CP or 4-CP by PMNPs. 57
Figure 18. Mechanistic sketch of the catalytic oxidation of 2-CP or 4-CP by the metal-doped MNPs. 57
Figure 19. Effect of metal doping on the catalytic degradation of 4-CP for a) 10 mg/mL catalysts dosage + 50 ppm 4-CP (MFe_2O_4 control experiments), and b) 10 mg/mL catalysts dosage + 50 ppm 4-CP + 1% H_2O_2. 61
Figure 20. Effect of metal doping on the catalytic degradation of 2-CP for a) 10 mg/mL catalysts dosage + 50 ppm 2-CP + 1% H_2O_2, and b) 10 mg/mL catalysts dosage + 50 ppm 2-CP (MFe_2O_4 control experiment). 61
Figure 21. Nanocatalyst dosage effect (2, 5, and 10 mg/mL) on 50 ppm 4-CP degradation in 1% H_2O_2 for a) Fe_3O_4 NPs, b) Chitosan-coated MNPs, c) PVP-coated MNPs, and d) Starch-coated MNPs. 65

Figure 22. Nanocatalyst dosage effect (2, 5, and 10 mg/mL) on 50 ppm 2-CP degradation in 1% H_2O_2 for a) Fe_3O_4 NPs, b) Chitosan-coated MNPs, c) PVP-coated MNPs, and d) Starch-coated MNPs. 66
Figure 23. Nanocatalyst dosage effect (2, 5, and 10 mg/mL) on 50 ppm 4-CP degradation in 1% H_2O_2 and their UV-vis absorption spectra for (a-d) $CoFe_2O_4$, (e-h) $ZnFe_2O_4$, and (i-l) $NiFe_2O_4$. 67
Figure 24. Nanocatalyst dosage effect (2, 5, and 10 mg/mL) on 50 ppm 2-CP degradation in 1% H_2O_2 and their UV-vis absorption spectra for (a-d) $CoFe_2O_4$, (e-h) $ZnFe_2O_4$, and (i-l) $NiFe_2O_4$. 68
Figure 25. Effect of pH on the degradation of 4-CP using the as-synthesized Fe_3O_4 NPs (10 mg/mL Fe_3O_4 catalyst + 1% H_2O_2 at room temperature). 70
Figure 26. Effect of pH on the degradation of 50 ppm 4-CP using 10 mg/mL catalyst, 1% H_2O_2, room temperature of as-prepared a) Chitosan-coated MNPs, b) PVP-coated MNPs, and c) Starch-coated MNPs. 74
Figure 27. Effect of initial pH on the degradation of 50 ppm 4-CP using 1% H_2O_2 at room temperature of as-prepared 74
Figure 28. Effect of H_2O_2 concentration on the degradation of 50 ppm 4-CP using $CoFe_2O_4$ nanocatalysts (2 mg/mL) 75
Figure 29. Effect of chlorophenol's concentrations on catalytic degradation at room temperature, 1% H_2O_2 for $CoFe_2O_4$ (2 mg/mL) + 50 & 10 ppm 4-CP. 76
Figure 30. Effect of temperature on 50 ppm 4-CP degradation using $CoFe_2O_4$ NPs (2 mg/mL) at two different temperatures of 22℃ and 35℃. 77
Figure 31. Complete degradation of 50 ppm 4-CP in 1% H_2O_2 and 2 mg/mL $CoFe_2O_4$ nanocatalyst, a) time-based degradation, b) chloride concentration increase over time, and c) TOC reduction over time. 79
Figure 32. Reusability of the different nanocatalysts at room temperature, in 1% H2O2, and pH 7.0 for a) CoFe2O4 NPs, b) Bare Fe3O4 NPs, and c) PVP-coated MNPs. 80
Figure 33. Catalytic degradation of 4-CP and 2-CP using (a-b) PMNPs and (c-d) MFe_2O_4 NPs under the influence of AMF. 82

Chapter 1. Introduction

Magnetic iron oxide nanoparticles (MNPs) have found extensive use in environmental applications such as in catalysis and heavy metals remediation (Giraldo, Erto, & Moreno-Piraján, 2013; Munoz, de Pedro, Casas, & Rodriguez, 2015). Among the different MNPs, magnetite (Fe_3O_4) and maghemite (γ-Fe_2O_3), are the most commonly studied NPs used due to their low toxicity, cost-effectiveness, and relatively ease of synthesis. In particular, the performance of polymer-coated MNPs (PMNPs) for various applications is intimately entwined with their structures, sizes, and magnetic properties. A diverse array of polymers with different molecular weights has been used to coat the surfaces of MNPs, including but not limited to polysaccharides such as hyaluronic acid (HA), starch, and chitosan, as well as synthetic polymers like polyethylene glycol (PEG), polyvinylpyrrolidone (PVP), and polyacrylic acid (PAA) etc., along with their respective copolymers and derivatives. Incorporating a complexing biocompatible polymer enhances the formulation by providing protective shielding, improving colloidal stability, and reducing particle agglomeration, thereby safeguarding the core material against degradation and oxidation over time. Polymer coatings are hypothesized to play a pivotal role in modulating the surface chemistry of MNPs. Specifically, hydrophilic polymers such as PVP and chitosan stabilize surface iron species by creating favorable microenvironments that enhance Fe^{2+} retention and facilitate electron transfer. This stabilization promotes redox cycling between Fe^{2+} and Fe^{3+}, which is essential for catalytic activity. Additionally, polymer coatings improve dispersion and accessibility of active sites due to their reduced nanoparticle size and improved crystallinity which further enhance the catalytic performance (Muzenda et al., 2023).

The incorporation of doped transition metals (i.e. Co, Ni, Zn, etc.) into MNPs yields multifunctional nanomaterials with enhanced magnetism and adsorption/catalytic activity utilized to efficiently remove various organic pollutants such as chlorophenols, methylene blue, methyl orange, Rhodamine B (RhB), etc. These metal-doped MNPs

(MMNPs) exhibit improved electronic structure and magnetic properties, which contribute to localized heating under alternating magnetic field (AMF) exposure. Dopants may also act as co-catalytic centers, accelerating the generation of reactive oxygen species (ROS) and facilitating pollutant degradation.

AMF exposure induces nanoscale heating *via* Neél and Brownian relaxation mechanisms, resulting in thermal energy generation quantified by specific absorption rates (SAR). This localized heating accelerates Fenton-like reactions, enhancing the decomposition of hydrogen peroxide (H_2O_2) and promoting the formation of hydroxyl radicals •OH, the primary agents responsible for chlorophenol degradation. These pollutants, including 4-chlorophenol (4-CP) and 2-chlorophenol (2-CP), are commonly found in wastewater from textile, petrochemical, pesticide, and insecticide industries, posing serious risks to human health and ecosystems. Consequently, the U.S. Environmental Protection Agency (EPA) has imposed stringent regulations limiting their concentrations to below parts per billion (ppb) levels.

Consequently, enhancing the heating responses of MNPs under AMF is highly demanded, particularly for biomedical and environmental motives. Application of AMF on MNPs evokes magnetization reversal and, consequently, production of thermal energy measured in terms of SAR. Consequently, the focus of most research groups is to prepare stabilized MNPs with high heating efficiencies in large quantities in an easy, robust, cheap, and reproducible procedure. To further enhance the heat dissipation efficiency of the MNPs, their magnetic properties can be optimized through doping with divalent metal ions (i.e. Co^{2+}, Ni^{2+} , or Zn^{2+}) to produce MMNPs or coating them with polymers (i.e. Starch, Chitosan, PVP) to produce polymer-coated MNPs (PMNPs) which is particularly promising for various fields (Aldaoud et al., 2022; K. El-Boubbou et al., 2024; Kheireddine El-Boubbou et al., 2022; Lemine, Algessair, Madkhali, Al-Najar, & El-Boubbou, 2023).

1.1. Research Problem

Wastewater pollution from the presence of hazardous CPs, particularly monochlorophenols, poses significant challenges due to their adverse effects on the environment and human health. Their contents in water have been strictly limited to below ppb levels owing to their persistence and toxicity. The most studied materials for CPs removal are carbonaceous materials, such as carbon nanofibers, nanoporous graphene, and activated carbon (Madannejad, Rashidi, Sadeghhassani, Shemirani, & Ghasemy, 2018; Radhika & Palanivelu, 2006). However, due to their relatively high synthetic cost, limited selectivity, low degradation efficiency, and reusability issues (Q. Wang et al., 2012), there is a great demand to design alternative nanomaterials for faster and more efficient CPs remediation. Herein, tailored-made colloidal and dispersed MNPs coated with different polymers or doped with different divalent metal ions are used to test their remediation capacities towards these CPs. The as-synthesized PMNPs and MMNPs are deployed for removal and degradation of two key monochlorophenol pollutants, 4-CP and 2-CP, *via* catalytic oxidation in the presence or absence of AMF. To the best of our knowledge, this is the first systematic study investigating the effects of different MNP formulations on the degradation of chlorophenol pollutants under the influence of an AMF. Therefore, this research will explore this important topic for the very first time.

1.2. Research Question

- How to improve the efficiency of monochlorophenols oxidative degradation using different PMNPs and MMNPs?
- In the presence of AMF, could the MNPs enhance the degradation of CPs effectively?

1.3. Research Objectives

The major objective of this proposed research is to develop and fully characterize a family of PMNPs and MFe_2O_4 (M ≅ Co, Ni, Zn, etc.) for monochlorophenols remediation applications using Fenton-like reaction. The secondary aim will be testing their respective heating properties and their utilization in improving CPs degradation efficiency. To meet the goals, the research project will be divided into five sub-objectives:

1. Preparation of PMNPs and MMNPs with different types of polymers and transition metals.
2. Investigation of the physicochemical properties of the as-synthesized PMNPs and doped MNPs using different techniques, such as transmission electron microscopy (TEM), scanning electron microscopy combined with energy-dispersive X-ray spectroscopy (SEM-EDX), X-ray diffraction (XRD), Fourier Transform Infrared spectroscopy (FTIR), and Vibrating Sample Magnetometer (VSM).
3. Studying the heating properties of the as-synthesized PMNPs and MMNPs.
4. Testing the degradation efficiency of the as-synthesized PMNPs and MMNPs for the degradation of 4-CP and 2-CP under different experimental conditions.
5. Exploring the possibility of degrading 4-CP and 2-CP in the presence of AMF.

1.4. Research Significance

The significance of the research lies in its potential to develop new generation of nanocatalysts based on stable recyclable cost-effective magnetic nanomaterials. Consequently, biocompatible PMNPs and metal-doped MNPs will be investigated as catalysts for the oxidation of monochlorophenols, where it has been proven that iron oxide MNPs can be effectively utilized for such applications (Cheng et al., 2015; Duan et al., 2020; Han, Zhang, Chen, Zhang, & Guo, 2018; Shen, Zhou, Li, Gu, & Xue, 2019;

L. Xu & Wang, 2012). Nonetheless, very few reports, if any, explored the comparison of using various polymer-coated MNPs and testing their effects and efficiencies towards monochlorophenols removal. The literature is scarce studying the effects of polymer coatings on MNPs and their consequences on CPs removal. In fact, most previous research work has focused on bare iron oxide NPs without polymer coat or metal doping. Thus, investigating the potential of using dopant metals or polymer coating with MNPs will be a great addition to the CPs remediation toolbox.

Tailoring PMNPs and MMNPs to generate heat efficiently across a range of magnetic field strengths and frequencies is critical for biomedical and environmental uses. Consequently, there is strong demand for stable, biocompatible PMNPs that deliver optimal heating efficiencies with high SAR values. Previous studies have shown that heating performance depends on saturation magnetization (M_s), particle size, crystallinity, nanoparticle concentration, interparticle magnetic interactions, and the amplitude and frequency of the applied field (Lemine et al., 2023). Improving the heating efficiency of the MNPs is influenced by multiple factors, primarily the intrinsic properties of the particles, such as size, composition, and magnetic characteristics, as well as the nature of the polymer coating, the dispersion medium, particle dispersity, interparticle interactions, and the parameters of the applied alternating current (AC) field, including amplitude and frequency. Therefore, designing tailored-made MNPs that can dissipate optimal heat under AMF to be utilized for CPs degradation is inimitable. The significance of the proposed work is to prepare high performance water-dispersible magneto-responsive thermal nano-agents and tune many of their physicochemical parameters which will be then employed for the degradation of monochlorophenols.

1.5. The Study's Setting

MNPs will be synthesized following the previously reported KHB methodology (Kheireddine El-Boubbou; Kheireddine El-Boubbou et al., 2022). Both PMNPs and metal-doped MNPs will be synthesized under similar conditions, and will be physically and chemically characterized using FTIR, XRD, TEM, SEM-EDX, and VSM. Following the characterization, the as-synthesized MNPs will be used as catalysts to derive Fenton-like reaction with the aid of H_2O_2 oxidant facilitating the degradation of monochlorophenols. The CPs degradation percentage using each of the as-prepared catalysts will be measured over time under different experimental conditions and will be reported in this study.

Chapter 2. Literature Review

2.1. MNPs and Environmental Applications

NPs are extremely small particles with diameters ranging from 1 to 100 nm. In particular, metal oxide MNPs have gained considerable researchers' interest in the last few decades due to their nanoscale size, high surface area to volume ratio, high stability, magnetic properties, and unique physicochemical properties, making them excellent candidates for catalysis, adsorption, magnetic hyperthermia, chemical sensing, and other applications (Villaseñor & Ríos, 2018). Magnetically-responsive MNPs are composed of elements possessing magnetic properties such as iron, nickel, cobalt, or metal oxides (i.e. magnetite (Fe_3O_4), maghemite (γ-Fe_3O_4), hematite (α- Fe_3O_4), cobalt ferrite ($CoFe_2O_4$), nickel ferrite ($NiFe_2O_4$), etc.). In particular, magnetite NPs are the most widely used in environmental and biomedical applications due to their low toxicity, cost-effectiveness, and ease of synthesis (El-Boubbou, 2018). However, for biomedical applications, it is desirable to modify the surface of the iron oxide using a protective coating layer (e.g. polymer or surfactants) to form nanostructures that will minimize iron oxide agglomeration and increase their stability against corrosion and oxidation. It is worth mentioning that the polymer coating will also enhance the biocompatibility and biodegradability of the MNPs, which is a key property in materials used for environmental remediations (Ramana et al., 2021). Moreover, their good magnetic properties allow them to be recycled and reused in multiple applications due to their rapid separation process simply by using hand-held magnets.

Ferrites, or metal ferrites, are mixed iron oxides with metal oxides that could crystallize into three structures, spinels, garnet, and magnetoplumbite, with the simplest structure being spinel ferrites having the formula MFe_2O_4 (where M = Co, Ni, Zn, Cu, Mg, Mn, etc.). As illustrated in **Figure 1** and **Table 1**, spinel ferrites have a face-centered cubic (fcc) crystalline lattice where oxygen and metal ions are positioned on the tetrahedral (A) and octahedral sites (B), and the positions of metals M^{2+} and M^{3+}

within A and B sites will vary depending on the synthesis method, crystal size, and lattice energies, hence, normal and inverse ferrites structures will be formed (Aisida, Ahmad, & Ezema, 2020; Al Maashani, Khalaf, Gismelseed, & Al-Omari, 2020; Bhushan Das, Kumar Singh, Kumar, Kumar, & Kumar, 2021). The availability of a transition metal atom in ferrites structure allows for controllable chemical and physical properties as well as enhanced magnetic and thermal properties due to the transition of the metal atoms between the A and B sites within the crystal, and this will vary depending on the ionic radius, ionic strength, and amount of the transition metal doped (Hazarika & Borah, 2023).

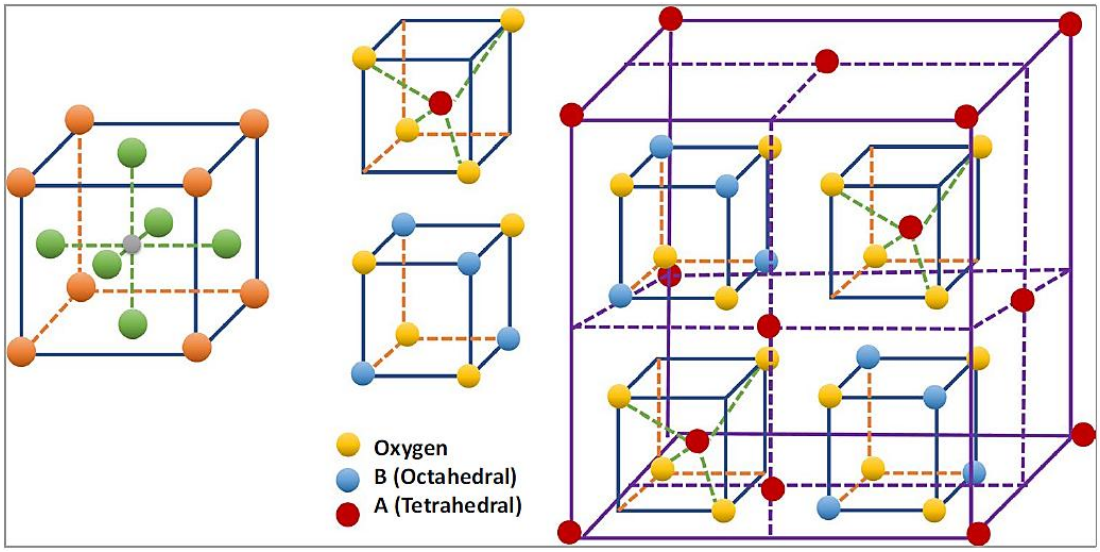


Figure 1. Spinel ferrite crystal structure. Reproduced with permission from (Hwang, Choi, Shin, Ju, & Chun, 2020).

Table 1. Structural cation distribution in different types of spinel ferrites.

Spinel ferrite	**Cation distribution**		**Spinel structure**
	Tetrahedral sites (A)	Octahedral sites (B)	
$CoFe_2O_4$	Fe^{3+}	$Fe^{3+} + Co^{2+}$	Inverse
$NiFe_2O_4$	Fe^{3+}	$Fe^{3+} + Ni^{2+}$	Inverse
$ZnFe_2O_4$	Zn^{2+}	$Fe^{3+} + Fe^{2+}$	Normal
Fe_3O_4	Fe^{3+}	$Fe^{2+} + Fe^{3+}$	Inverse

MNPs and ferrites are used in our daily life as essential components in transformers, electronic conductors, electromagnets, recording tapes, and aircrafts. However, they are also important in other applications such as environmental remediation in photocatalysis, catalysis, and adsorption. Additionally, they can be used in biomedical applications such as biosensing, drug delivery, and hyperthermia (K. El-Boubbou et al., 2024; Patil et al., 2018). Their use in environmental application is mainly due to their high surface area to volume ratio and small sizes that are crucial for catalysis and adsorption applications, large number of surface's active sites that will prompt higher adsorption and catalytic capabilities, biodegradability and nontoxic nature, and superparamagnetic behavior that allow their ease of separation with a magnet from water bodies (Kaur, Kaur, & Vibha, 2016). Before proceeding to the particular remediation application, it is important to note the different synthetic approaches utilized for the syntheses of MNPs. Recent studies have increasingly focused on various synthetic approaches for MNPs, with particular attention to controlling their size, magnetic properties, stability, and surface functionalization. These aspects will be explored in greater detail in the following section.

2.2. MNP Synthetic Methods

Special emphasis should be placed on the synthetic strategies employed for MNPs, as these methods critically influence the size, morphology, structural integrity, dimensional attributes, and overall physicochemical properties, which ultimately determine their behavior and performance in targeted applications. When selecting or designing a synthesis approach, the following key parameters must be carefully considered:

1) Size-control and narrow-dispersion
2) Stability and colloidality
3) Scalability and reproducibility

A substantial body of literature has explored efficient synthetic methodologies for producing MNPs and ferrites with controlled size, high stability, colloidal integrity, and biocompatibility. These methods encompass sol-gel processes, spray and laser pyrolysis, sonochemical synthesis, microemulsion techniques, hydrothermal approaches, mechanical milling, microwave-assisted synthesis, and, most notably, co-precipitation and thermal decomposition techniques as illustrated in **Figure 2**. Depending on the desired physicochemical properties of the NPs, the synthetic route can be selected, as it affects the quality, size, shape, and, hence, the catalytic properties of the NPs.

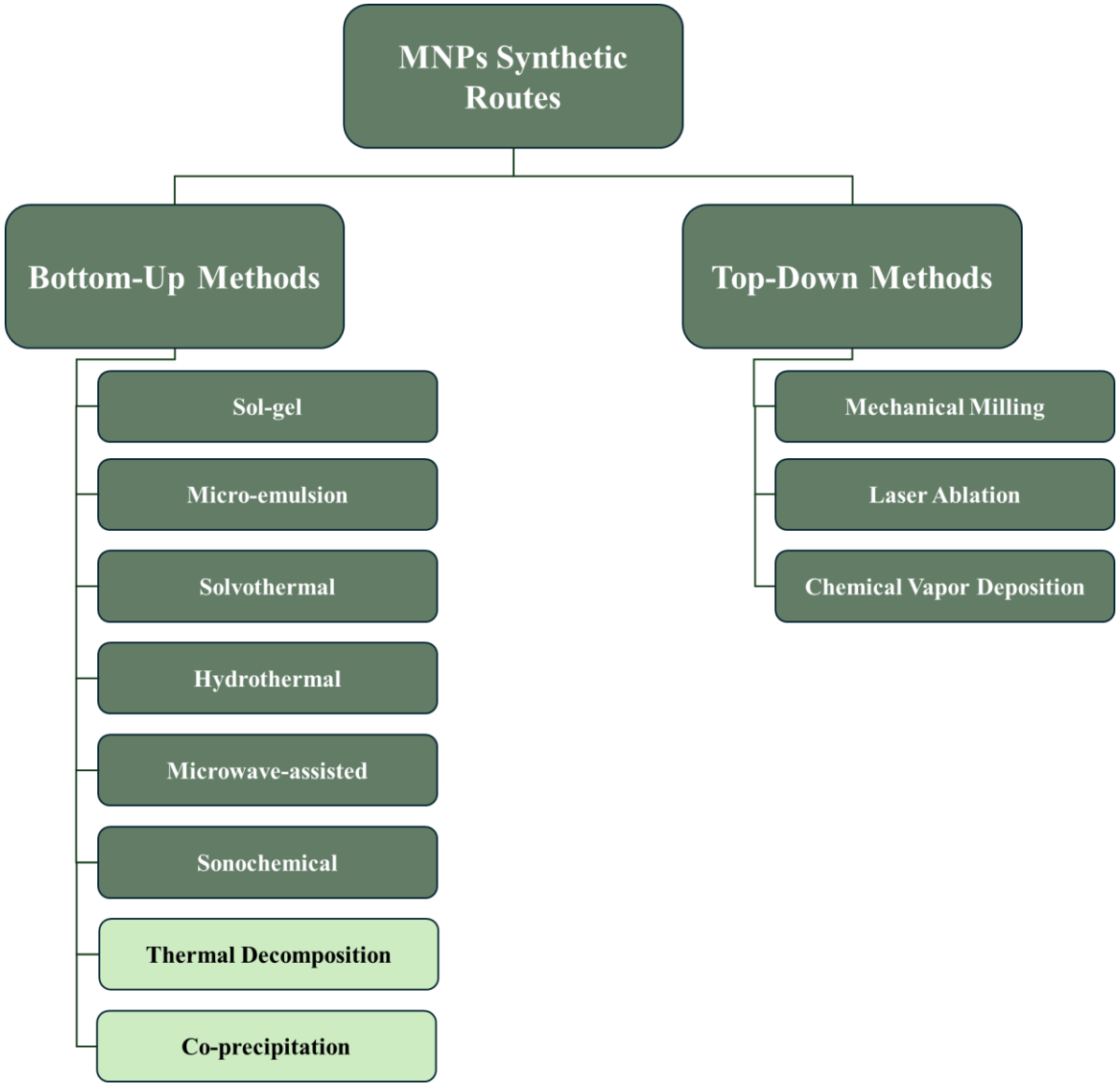


Figure 2. Overview of the synthetic methods used to prepare MNPs.

The main challenge in developing a synthetic route lies in identifying a simple, practical, and cost-effective way to produce large quantities of magnetite nanoprobes that maintain stable dispersion for months without precipitation. Equally important is ensuring the production of uniform nanocolloids with precise control over their size and morphology. Of the many reported methods, two solution-based approaches prevail:

1) *Co-precipitation of iron salts in basic aqueous media*. The co-precipitation of iron salts in basic aqueous media is a widely used method, based on the Massart method, for synthesizing iron oxide nanoparticles, typically magnetite or maghemite. This process involves mixing aqueous solutions of iron(II) and iron(III) salts (e.g., chlorides, sulfates, nitrates) in a precise molar ratio with a strong base (e.g., NaOH or NH_4OH). The ideal stoichiometric molar ratio of Fe^{3+} to Fe^{2+} is 2:1 to produce high-purity magnetite. The overall chemical reaction for producing magnetite using iron chlorides and ammonium hydroxide is:

$$FeCl_2 + 2FeCl_3 + 8NH_4OH \rightarrow Fe_3O_4 + 8NH_4Cl + 4H_2O$$

2) *High-temperature thermal decomposition of organometallic precursors* (e.g., $Fe(CO)_5$, $Fe(acac)_3$, Fe-oleate, or mixed oleates) in high boiling solvents at elevated temperatures (200-360 °C). This process is typically followed by ligand exchange to replace the hydrophobic coating with a hydrophilic one. However, each synthetic method comes with its own set of advantages and disadvantages. A comparison of these methods is presented in **Table 2**.

Table 2. Summary of MNPs' synthetic methods and main advantages of each.

Synthetic Method	Brief Description	Advantages	Approach	Reference
Sol-gel	NPs formed by chemical process in solution	Controlled shape and size; enables hybrid NP formation	Bottom-up	(Hashemi, Ataollahi, Hasani, & Seifoddini, 2023)
Micro-emulsion	NPs formed in droplets by surfactants	Produces uniform and stable NPs with narrow size distribution	Bottom-up	(Salvador et al., 2021)
Solvothermal	NPs formed at high temperature and pressure in various solvent systems	Yields high purity with good crystalline NPs	Bottom-up	(Ni et al., 2022)
Sonochemical	NPs formed by using ultrasound-induced synthesis with localized energy spikes	Fast and eco-friendly method	Bottom-up	(Ilosvai et al., 2022)
Microwave-assisted	NPs formed using microwave energy for uniform heating	Provide rapid and uniform heating that ensures consistent particle properties	Bottom-up	(Porru et al., 2022)
Mechanical Milling	NPs formed by physical grinding of bulk materials	Scalable and solvent-free method	Top-down	(Velásquez & Urquijo, 2021)
Laser Ablation	NPs formed from materials vaporization and condensation using high-energy laser	Produces high-purity NPs without chemical contamination.	Top-down	(Attallah, Abdulwahid, Ali, & Haider, 2024)
Chemical Vapor Deposition	NPs formed via gaseous precursors decomposition on a substrate	Offers precise control over composition and uniformity of NPs	Top-down	(H. Jiang, Zhang, Wang, & Gong, 2021)
Thermal Decomposition	NPs formed in the presence of hydrophobic acids in the presence of high-boiling point organic solvents (widely used)	Offers precise control over composition, uniformity, dispersity, and narrow size distribution of NPs	Bottom-up	(Bakr, El-Nahass, Hamada, & Fayed, 2021)
Co-precipitation	NPs formed by precipitation of iron salts in aqueous solution using a strong base (the most widely used)	Facile, simple, cost-effective, and easy with limited control of size and dispersity	Bottom-up	(Mohammadi et al., 2021)
Ko-precipitation Hydrolytic Basic (KHB)	NPs formed by sequential *in situ* co-precipitation of iron salts in aqueous solution in the presence of polymers	Facile, simple, cost-effective, easy with good control over particle size, dispersity, and morphology	Bottom-up	(Kheireddine El-Boubbou, 2020)

2.3. MNPs Characterization Techniques

Several spectroscopic and analytical techniques are used for analyzing the characteristics of MNPs including mainly FTIR, XRD, TEM, SEM-EDX, and VSM. FTIR is used to obtain qualitative information about the MNPs to identify the functional groups present in their structures. The functional groups are identified based on their bonds' absorption frequencies in the IR range (400 – 4000 cm^{-1}). XRD is utilized to obtain information about the composition and crystallinity of the MNPs, crystal structure, and crystalline size. Hence, using XRD analysis can give information about the magnetic phase, and can distinguish between a maghemite, magnetite, or other phases of iron oxide NPs. For example, hematite (α- Fe_2O_3) displays strong peaks at (012), (104), (110), (024), and (116), while magnetite (Fe_3O_4) shows diffraction peaks at (220), (311), (400), (511), and (440), and maghemite (Fe_3O_4) often exhibits additional peaks at (210) and (211) (Bhateria & Singh, 2019; Samrot, Sahithya, Selvarani A, Purayil, & Ponnaiah, 2021). TEM is used to examine the morphology, size, and even the internal structure of MNPs but only at a high resolution. It provides detailed imaging of the particles at the nanoscale, allowing for the observation of particle shape, size distribution, and any potential defects. SEM equipped with EDX provides the elemental composition of the MNPs. VSM, on the other hand, is utilized to study the magnetic properties of the MNPs by recording saturation magnetization (M_S), remnant magnetization (M_r) and coercivity (H_c) from magnetization loops. This will allow researchers to know if their NPs possess superparamagnetic, ferrimagnetic, or ferromagnetic behavior. Several factors can affect the magnetization of MNPs including but not limited to the synthetic method, crystalline sizes, iron distribution, doping, and dopant type (Yew et al., 2020). Moreover, the magnetic hyperthermia measurements will give information about the heat dissipation efficiencies for the MNPs.

2.4. Chlorophenol Remediation using MNPs

CPs are class of compounds known as aromatic phenol derivatives, such as 2-CP, 4-CP, or 2,4-dichlorophenols (2,4-DCP) to name few. CPs are formed by replacing the hydrogen atom/s in the phenol's structure with a chlorine atom(s). This substitution creates a family of compounds well-known as CPs and depending on the number and position of hydrogen atoms to be substituted, there could be 19 possible CPs to be formed. These compounds are very well known to be carcinogenic, toxic to both environment and human beings, and mutagenic. The toxicity of CPs is defined by the degree of chlorination based on the position of the chlorine atoms in the aromatic ring. For instance, CPs with meta-positioned chlorine atoms are more toxic than para and ortho-substituted CPs, and as the number of chlorine atoms is higher, the toxicity of CPs increases (Nair & Kurian, 2017a; Olaniran & Igbinosa, 2011). Moreover, some of these derivatives are listed as priority pollutants by EPA and as per the World Health Organization (WHO), the maximum acceptable concentration of monochlorophenols, dichlorophenols, and trichlorophenols in fresh water is 7.0, 0.2, and 18.0 μg/L, respectively (Abu-Alsoud & Bottaro, 2021). The toxicity of these pollutants largely comes from their persistent nature where they are classified as Persistent Organic Pollutants (POPs). POPs are hazardous chemicals that enter the environment but are very difficult to remove from the environment. CPs can be found in air, surface water, groundwater, and soil (Gallego et al., 2018; Kallawar, Barai, & Bhanvase, 2021; Kayan, Oz, & Kantar, 2021; Zada et al., 2021). Extensive usage of such chemicals in everyday life have increased their concentration in the environment, especially in water, where they get introduced through industrial effluents discharges, such as resins, plastic, papers, textiles, steel, pharmaceuticals, dyes, pesticides, insecticides, herbicides, fungicides, bactericides, and leachates from landfills (Oluwasanu, 2018). Different efficient methods are used to remediate aqueous medium that is polluted with CPs, such as photocatalytic oxidation (Choi, Min, Park, Park, & Jung, 2019; Tseng & Huang, 1991), adsorption (Garba et al., 2019; Radhika & Palanivelu, 2006; Rangabhashiyam et

al., 2022), catalytic wet air oxidation (Tu, Xiong, Tian, Kong, & Descorme, 2014), oxidation (T. Jiang et al., 2022; Li et al., 2021; Pera-Titus, García-Molina, Baños, Giménez, & Esplugas, 2004), and filtration (Kim et al., 2022). However, their elimination is currently restricted because of their moderate to poor water solubility, strong chemical stability and non-degradability in conventional ways such as biological treatment methods, allowing them to persist in the environment and to pass through typical water purification systems. Thus, their removal using more efficient methods and novel nano-based systems is highly demanded and hot research topic, particularly for industrial water treatment applications (Chaliha, Bhattacharyya, & Paul, 2008). In this sense, MNPs have emerged as promising and new materials that can promote the degradation of these persistent pollutants *via* highly reactive radical-mediated pathways, Fenton, and Fenton-like reactions. **Table 3** summarizes some of the reported iron-based materials that have been explored for environmental applications such as adsorption, photodegradation, and catalytic degradation. For instance, Fe_3O_4-PEDOT composite exhibited high removal efficiency for Ag^+, Hg^{2+}, and Pb^{2+} achieving 95% removal within 24 hours and reusability over 10 cycles (S. Shin & Jang, 2007). Similarly, Fe_3O_4/WO_3 demonstrated near-complete photodegradation of RhB and MB within two hours (Xi, Yue, Cao, & Ye, 2011). CP degradation using iron-based NPs has shown promising results across various removal techniques, including adsorption, catalytic degradation, photodegradation, and persulfate activation. For 4-CP, MAC composite achieved 90% removal within one hour through a combination of adsorption and catalytic degradation, demonstrating both fast kinetics and reusability up to five cycles (Duan et al., 2020). In another study, nitrogen- and sulfur-doped $ZnFe_2O_4$ have an improved 4-CP removal, reaching complete degradation within just one hour *via* persulfate-activated oxidation (Hareendran et al., 2022). Regarding 2-CP, $Fe_3O_4/SiO_2/TiO_2$ composite facilitated 100% degradation of 25 ppm within 130 minutes, while $CaFe_2O_4$ achieved 86.1% degradation within 180 minutes under photodegradation, both demonstrating notable efficiency and recyclability (Chaveanghong et al., 2023; Rashid, Barakat, Ruzmanova, & Chianese, 2015). For 2,4-DCP, both Ni/Fe– Fe_3O_4 and PAOT/$NiFe_2O_4$ nanomaterials

achieved high removal efficiencies, 100% and >83%, respectively, within 2-3 hours, while also showing good reusability (Fathy, Kamel, & Hassan, 2022; C. Xu, Liu, Chen, & Tang, 2016).

Table 3. Various MNPs and ferrites used for removal of organic dyes and CPs from wastewater.

Nanomaterial	Targeted Pollutants	Environmental Application	Key Advantages	References
Fe_3O_4–PEDOT	Ag^+, Pb^{2+} and Hg^{2+}	Adsorption	- **95% removal** in 24h with the order of $Ag^+ > Hg^{2+} > Pb^{2+}$. - Reusable for up to 10 cycles.	(S. Shin & Jang, 2007)
rGO-Fe_3O_4	BPA	Adsorption	- Adsorption within 2 hours. - Reusable for up to 5 cycles.	(Yixuan Zhang et al., 2014)
γ-Fe_2O_3	Acridine orange dye	Adsorption	- **98% adsorption** within 20 minutes. - 60–90% dye recovery. - Recyclable.	(Qadri, Ganoe, & Haik, 2009)
Chitosan-coated MNPs	Pb^{2+}	Adsorption	- **67% removal** for Pb^{2+}.	(Osuna et al., 2012)
Fe_3O_4/WO_3	RhB and MB	Photodegradation	- **~100% degradation** achieved within 1.5 - 2 hours. - Reusable for up to 4 cycles.	(Xi et al., 2011)
α-Fe_2O_3	CR	Photodegradation	- **~91.2% degradation** for the dye within 140 minutes.	(Sundaramurthy et al., 2012)
Fe_3O_4/SiO_2/TiO_2	2-CP	Photodegradation	- **100% degradation** within 130 minutes for 25 ppm 2-CP. - **97.2% degradation** within 3 hrs for 50 ppm 2-CP.	(Rashid et al., 2015)
Ni/Fe–Fe_3O_4	2,4-DCP	Catalytic degradation	- **100% degradation** within 3 hrs for 20 ppm 2,4-DCP. - Reusable for up to 10 cycles.	(C. Xu et al., 2016)
MAC	4-CP	Adsorption & Catalytic degradation	- Catalytic degradation removed **90%** of 4-CP within 1 hour. - Reusable for up to 5 cycles.	(Duan et al., 2020)
$CaFe_2O_4$	2-CP	Photodegradation	- **86.1% degradation** within 180 minutes. - Reusable for up to 3 cycles.	(Chaveanghong et al., 2023)
PAOT/$NiFe_2O_4$	2,4-DCP	Adsorption	- **>83% Removal** within 120 minutes. - Reusable for up to 5 cycles.	(Fathy et al., 2022)
Nitrogen- and sulphur-doped $ZnFe_2O_4$	4-CP	Persulfate activated oxidation	- **100% Removal** within 1 hour. - Reusable for up to 5 cycles.	(Hareendran et al., 2022)

*PEDOT (Poly(3,4-ethylenedioxythiophene)), BPA (Bisphenol A), 2-CP (2-Chlorophenol), 2,4-DCP (2,4-Dichlorophenol), HDC (Catalytic hydrodechlorination), MAC (activated carbon/Fe_3O_4), 4-CP (4-Chlorophenol), PAOT (poly(aniline-*co*-*o*-toluidine)).

2.5. Fenton and Fenton-like Reactions

In the last decades, the remediation of different contaminants using advanced oxidation processes (AOPs) has been widely investigated over other removal techniques owing to the rapidity and the eco-friendliness of these processes (Ali R. Tehrani-Bagha & Balchi, 2018). The Fenton-reactions or Fenton-like reactions are an example of AOPs. In these techniques, the organic contaminants are thoroughly degraded to less-hazardous species (i.e. smaller molecules) or even CO_2 and H_2O in case complete degradation took place (Gao et al., 2007; Seoyoun Shin, Yoon, & Jang, 2008). This approach exploits hydroxyl radicals (•OH) as the key reactive species that are generated in a series of redox reactions to fully mineralize the contaminants. Notably, •OH possesses a standard reduction potential of 2.80 V, making it a far stronger oxidant than other oxidizing agents such as H_2O_2 (E^0= 1.78 V), and ozone (E^0= 2.08 V) (Hübner et al., 2024; Neyens & Baeyens, 2003).

Homogeneous Fenton reactions are nowadays used less frequently in comparison to the heterogenous Fenton-like reactions. The reason is because Fenton reactions use homogeneous ferrous or ferric salts that suffers from considerable drawbacks, especially the formation of iron-containing sludge at the end of the process which is not easy to remove. Furthermore, the reaction can be performed only within a narrow pH range (i.e. it will only work under strong acidic conditions), and the catalysts used are of low efficiency and cannot be recovered or recycled, which adds a considerable cost to the treatment method. Hence, to overcome the above-mentioned drawbacks, the conventional homogeneous Fenton reactions are replaced now with the heterogeneous Fenton-like reactions, that use solid supports such as magnetite (Fe_3O_4) and ferrites (MFe_2O_4, where M= Fe, Co, Ni, Mn, Zn, Mg, Cu, etc.). Main advantages include their intrinsic magnetic nature allows them to be reused and recycled after their separation from the reaction medium, good catalytic properties, high stability, and large surface

area to volume ratio (Amiri, Eskandari, & Salavati-Niasari, 2019; L. Xu & Wang, 2012; Yan et al., 2009; S. Zhang et al., 2009).

The •OH radicals used for the degradation of organic contaminants are produced from the reaction between iron ions (e.g. Fe^{2+} and Fe^{3+}), in the solid iron-containing catalysts and H_2O_2, known as Fenton-like reactions (**Equations 1-3**). These reactions involve the decomposition of H_2O_2 to the reactive species, •OH by means of chain reactions with the help of iron-containing catalysts (ferrous or ferric salts). These reactions will prompt the regeneration of Fe^{2+} and Fe^{3+} at the surface of the catalysts and in the reaction medium due to their redox potential, and as long as these reactions are taking place, •OH will be ultimately generated and, hence, organic contaminants can undergo oxidative degradation due to the •OH oxidative properties. Either the degradation will form secondary intermediates that can further undergo oxidative degradation to smaller and smaller molecules with the help of radicals formed, or the degradation can be complete and organic molecules will be completely mineralized to CO_2 and H_2O as shown in **Equation 4-7.** However, side reactions might occur and affect the organic molecules degradation rate, as shown in **Equation 8-11**.

$$Fe^{2+} + H_2O_2 \rightarrow Fe^{3+} + HO\bullet + HO^- \quad \textbf{Equation 1}$$

$$Fe^{3+} + H_2O_2 \rightarrow Fe^{2+} + HO_2^{\bullet} + H^+ \quad \textbf{Equation 2}$$

$$Fe^{3+} + HO_2^{\bullet} \rightarrow Fe^{2+} + O_2 + H^+ \quad \textbf{Equation 3}$$

$$HO\bullet + RH \rightarrow R\bullet + H_2O \quad \textbf{Equation 4}$$

$$R\bullet + H_2O_2 \rightarrow ROH + HO\bullet \quad \textbf{Equation 5}$$

$$R\bullet + Fe^{3+} \rightarrow R^+ + Fe^{2+} \quad \textbf{Equation 6}$$

$$R\bullet + O_2 \rightarrow ROO\bullet \quad \textbf{Equation 7}$$

$$Fe^{2+} + HO\bullet \rightarrow Fe^{3+} + HO^- \quad \textbf{Equation 8}$$

$$H_2O_2 + HO\bullet \rightarrow HO_2^{\bullet} + H_2O \quad \textbf{Equation 9}$$

$$HO_2^{\bullet} + HO\bullet \rightarrow H_2O + O_2 \quad \textbf{Equation 10}$$

$$HO\bullet + HO\bullet \rightarrow H_2O_2 \quad \textbf{Equation 11}$$

During the Fenton or Fenton-like reactions, one must consider the following aspects for optimum reaction conditions (i.e. pH, temperature, iron catalyst dosage, H_2O_2, and contaminant's concentrations). The pH of the reaction medium is preferable to be less than 7 (S. Wang, 2008). At very low pH, •OH will be utilized with the excess H^+ ions and Fe^{2+} electron transfer to produce water. However, at higher pH values, Fe^{2+} and Fe^{3+} can precipitate into their hydroxides which reduces their availability and, hence, •OH generation will be less. Moreover, at higher pH values and presence of HO^- ions, H_2O_2 undergoes decomposition to H_2O and O_2 at higher rates, **Equation 12** & **Equation 13** (Granados-Oliveros et al., 2013; Sahni & Locke, 2006; Tai, Peng, Liu, Jiang, & Zou, 2004; Yang, Zhang, He, & Abliz, 2007).

$$H_2O_2 + HO^- \rightarrow H_2O + HO_2^- \qquad \textbf{Equation 12}$$

$$H_2O_2 + HO_2^- \rightarrow H_2O + O_2 + HO^- \qquad \textbf{Equation 13}$$

Temperature plays another critical role in the efficiency of Fenton and Fenton-like reactions. Most of the organic molecule's degradation reported in the literature to be carried around 25-30 °C. Studies consistently show that increasing temperature from 20 °C to 40 °C improves degradation efficiency by overcoming the reaction's activation energy and accelerating reaction kinetics (Munoz, Pliego, de Pedro, Casas, & Rodriguez, 2014). However, above 40 °C, results vary; some researchers observed enhanced removal of organic material, while others reported negligible change or even decreased efficiency (Carbajo, Silveira, Pliego, Zazo, & Casas, 2021; Hashemian, 2013; Mesquita et al., 2012).

In addition, the concentration of H_2O_2 is also an additional factor. The concentration of H_2O_2 must be enough for the degradation of organic contaminants, however, at higher concentrations, H_2O_2 contributes to the chemical oxygen demand of the water body being treated, thus it is important not to increase the concentration too much as it will affect the oxygen availability in a water body (Tai, Gu, Zou, & Guo, 2002). Notably, as the iron catalyst increases, the degradation of organic contaminants shall increase until

it reaches equilibration, where degradation is not enhanced further. In contrast, as the organic contaminant concentration decreases, the degradation rate will increase due to less time required to fully degrade the contaminated water body (Nakatani et al., 2007).

2.6. Advanced Physicochemical Insights and Emerging Catalytic Mechanisms

The efficacy of Fenton and Fenton-like reactions hinges on the redox cycling between Fe^{2+} and Fe^{3+}, which governs the generation of hydroxyl radicals •OH. The standard reduction potential of Fe^{3+}/ Fe^{2+} ($E^{o} = +0.77$ V) is thermodynamically favorable for electron transfer from Fe^{2+} to H_2O_2, initiating radical formation (**Equation 1**). However, the kinetics of this redox pair are influenced by the coordination environment, surface states, and pH. In heterogeneous systems, surface-bound Fe^{2+} exhibits slower electron transfer rates compared to its homogeneous counterpart, but this is offset by enhanced stability and recyclability. The presence of surface defects and oxygen vacancies can further modulate electron transfer rates, enhancing catalytic turnover (Yamaguchi, 2025).

Doping transition metals into spinel ferrites (MFe_2O_4) alters the cation distribution between tetrahedral (A) and octahedral (B) sites, thereby tuning magnetic, electronic, and catalytic properties. For instance, Co^{2+} and Ni^{2+} preferentially occupy B sites, increasing the degree of inversion and enhancing electron hopping between Fe^{3+} and Fe^{2+}, which is critical for redox cycling. This redistribution is governed by factors such as ionic radius, crystal field stabilization energy (CFSE), and lattice strain.

Recent studies have highlighted the potential of magnetothermal catalysis, where AMF induce localized heating in MNPs, which might be helpful in accelerating Fenton-like reactions (K. Wang et al., 2023). This approach enhances •OH generation by increasing the mobility of surface-bound species and lowering activation energy barriers (Trotsenko, Shabalkin, Krivoshapkina, & Krivoshapkin, 2026).

Chapter 3. Research Methodology

3.1. Materials and Methods

All chemical reagents and solvents were sourced from commercial suppliers and used as received without additional purification. The chemicals used are iron(II) sulfate heptahydrate ($FeSO_4 \cdot 7H_2O$), iron(III) chloride hexahydrate ($FeCl_3 \cdot 6H_2O$), nickel(II) chloride hexahydrate ($NiCl_2 \cdot 6H_2O$), cobalt(II) chloride hexahydrate ($CoCl_2 \cdot 6H_2O$), zinc(II) chloride hexahydrate ($ZnCl_2 \cdot 6H_2O$), Starch, Chitosan, polyvinylpyrrolidone (PVP K30 Mw ~40000), ethanol, isopropanol, 4-CP, 2-CP, hydrogen peroxide (H_2O_2), and 28% ammonium hydroxide (NH_4OH) were all purchased from Sigma-Aldrich or Fisher Scientific and used as supplied. All reactions were carried out under inert nitrogen atmosphere.

3.2. Characterization

XRD patterns were recorded on a Rigaku Ultima IV diffractometer using Cu-Kα radiation (λ = 0.15418 nm) over a 2θ range of 20°-80°. Crystal structure parameters were extracted via Rietveld analysis. TEM was carried out on a JEOL JEM-1230 at 120 kV, with images captured by a Gatan camera and Digital Micrograph software. For TEM, 5 μL of nanoparticle dispersion was dropped-cast onto a 400-mesh formvar/carbon copper grid and air-dried before imaging. Elemental composition was determined by SEM-EDX on a SEM-SERONAIS1800C equipped with an EDX detector, alongside nanoscale core-loss electron energy loss spectroscopy (EELS). FTIR spectra (400–4000 cm^{-1}) were collected as KBr pellets using a Shimadzu IRAffinity-1 spectrometer. Magnetic properties were measured at ambient temperature with a VSM featuring a 1.8 T field. The magnetic hyperthermia experiments were conducted using the calorimetric method with a Nanotherics Magnetherm system equipped with a 9-turn copper coil. The AMF generator operated strictly within the manufacturer's allowed parameters, with frequencies between 110–633 kHz and magnetic field strengths

ranging from 0–25 mT. To ensure precise temperature monitoring without electromagnetic interference, the sample temperature was recorded using a fiber-optic thermometer positioned directly in the solution throughout the experiment.

3.3. Preparation of PMNPs and metal-doped MNPs

PMNPs and metal-doped MNPs were synthesized using KHB methodology reported in our previous works (Aldaoud et al., 2022; K. El-Boubbou et al., 2024; Kheireddine El-Boubbou et al., 2022; Lemine et al., 2023). In a specific example, Fe^{3+} salt (0.30 g) was mixed with the respective polymer (~ 0.30 g) and dissolved in water (10 mL), then stirred for few minutes at 80 °C under nitrogen. An aqueous solution of Fe^{2+} (0.2 g in 1.0 mL of water) was subsequently injected into the above solution. Then, ~ 3 mL of 28% NH_4OH was added, and the mixture was stirred continuously for at least 3 hours. The resulting MNP suspensions were purified by centrifugation (4500 rpm, 5 minutes) and subjected to multiple washing steps with isopropanol, ethanol, and water, yielding stable aqueous colloidal dispersions of PMNPs (**Figure 3**). For the synthesis of MMNPs, the same procedure was followed without adding the polymer and injecting aqueous solution of 0.10 g of $Fe^{2+}$and 0.10 g of the respective metal-dopant salt (M = Co^{2+}, Ni^{2+}, or Zn^{2+}; 1:1 Fe^{2+}: M^{2+}) instead (**Figure 4**).

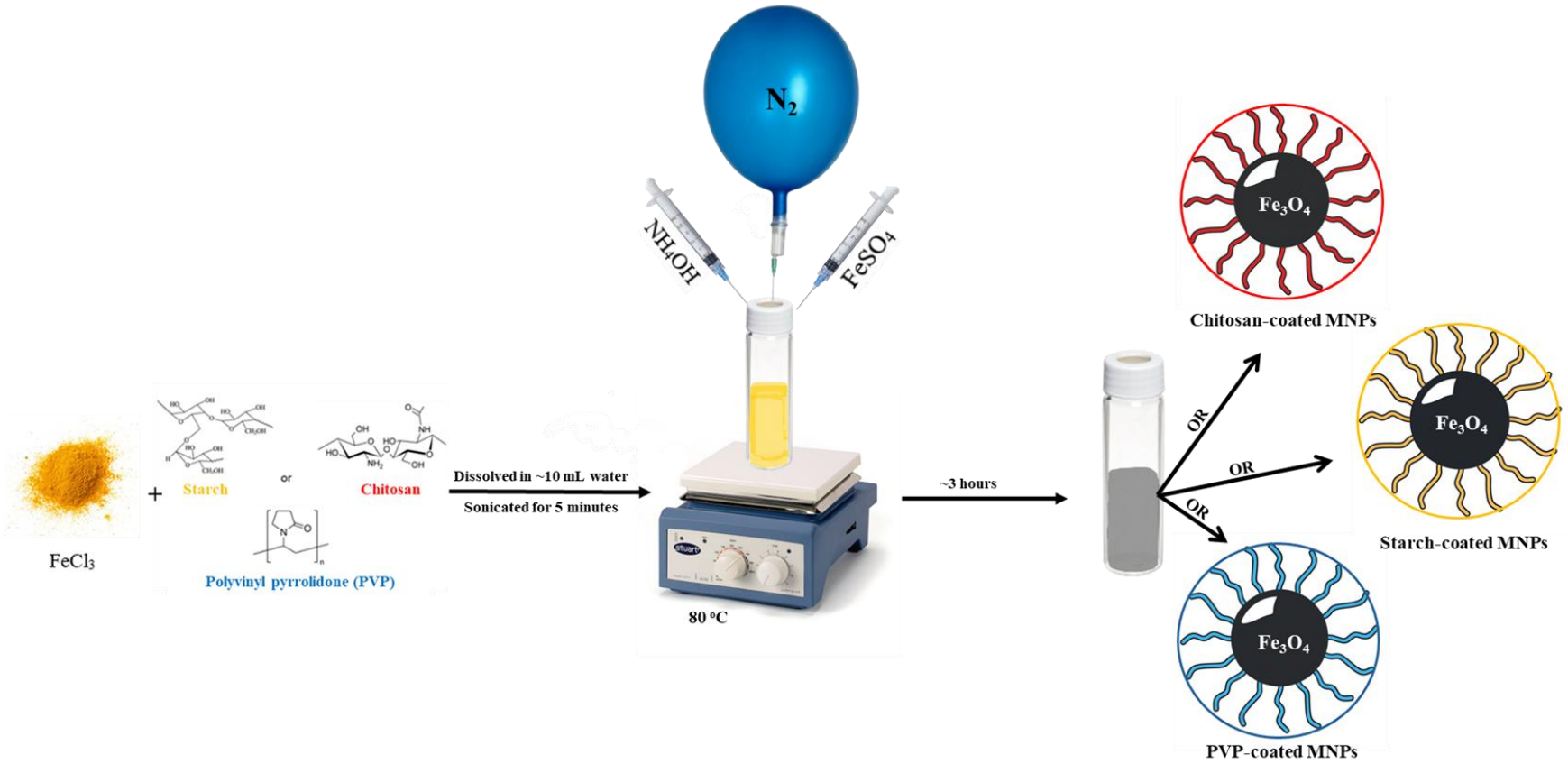


Figure 3. Schematic illustration of the KHB synthetic methodology utilized to prepare PMNPs.

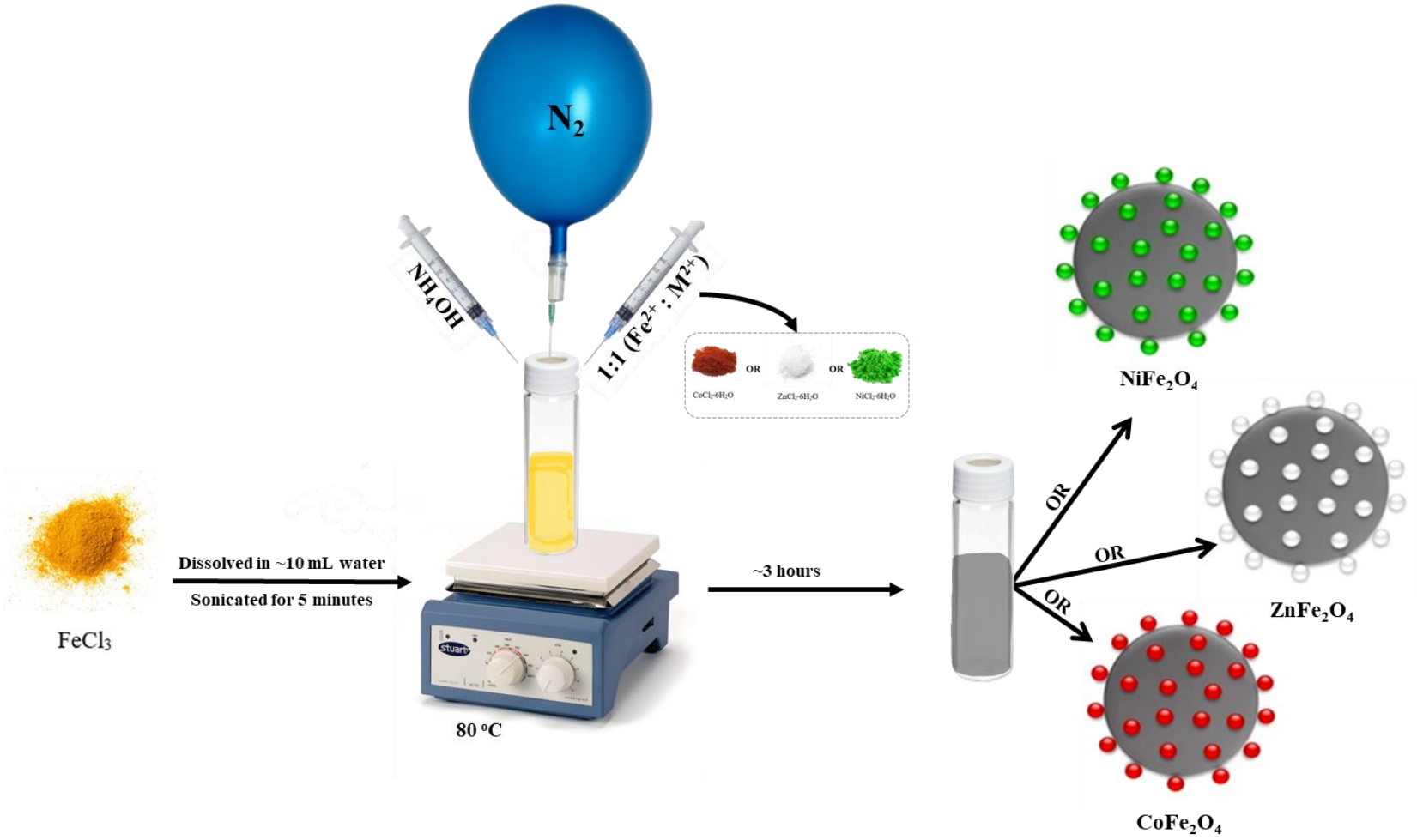


Figure 4. Schematic illustration of the KHB synthetic method used to prepare metal-doped MNPs

3.4. Catalytic Degradation of Chlorophenols

In each catalytic experiment, 10 mL 4-CP or 2-CP solution was placed in 25 mL stoppered vials, and the initial CPs concentration was set at 10, 50, or 70 $mg \cdot L^{-1}$ depending on the required concentration to be examined. The initial pH of the CP solution was adjusted using HCl (0.5 $mol \cdot L^{-1}$) and NaOH (0.5 $mol \cdot L^{-1}$), followed by measurement of the solution's pH. All experiments were conducted at room temperature, except for the temperature control experiments where the vials were placed on a hot plate with magnetic stirrer to adjust the temperature of the solution. Thereafter, precise amounts of the catalysts (e.g. 100, 50, or 20 mg) were introduced to the chlorophenol solution inside the vials to prepare 10, 5, and 2 $mg \cdot mL^{-1}$ catalyst dosages. The heterogeneous mixture was briefly sonicated followed by shaking on a rotatory shaker at 150 rpm at room temperature to allow efficient mixing and the catalytic reactions were initiated after adding the required volume from 35% H_2O_2 into the vials (286 µL and 571 µL to prepare 1% and 2% H_2O_2 solutions, respectively). At designated time points, samples were withdrawn and isolated *via* a hand-held magnet to separate the magnetic NP catalysts from the solution. 2 mL aliquots were taken, and UV-vis absorption spectra (200-800 nm) were then recorded at different time intervals in a quartz cuvette on an Orion AquaMate 8000 spectrophotometer. A schematic illustration is given in **Figure 5**. The concentrations for the various samples were obtained through a calibration curve, and the % degradation was calculated as follows:

$$\% \text{ Degradation} = \frac{C_i - C_t}{C_i} \times 100 \qquad \textbf{Equation 14}$$

where C_i and C_t are the initial chlorophenol's concentration at time equal zero, and the concentration of the chlorophenol at time equal t, respectively.

Chloride and total organic carbon (TOC) concentrations were measured using ion chromatography (Metrohm, 940 Professional IC Vario equipped with conductivity detector and Metrosep A Supp 7 -250/4.0 anion column) and TOC-L (Shimadzu, TOC-L CSH), respectively. The reusability of selected as-prepared MNP catalysts was evaluated

by collecting the catalysts using the magnet after the first reaction is completed, washing it with deionized water several times, and then using it for subsequent reactions under the same experimental conditions.

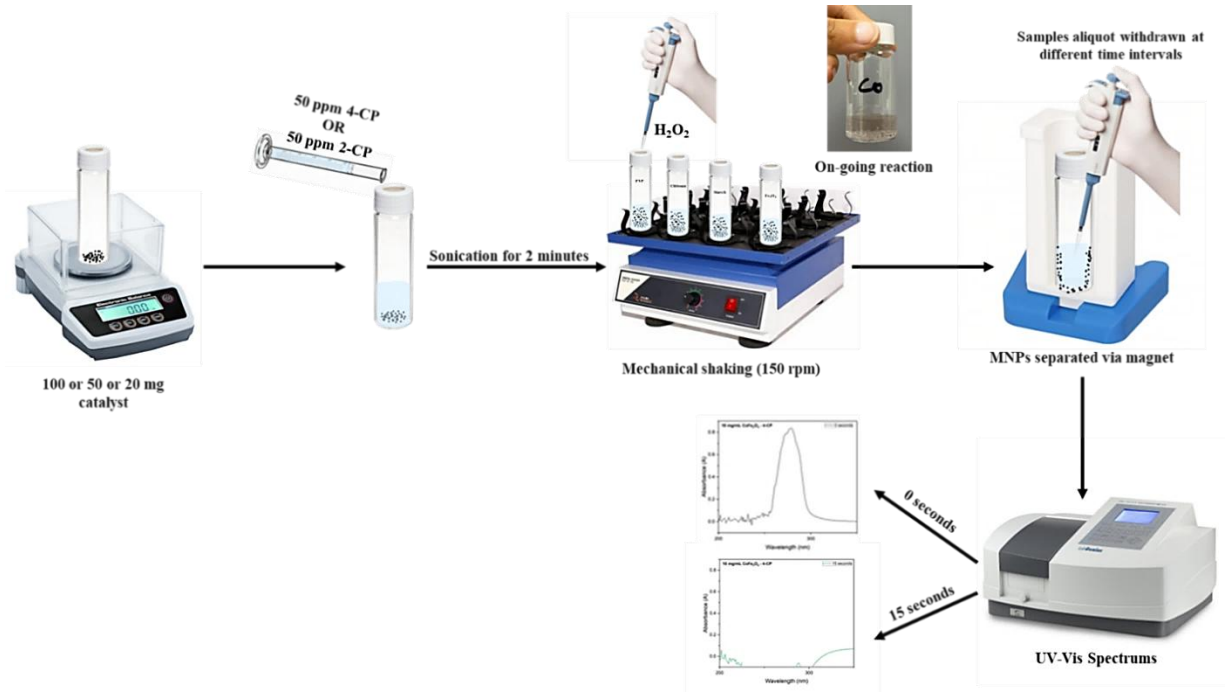


Figure 5. Schematic illustration of the experimental setup for the catalytic degradation of chlorophenols.

3.5. Catalytic Degradation of Chlorophenols under AMF

PMNPs and metal-doped-MNPs (10 mg/mL) have been investigated under the effect of AMF (H_0 = 170 Oe and f = 472 kHz) for the field amplitude and frequency, respectively, using Magnetotherm self-heating apparatus from Nanotherics equipped with a 9-turn copper coil using the calorimetric method. To ensure precise temperature monitoring without electromagnetic interference, the sample temperature was recorded using a fiber-optic thermometer positioned directly in the solution throughout the experiment. First, the samples were dissolved in 2 mL of 50 ppm 4-CP or 2-CP and sonicated for 2 minutes, then the catalytic reactions were initiated after adding the required volume from 35% H_2O_2 into the vials (286 µL to prepare 1% H_2O_2) and immediately the cells were inserted inside the magnetotherm instrument under the

previously mentioned magnetic field and amplitude, and the temperature increase of the samples was then recorded under AMF for 10 min only. After that, MNPs were separated from the solution using a hand-held magnet, and the absorbance spectra of the supernatant were measured by UV-Vis spectroscopy as previously described. A schematic illustration is shown in **Figure 6**.

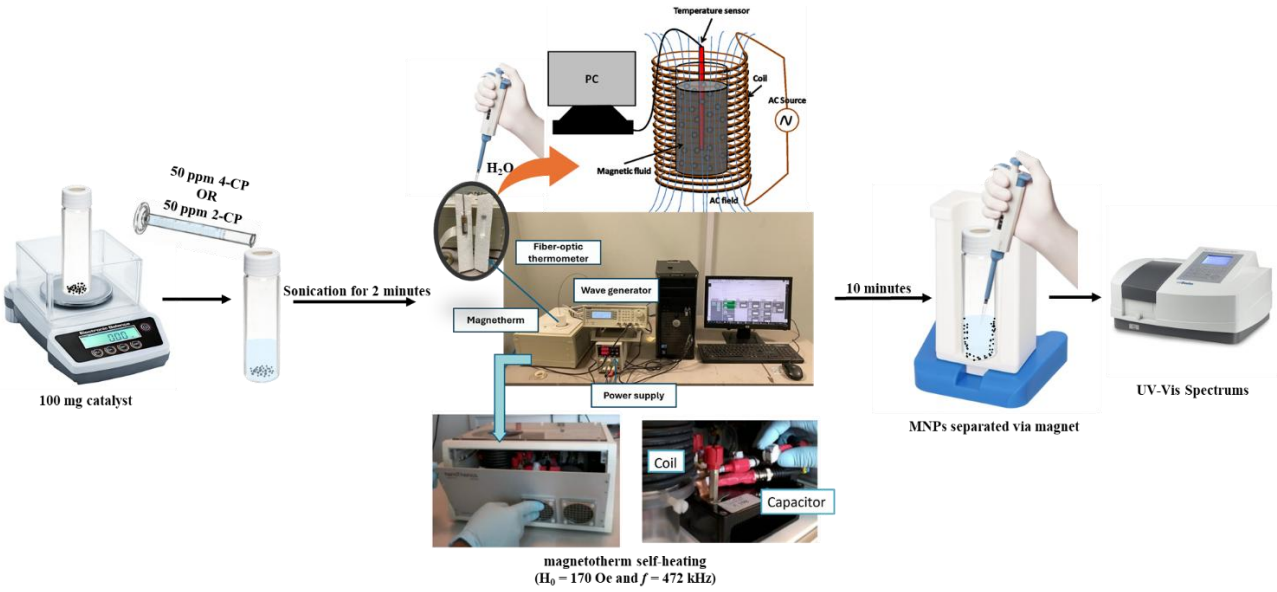


Figure 6. Schematic illustration for the experimental setup for the catalytic degradation of chlorophenols under AMF.

Chapter 4. Results and Discussion

4.1. Preparation and Characterization of various MNPs

4.1.1. Synthesis and characterization

As illustrated in Error! Reference source not found., various polymer-capped Fe_3O_4 MNPs were synthesized using our recently developed *Ko-precipitation Hydrolytic Basic* (KHB) method, which yields well-dispersed, colloidally stable PMNPs. The method is based on sequential *in situ co-precipitation* under alkaline hydrolytic conditions (*Ko-precipitation*) of metal salts (i.e. Fe^{3+} and Fe^{2+}) compartmentalized by stabilizing organic polymers in aqueous solutions at relatively low temperatures. Herein, hydrophilic polymers were used to coat the MNPs (i.e. PVP, Starch, and Chitosan), and divalent metal ions were used to dope the MNPs. Adding NH_4OH base afforded blackish tailor-made polymerylated iron oxide MNPs. The obtained MNPs were recovered through successive centrifugation cycles, purified, and oven-dried before further experimentation.

To verify the formation of PMNPs, TEM, XRD, FTIR, and VSM analyses were carried out. TEM micrographs (**Figure 7a**) show quasi-spherical particles with average sizes of 10 -15 nm, as confirmed by their corresponding size-distribution (**Figure 7b**). XRD patterns of all polymer-functionalized samples (**Figure 8a**) exhibit sharp reflections indicative of a well-crystallized, single-phase inverse spinel structure. The prominent peaks at the (220), (311), (400), (422), (511), (440), and (533) planes correspond to the cubic Fe_3O_4 spinel phase (JCPDS # 01-088-0315).

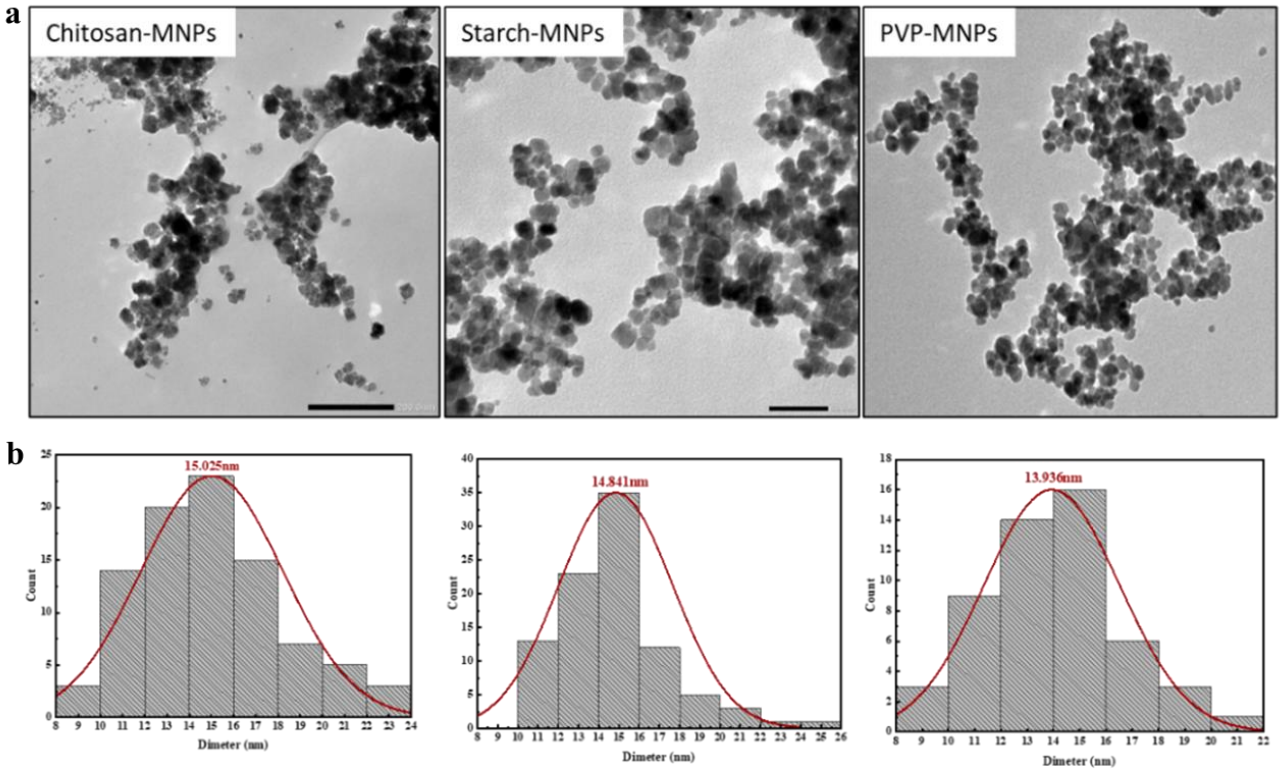


Figure 7. a) TEM images of the various polymer-coated MNPs showing sizes ~ 10 – 15 nm, b) corresponding size distributions.

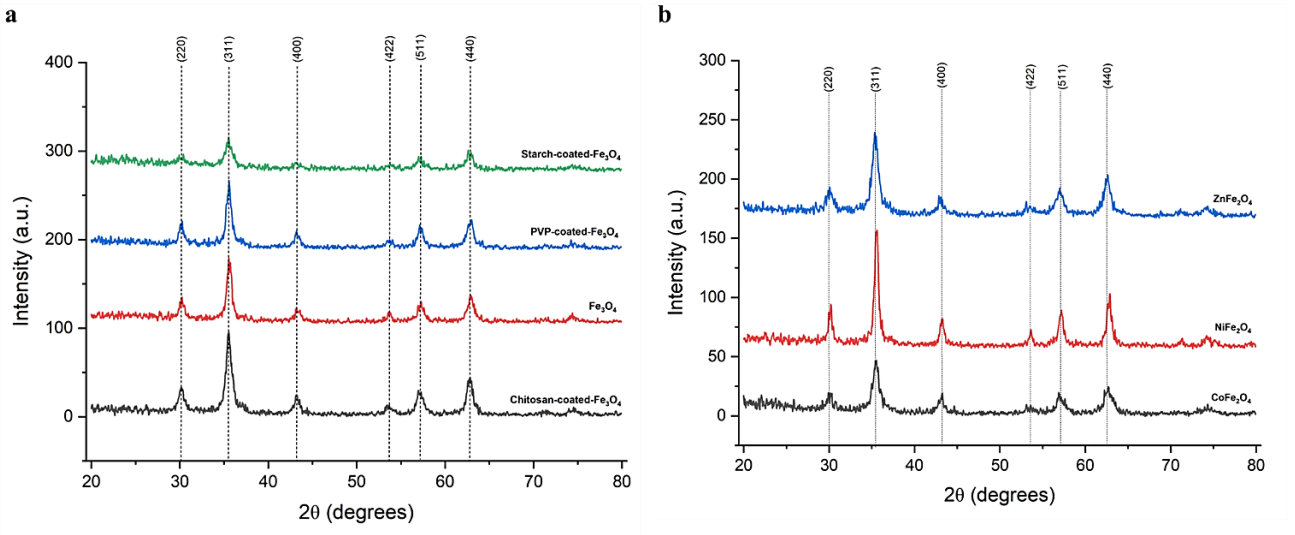


Figure 8. Powder XRD patterns of the as-synthesized a) polymer-coated MNPs and b) metal-doped ferrites.

For the as-synthesized metal-doped samples, the same main XRD peaks were observed which are related to the spinel structure (**Figure 8b**). Very slight peak shifting was observed, in agreement with previous reports (K. El-Boubbou et al., 2024). Both Co and Ni ferrite possess a fully inverse structure where Fe^{3+} ions mainly occupy tetrahedral sites, while Co^{2+} or Ni^{2+} and the remaining Fe^{3+} ions share octahedral sites. $ZnFe_2O_4$, on the other hand, typically exhibits a normal spinel structure, where the divalent Zn^{2+} ions preferentially occupy the tetrahedral A-sites, while the trivalent Fe^{3+} ions reside in the octahedral B-sites. This arrangement is favored due to the smaller ionic radius of Zn^{2+} compared to Fe^{3+}, allowing it to fit comfortably in the smaller tetrahedral voids. The different cationic distribution at the A and B sites directly influences the magnetic properties of the material, such as its coercivity and saturation magnetization. Rietveld analysis of these XRD patterns confirmed the formation of MFe_2O_4 cubic spinel phases with space group *Fd3m* for $NiFe_2O_4$, $CoFe_2O_4$, and $ZnFe_2O_4$ which matches well with JCPDS # 01-071-3850, # 01-074-6402, and # 01-071-5149, respectively. The refinements show an excellent agreement between the observed and calculated patterns. Moreover, only slight differences in sizes of crystals were obtained, probably due to the difference in the ionic radii of the dopant metals. In all cases, however, no extra peaks were detected, confirming the formation of pure spinel magnetite or ferrite phases (Srivastava, Ojha, Chaubey, & Materny, 2009; Tipsawat et al., 2018). Notably, Rietveld analysis confirmed the XRD and TEM findings, yielding lattice parameters a = b = c = 8.38/9 and crystallite sizes of 7.313-12.44 nm across all samples (**Table 4**).

Next, SEM–EDX was performed to assess the elemental composition of the doped ferrite samples. Analyses on representative areas confirmed phase purity, revealing atomic percentages of 7.8-16.2% for the dopant metals (Co, Ni, Zn), ~56.9% Fe, and 23.7-37.7% O (**Figure 9**). These results nicely corroborated the pure XRD MFe_2O_4 phases obtained by Rietveld analysis.

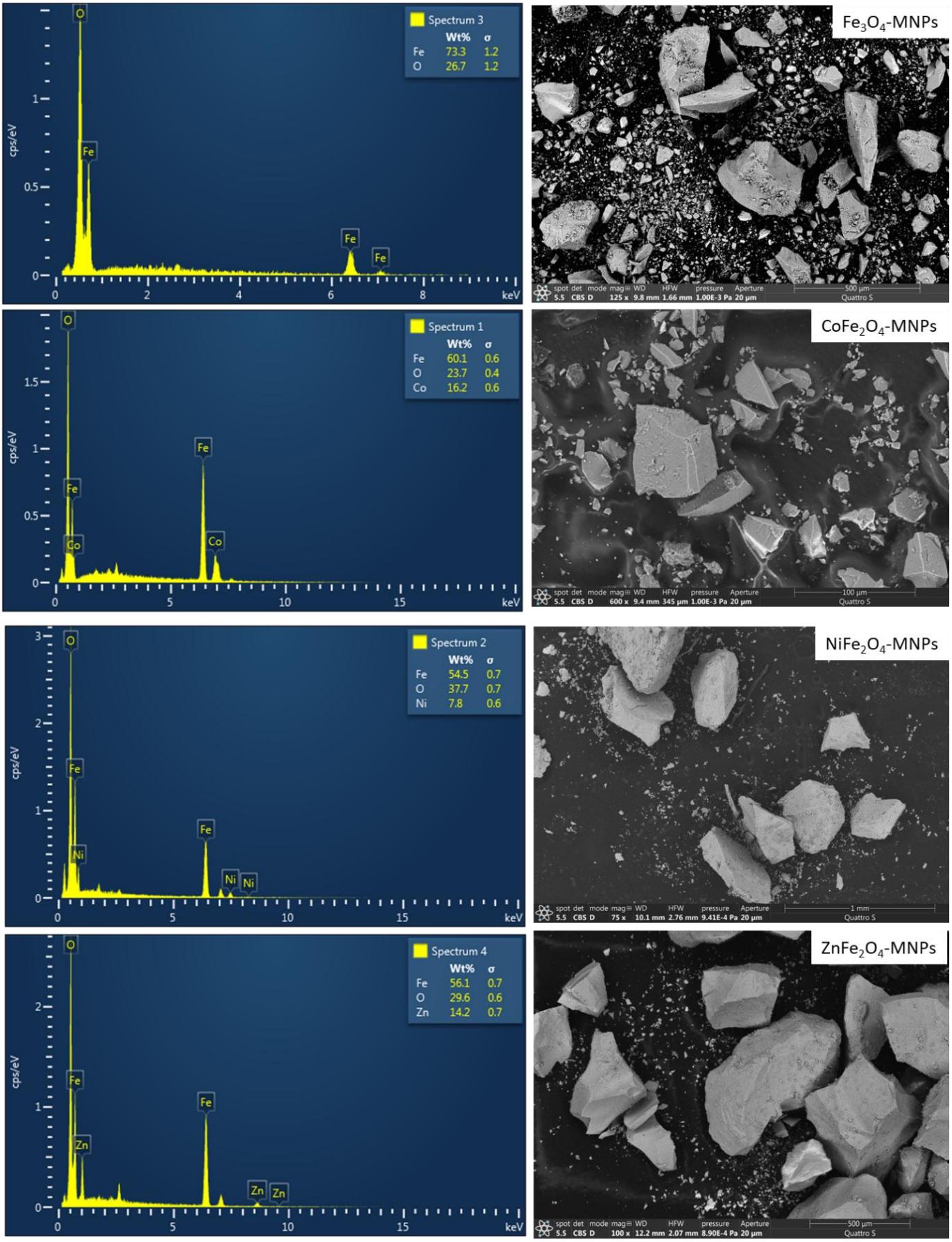


Figure 9. SEM-EDX elemental analysis of the various metal-doped ferrites.

FTIR spectroscopy was subsequently conducted to confirm the successful deposition of polymers onto the Fe_3O_4 NP surfaces. As shown in **Figure 10a**, the presence of iron oxide (Fe_3O_4) in the core is clear from the Fe-O stretching vibrations at 560 and 600 cm $^{-1}$. The prominent broad peak ~3400 cm^{-1} in all samples is due to the O-H stretching vibration of the hydroxyl groups, while the distinctive peaks at 2920 and 2850 cm^{-1} is responsible for the symmetric and asymmetric C-H stretching modes of the carbon chains in polymer coatings. The signature sharp peak at 1635 cm^{-1} is responsible of the stretching vibration of the C=O carbonyl groups present in PVP-coated-Fe_3O_4, and it was observed as well in the spectrums of other MNPs (Fe_3O_4, Chitosan-coated Fe_3O_4, Starch-coated Fe_3O_4) which is due to the bending vibrations of the hydroxyl groups on the surface of the magnetite (Jannah & Onggo, 2019; Lori et al., 2016; Petcharoen & Sirivat, 2012). The broad peak from 1000 to 1150 cm^{-1} responsible of C-O, C-C stretching vibrations (Gangwar et al., 2012; Hebeish, Aly, El-Shafei, & Zaghloul, 2009; Lawrie et al., 2007; Warren, Gidley, & Flanagan, 2016). Similar peaks were observed for Chitosan-coated and Starch-coated MNPs clearly indicating the successful coating of Fe_3O_4 MNPs surfaces with the respective polymers.

For the metal-doped ferrites, as shown in **Figure 10b,** only four prominent and significant peaks appeared (i.e. broad O-H stretching vibration peak at ~3400 cm^{-1}, O-H bending vibration band at 1635 cm^{-1}, and two absorption bands at ~ 400 -590 cm^{-1} corresponding to the octahedral and tetrahedral sites of the ferrites responsible particularly to the M-O bonds (Fe-O, Zn-O, Ni-O, and Co-O) because of metal doping the crystallites (K. El-Boubbou et al., 2024; Lori et al., 2016).

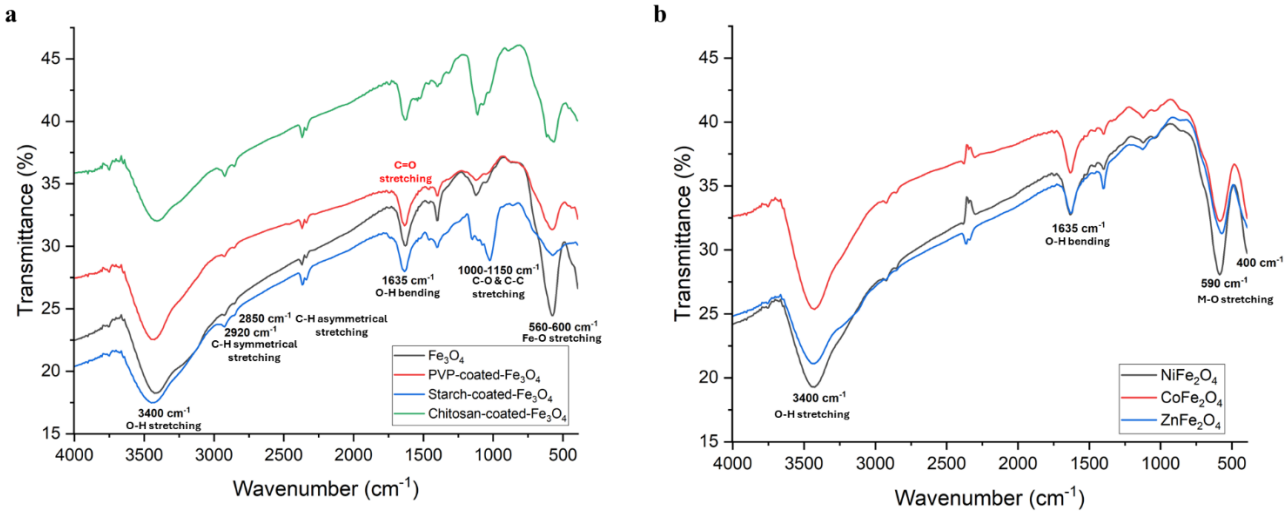


Figure 10. FTIR spectra of the as-synthesized a) polymer-coated-MNPs and b) metal-doped ferrites.

Table 4. Rietveld analysis of the different polymer-coated and metal-doped MNPs.

Sample	Phase Composition (%)	Crystallite size (nm)	Microstrain (%)	Lattice parameters (Å)	Fit parameters
Fe_3O_4	Fe_3O_4 100(6) 01-076-2948	12.25 (11)	0.372 (18)	a= b=c=8.369 (5) α=β=γ=90°	R_{wp}=43.05% R_p=32.63% R_e=38.71% S=1.1105 χ_2=1.2331
$NiFe_2O_4$	$NiFe_2O_4$ 100(5) 01-078-6781	12.44 (6)	0.17 (2)	a= b=c=8.379 (16) α=β=γ=90°	R_{wp}=41.41% R_p=30.43% R_e=38.80% S=1.0660 χ_2=1.1363
$ZnFe_2O_4$	$ZnFe_2O_4$ 100(6) 01-089-7412	7.313 (7)	0.293 (7)	a= b=c=8.3948 α=β=γ=90°	R_{wp}=38.63% R_p=28.90% R_e=37.40% S=1.0315 χ_2=1.0640
$CoFe_2O_4$	$CoFe_2O_4$ 100(7) 01-076-2948	8.33 (8)	0.55 (3)	a= b=c=8.386 (7) α=β=γ=90°	R_{wp}=41.70% R_p=32.48% R_e=40.94% S=1.0173 χ_2=1.0349
PVP-Fe_3O_4	Fe_3O_4 100(7) 01-076-2948	10.214 (19)	0.266 (7)	a= b=c=8.362 (6) α=β=γ=90°	R_{wp}=39.31% R_p=28.55% R_e=37.13% S=1.0575 χ_2=1.1183
Starch-Fe_3O_4	Fe_3O_4 100(11) 01-076-2948	8.12 (4)	0.41 (2)	a= b=c=8.395 (5) α=β=γ=90°	R_{wp}=39.39% R_p=30.21% R_e=37.4% S=1.0520 χ_2=1.1066
Chitosan-Fe_3O_4	Fe_3O_4 100(5) 01-085-1436	8.82 (5)	0.32 (3)	a= b=c=8.382 (6) α=β=γ=90°	R_{wp}=38.87% R_p=28.27% R_e=35.33% S=1.0986 χ_2=1.2070

4.1.2 Magnetic Properties

Field-dependent magnetization measurements were carried out at room temperature to assess the magnetic behavior of bare Fe_3O_4 NPs, polymer-coated MNPs, and metal-doped ferrite samples. **Figure 11a,c** present the corresponding hysteresis loops (M-H curves), from which saturation magnetization (M_s), coercivity (H_c), and remanence (M_r) values were determined and compiled in **Table 5**. All samples exhibited superparamagnetic behavior, with negligible H_c and M_r. The M_s values for PVP- MNPs, starch-MNPs, and chitosan-MNPs were 68.13, 37.71, and 19.75 emu/g, respectively, while those for $NiFe_2O_4$, $CoFe_2O_4$, and $ZnFe_2O_4$ ferrites were 59.86, 62.42, and 53.96 emu/g. These trends align closely with our earlier observations (K. El-Boubbou et al., 2024; Kheireddine El-Boubbou et al., 2022). Here, the synthesized MNPs exhibit notably high saturation magnetizations, reflecting a strong degree of magnetic ordering and crystallinity, which is an outcome of our optimized synthetic protocol. To further characterize their magnetic behavior, we calculated the effective anisotropy constant (K_{eff}), a key parameter directly influencing magnetization. K_{eff} was determined by applying the law of approach to saturation (LAS) to the experimental magnetization data, using the following equation:

$$\mathbf{M(H) = M_s\left(1 - \frac{b}{H^2}\right)}$$

where b is a parameter which is deduced from the fitting of experimental magnetization with the above equation. K_{eff} is then determined by:

$$\mathbf{K_{eff} = \mu_0 M_s\sqrt{\frac{15b}{4}}}$$

Fitting the equation to the experimental magnetization shows that all the obtained M-H curves fit well with the LAS model with very high K_{eff} values of ~ 0.455 $\times 10^5$ - 2.60 $\times 10^5$ erg/cm^3 (**Figure 11 b,d)**.

4.1.3 Thermal Properties

We evaluated the heating efficiencies of various PMNPs under AMF to determine how different polymers influence heat generation. Since any barrier between the iron oxide core and the surrounding medium can affect heat transfer, hence, achieving rapid temperature rises with minimal NP doses is essential. Heat production in MNPs arises mainly from hysteresis losses, Brownian relaxation (frictional heating due to particle rotation in the medium), and Néel relaxation (internal heating from magnetic moment reorientation). Smaller particles predominantly relax via the Néel mechanism, whereas larger particles dissipate heat chiefly through Brownian relaxation in liquids. Key factors governing heating efficiency include nanoparticle characteristics (size, composition, structure, magnetic properties), the nature of the polymer coating, the dispersion medium, particle concentration and interactions, and AMF parameters (field amplitude and frequency). In our experiments, we recorded heating curves (temperature increase versus time) for PMNPs at varying concentrations in aqueous dispersions under an AMF (H_0= 160 Oe, f = 472 kHz), as depicted in **Figure 12** and **Figure 13**.

Figure 12 shows the temperature rise of Fe_3O_4, PVP-coated-Fe_3O_4, Chitosan-coated-Fe_3O_4, and Strach-coated-Fe_3O_4 each at different concentrations of 2.5, 5, 7.5, and 10 mg/mL for 15 minutes. All samples except Starch-coated-Fe_3O_4 reached 42 ℃, the temperature required for hyperthermia, shortly after applying AMF. It was observed that for all MNPs, increasing their concentration led to a rapid rise in temperature. This can be attributed to the greater amount of MNPs, which serve as the primary source of heat dissipation under an AMF as the NPs return to their relaxed states. PVP-coated-Fe_3O_4 and Chitosan-coated-Fe_3O_4 exhibited higher heating abilities compared to the Starch-coated-Fe_3O_4, where the time required to reach hyperthermia at 42 ℃ was 4.08 and 4.2 minutes for PVP-coated-Fe_3O_4 and Chitosan-coated-Fe_3O_4, respectively, as illustrated in **Figure 13** and **Table 6**. However, at the same concentration, the uncoated bare-Fe_3O_4 exceeded the heating ability of all PMNPs and reached 42 ℃ within 2.65 minutes. Similarly, when the MNPs concentration was 7.5 mg/mL, the highest heating

ability was Fe_3O_4, followed by PVP-coated-Fe_3O_4, Chitosan-coated-Fe_3O_4, and Strach-coated-Fe_3O_4, where 42 ℃ reached within 3.42, 5.05, 5.38, and 12.27 minutes, respectively, and the same was obtained with concentrations of 5 and 2.5 mg/mL. For the metal-doped MNPs, all samples exhibit high heating efficiencies, with $CoFe_2O_4$ showing the highest performance (i.e. SAR values reaching ~ 150 W/g), followed by $NiFe_2O_4$ and the least is for $ZnFe_2O_4$ (**Table 7**). This is expected and is in accordance with magnteization data (**Figure 11c-d** and **Table 5**). Importantly, all the samples show high heating abilities, reaching high temperatures in very short times.

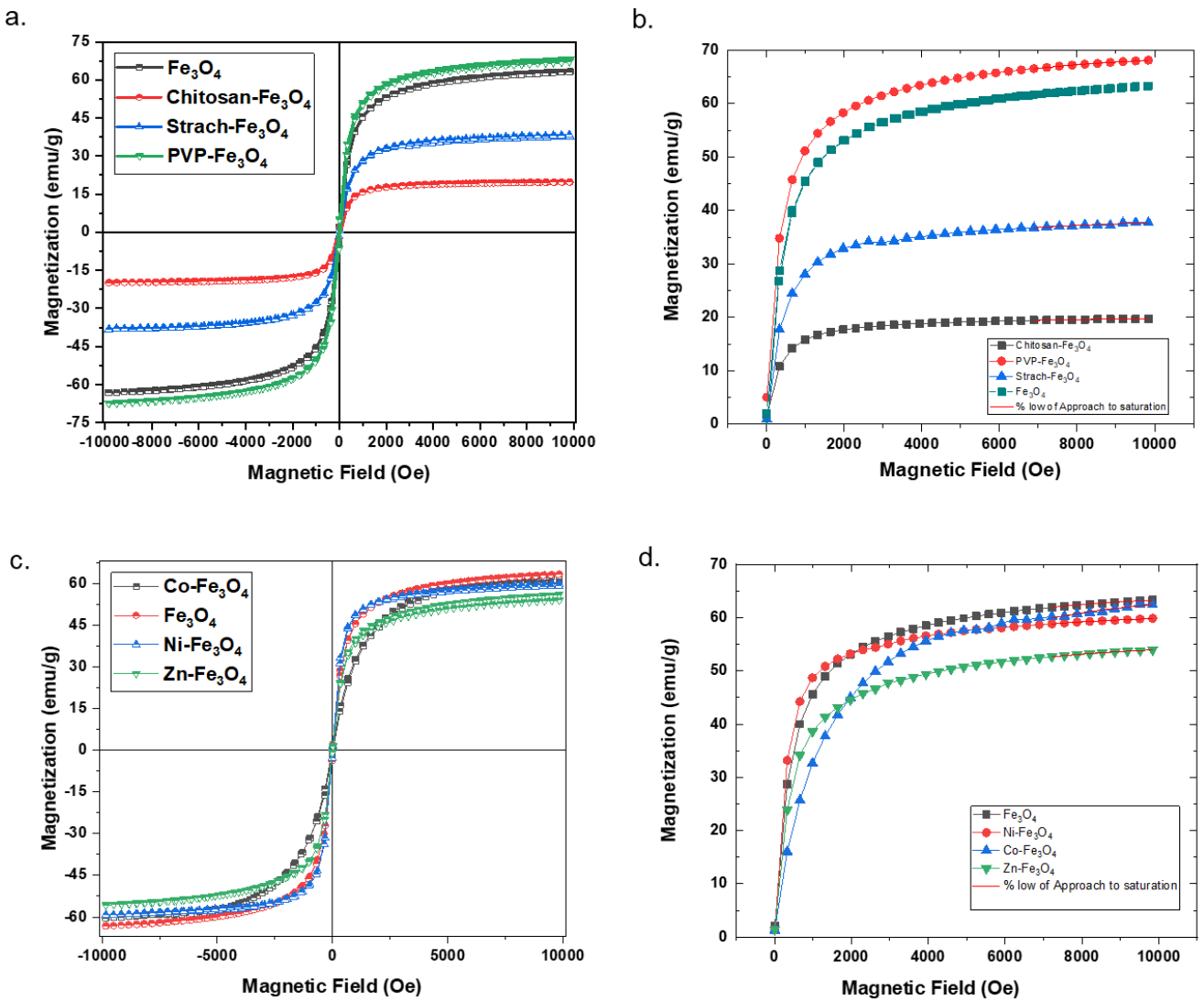


Figure 11. Field-dependent magnetization hysteresis loops at room temperature for a) polymer-coated MNPs, and b) law of saturation *(LAS)*; c) metal-doped MNPs and d) LAS fitting.

Table 5. Magnetic parameters obtained from M–H curves and law of approach to saturation (LAS) for polymer-coated and metal-doped MNPs.

Sample	**Experimental**				**Law of Saturation**	
	H_c (Oe)	**M_r (emu/g)**	**M_s (emu/g)**	**M_r/M_s**	**M_s (emu/g)**	**K_{eff} (erg/cm^3)**
Fe_3O_4-MNPs	20.20	1.584	63.30	0.025023	64.84 ± 0.04748	**1.93 x 10^5**
PVP-MNPs	39.17	4.145	68.13	0.060837	69.61 ± 0.05925	**1.97 x 10^5**
Chitosan-MNPs	15.15	1.412	19.75	0.07153	20.02 ± 0.0116	**4.55 x 10^4**
Starch-MNPs	10.44	0.485	37.71	0.012863	38.55 ± 0.1861	**1.12 x 10^5**
$NiFe_2O_4$-MNPs	13.13	1.064	59.86	0.017775	60.99 ± 0.04635	**1.62x 10^5**
$CoFe_2O_4$-MNPs	19.93	1.039	62.42	0.016646	65.29 ± 0.3727	**2.60 x 10^5**
$ZnFe_2O_4$-MNPs	6.611	0.519	53.96	0.009618	55.44 ± 0.04564	**1.75 x 10^5**

Table 6. Heating properties of metal-doped MNPs at different concentrations (field = 160 Oe, frequency = 472 kHz).

Sample	Concentration (mg/mL)	Maximum temperature (°C)	Time to reach 42°C (min)	SAR (W/g) (0-30 sec)	ILP ($nHm^2.kg^{-1}$)
Fe_3O_4-MNPs	10	63.62	2.65	60.099	0.785
	7.5	60.48	3.42	92.291	1.206
	5	55.58	4.07	103.604	1.354
	2.5	51.75	5.45	245.778	3.212
PVP-MNPs	10	54.85	4.08	68.322	0.893
	7.5	52.76	5.05	81.727	1.068
	5	52.28	5.52	105.846	1.383
	2.5	48.11	7.93	188.370	2.462
Chitosan-MNPs	10	54.78	4.20	51.578	0.674
	7.5	50.75	5.38	66.976	0.875
	5	46.90	8.02	76.245	0.996
	2.5	41.94	Not reached	135.746	1.774
Starch-MNPs	10	44.64	10.62	34.235	0.447
	7.5	43.47	12.27	37.275	0.487
	5	42.14	14.67	46.046	0.602
	2.5	38.55	Not reached	107.042	1.399

Table 7. Heating properties of metal-doped MNPs at different concentrations (field = 160 Oe, frequency = 472 kHz).

Sample	Concentration (mg/mL)	Maximum temperature (°C)	Time to reach 42°C (min)	SAR (W/g) (0-30 sec)	ILP ($nHm^2.kg^{-1}$)
$CoFe_2O_4$-MNPs	10	68.44	3.17	27.254	0.411
	7.5	57.9	4.88	55.956	1.017
	5	47.36	9.77	76.150	1.321
	2.5	48.2	9.57	149.501	2.113
$NiFe_2O_4$-MNPs	10	56.58	3.18	24.335	0.396
	7.5	51.91	5.23	37.368	0.568
	5	47.24	8.63	46.164	0.734
	2.5	42.80	13.73	59.134	0.778
$ZnFe_2O_4$-MNPs	10	42.50	14.10	18.031	0.237
	7.5	41.45	Not reached	22.873	0.301
	5	40.40	Not reached	25.104	0.330
	2.5	39.40	Not reached	46.303	0.954

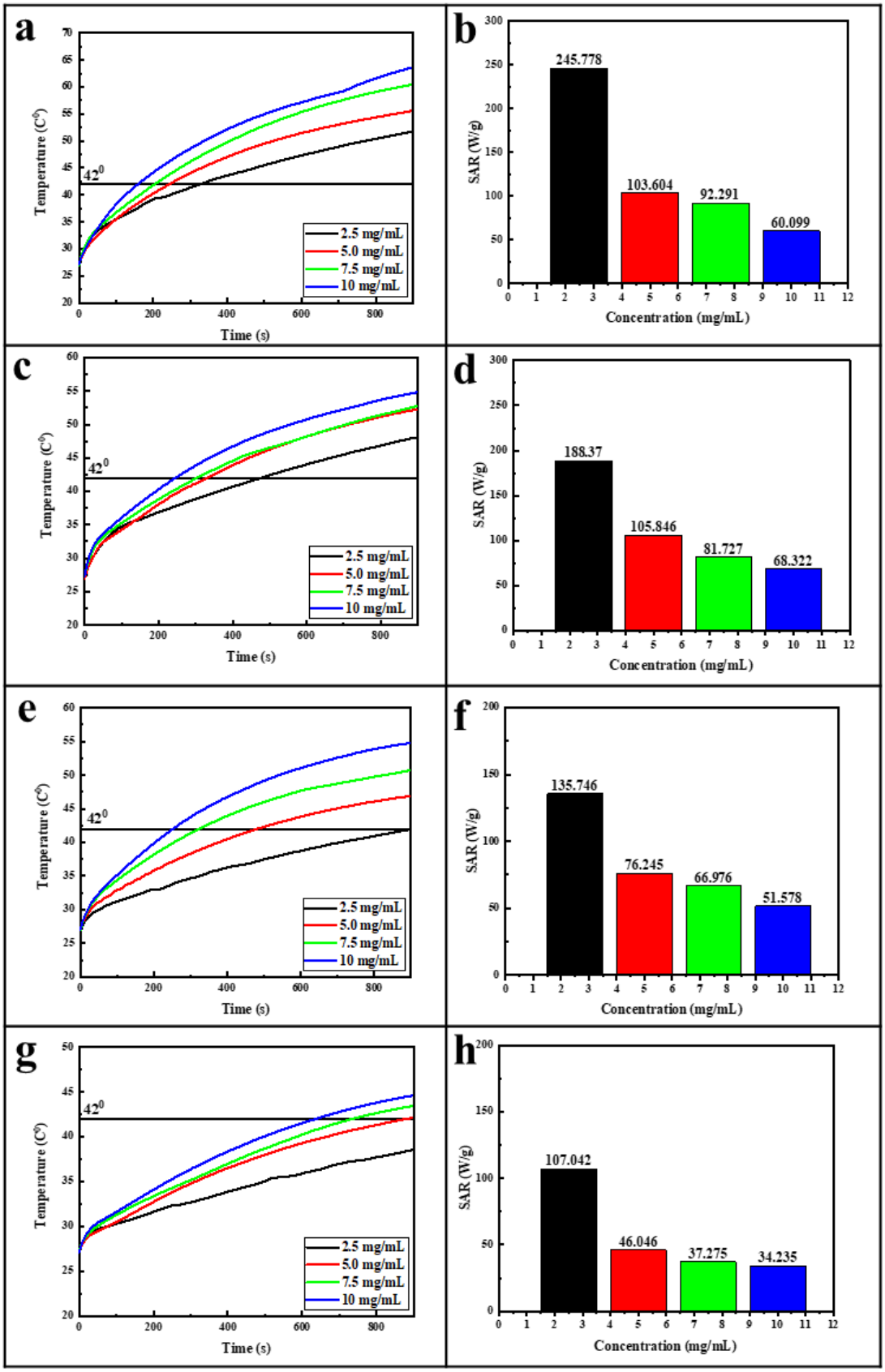


Figure 12. Heating efficiencies of (a-b) Fe_3O_4-MNPs, (c-d) PVP-MNPs, (e-f) Chitosan-MNPs, (g-h) Starch-MNP at H_0 = 160 Oe, f = 472 kHz.

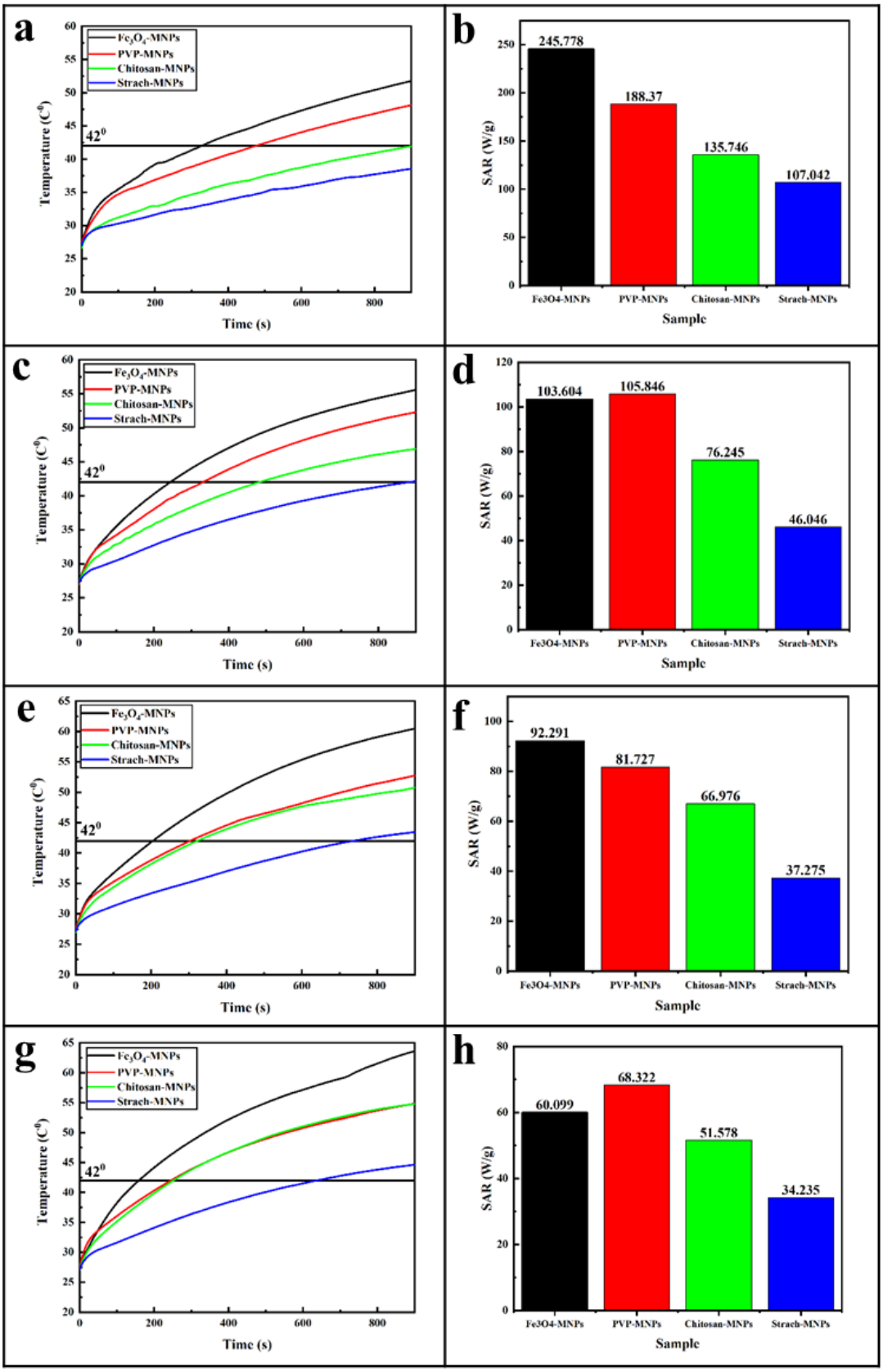


Figure 13. Heating efficiencies of the different MNPs at different concentrations (a-b) 2.5 mg/mL, (c-d) 5 mg/mL, (e-f) 7.5 mg/mL, (g-h)10 mg/mL at H_0 = 160 Oe, f = 472 kHz.

4.2 Catalytic Degradation of Chlorophenols

4.2.1 Control Experiments for Degradation of Chlorophenols

The degradation of 4-CP and 2-CP with time were examined under oxidative environment in the presence of 1% H_2O_2 alone or MNPs (10 mg/mL) alone. First, H_2O_2 was tested and it was observed to be not effective towards the degradation of 2-CP, where only 5.3% degradation was achieved within 90 minutes, and its effect was almost negligible, with only 0.74% degradation towards 4-CP within the same period (**Figure 14**). This is mainly attributed to the weak oxidative ability of H_2O_2 alone. Control reactions in the presence of 10 mg/mL bare Fe_3O_4 NPs show almost similar trend, where ~ 4.6% degradation of 2-CP and ~ 0.53% degradation of 4-CP was achieved within 90 minutes reaction (**Figure 14**).

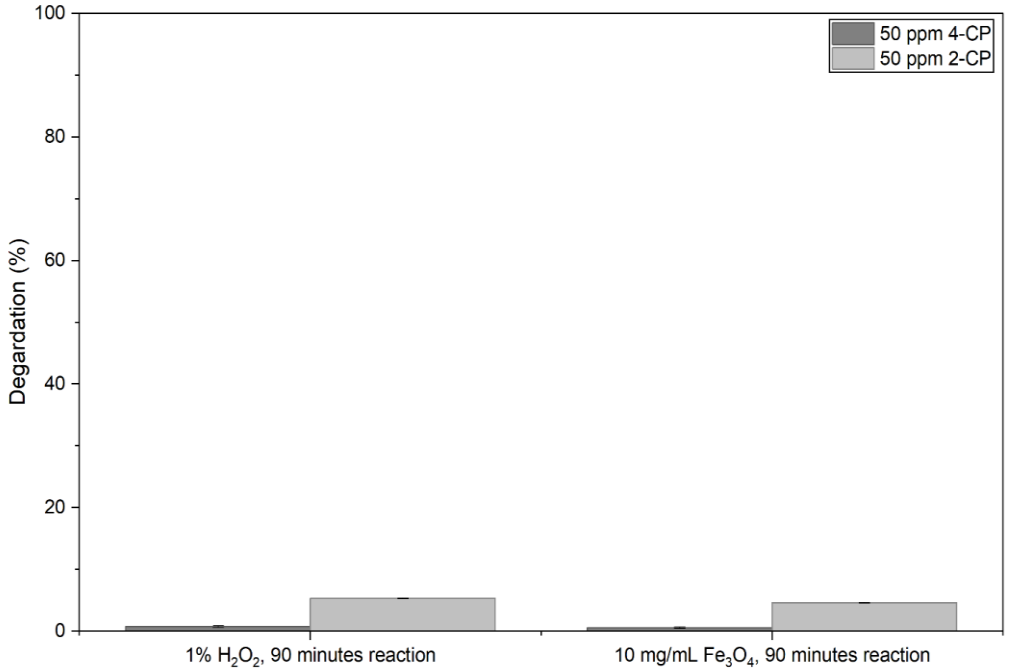


Figure 14. Control degradation experiments for 4-CP & 2-CP in the presence of either 1% H_2O_2 only or Fe_3O_4 NPs (10 mg/mL) only.

4.2.2 Degradation of Chlorophenols using PMNPs

To examine the utilization of PMNPs towards catalytic degradation of 4-CP and 2-CP, experiments were conducted in the presence or absence of 1% H_2O_2. As shown in **Figure 15a** and **Figure 16a,** even after 90 minutes exposure, negligible amounts of both pollutants were found to be removed and, thus, the removal percentages were relatively low, which clearly indicates the limited adsorption capacities of the NPs. For instance, 0.93, 1.07, and 4.8% removal of 50 ppm 4-CP were only achieved with Chitosan-coated MNPs, Starch-coated MNPs, and PVP-coated MNPs (10 mg/mL), respectively (**Figure 15a**). Similarly, only 0.53, 7.84, and 8.05% removal of 50 ppm 2-CP were achieved with Starch-coated MNPs, Chitosan-coated MNPs, and PVP-coated MNPs, respectively, at the same concentrations (**Figure 16a**).

Next, oxidative degradations of 4-CP and 2-CP with time were examined for the as-synthesized PMNPs and bare Fe_3O_4 NPs in the presence of 1% H_2O_2. As illustrated in **Figure 15b** and **Figure 16b**, the degradation of 4-CP and 2-CP was very effective reaching 100% degradation, albeit at different times for the different nanoformulations. For instance, 100% degradation of 50 ppm 4-CP was accomplished within 13, 16, 23, and 30 minutes using 10 mg/mL of Fe_3O_4 NPs, Chitosan-coated MNPs, PVP-coated MNPs, and Starch-coated MNPs, respectively (**Figure 15b**). Similarly, complete degradation of 50 ppm 2-CP was accomplished within 5, 9, 10, and 50 minutes using 10 mg/mL of Fe_3O_4 NPs, Chitosan-coated MNPs, PVP-coated MNPs, and Starch-coated MNPs, respectively (**Figure 16b**). Given these findings, the results clearly indicate the varying levels of removing CP pollutants, due to the polymer nature coating the MNP surface, which does not only affect the MNP surface area but will also influence the accessibility of the PMNPs active sites where the pollutants can get adsorbed onto it. Chitosan coated-MNPs were having the highest % removal amongst the PMNPs, followed by PVP-coated-MNPs and Starch-MNPs.

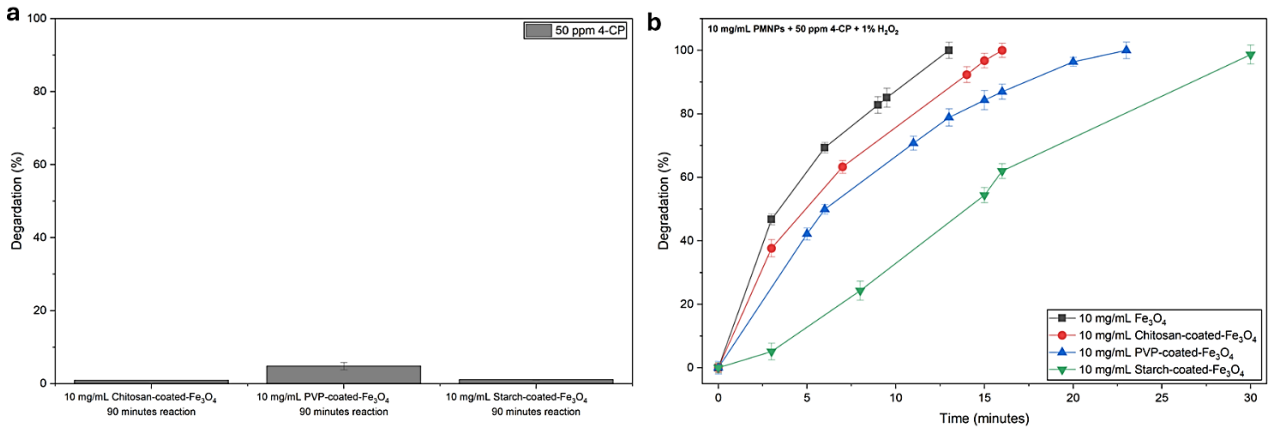


Figure 15. Effect of polymer coatings on the catalytic degradation of 4-CP for a) 10 mg/mL catalysts dosage + 50 ppm 4-CP (PMNPs control experiments), and b) 10 mg/mL catalysts dosage + 50 ppm 4-CP + 1% H_2O_2.

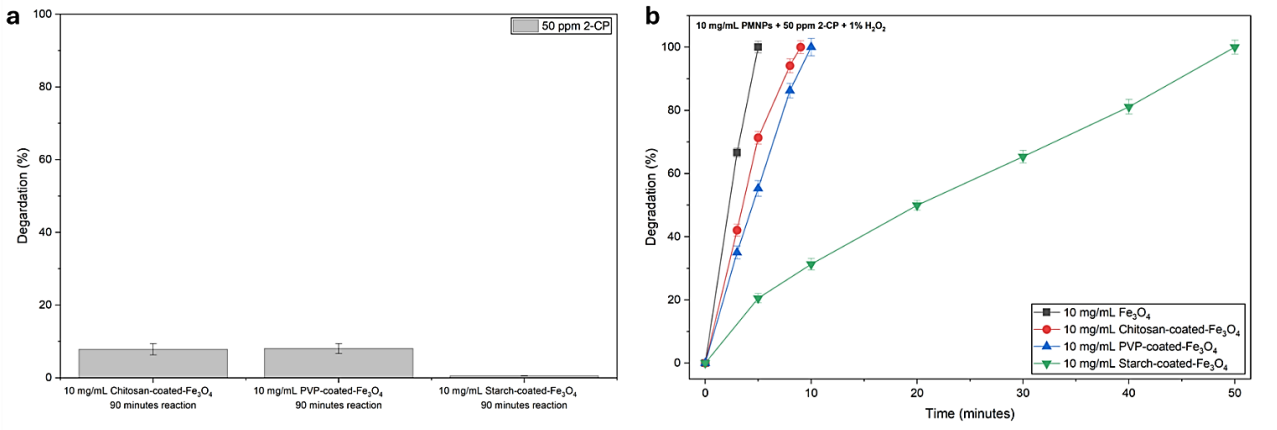


Figure 16. Effect of polymer coatings on the catalytic degradation of 2-CP for a) 10 mg/mL catalysts dosage + 50 ppm 2-CP (PMNPs control experiments), and b) 10 mg/mL catalysts dosage + 50 ppm 2-CP + 1% H_2O_2.

Overall, it was observed that the trend in catalytic behavior towards both 2-CP and 4-CP was the same. Despite the fact that it was expected that polymer coatings would enhance the catalytic behavior of the modified MNP catalysts (i.e. PMNPs) and consequently increase CP degradation rates, it was found that bare Fe_3O_4 NPs were the most effective nanocatalysts among others possessing the highest catalytic behavior towards 2-CP and 4-CP degradation. This can be attributed to the ease and accessible active sites on uncoated bare Fe_3O_4 NPs, in comparison to the protected PMNPs with polymers surrounding the iron oxide core. This would reduce the availability of iron ions that are essential for Fenton-like reactions that generate hydroxyl radicals (·OH) involved in chlorophenols oxidative degradation reactions as mentioned earlier in **Equation 1** and illustrated in **Figure 17.** For instance, Chitosan, Starch, or PVP polymers can form a branched and dense network around MNPs which can increase steric hindrance and reduce the availability of active sites available for adsorption and, in turn, prevent the diffusion of 2-CP or 4-CP onto the surface. Moreover, the polymer coats make it difficult for H_2O_2 to directly contact iron oxide core due to the physical barrier, resulting in generating less number of radicals that are essential to degrade chlorophenols. Thus, the less effective PMNPs were Starch-coated MNPs, due to the bulkiness and rigidity of the starch coating. On the other hand, Chitosan and PVP coatings showed better degradation efficiencies, with ~ 7 minutes difference to reach 100% 4-CP degradation and 1 minute difference to reach 100% 2-CP degradation. This can be attributed to the amine and amide functional groups in both polymers that can aid in increasing the interaction of the catalyst with the chlorophenols, thus reducing the time required to fully degrade both 2-CP and 4-CP.

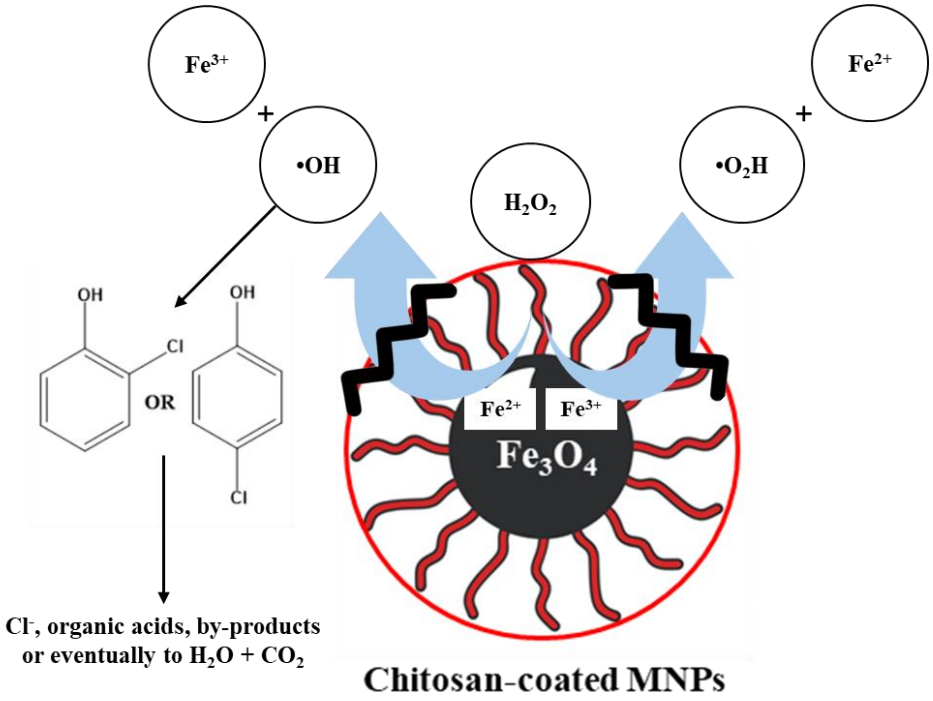


Figure 17. Mechanistic sketch of the catalytic oxidation of 2-CP or 4-CP by PMNPs.

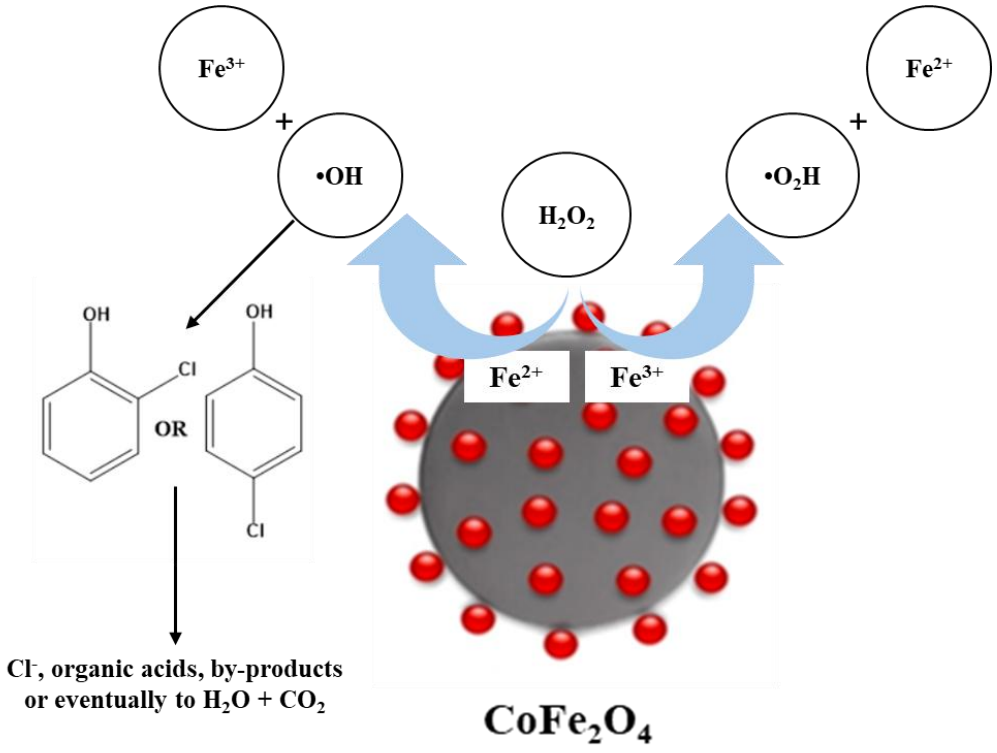


Figure 18. Mechanistic sketch of the catalytic oxidation of 2-CP or 4-CP by the metal-doped MNPs.

4.2.3 Degradation of Chlorophenols using metal-doped MNPs

Next, the efficiency of different metal-doped ferrites (MFe_2O_4 where M = Co, Ni, and Zn) towards the catalytic oxidation of chlorophenols was evaluated. As discussed earlier, the rate of catalytic degradation of chlorophenols can be influenced by several factors, such as the diffusion of the pollutants into the catalyst surface, adsorption of these pollutants onto the active sites of the catalyst, and regeneration of active sites on the catalyst surface, and how the pollutants interact with the metal oxide core generating the free radicals (Kurian & Nair, 2015). One of the advantages of using ferrites lies in their affordability, relatively low toxicity, and the flexibility in how they can be synthesized. Moreover, doping NPs with selected metal ions has been shown to significantly enhance catalytic degradation efficiencies. This is mainly because doping enhances the production of reactive oxygen species, such as hydroxyl radicals and superoxide anions, which are crucial for pollutant degradation *via* oxidative pathways. (Ariza-Tarazona et al., 2020). The structural tunability of the doped ferrites allows for optimization in terms of efficiency, cost, and environmental impact. As such, they are becoming strong candidates for sustainable wastewater treatment technologies, especially when it comes to tackling persistent and hazardous contaminants like CPs (Al-Najar, Kamel, Albuflasa, & Hankins, 2023).

First, control experiments were conducted to investigate the adsorption capabilities of three as-synthesized metal-doped ferrites (i.e. $CoFe_2O_4$, $ZnFe_2O_4$, $NiFe_2O_4$) towards monochlorophenols removal in the absence of 1% H_2O_2. As shown in **Figure 19a** and **Figure 20a**, even after 90 minutes exposure, removal percentages were relatively low, which, as before, clearly indicates the limited adsorption capacities of MFe_2O_4 ferrites for 4-CP and 2-CP. For instance, 5.87, 4.93, and 1.73% removal of 50 ppm 4-CP were achieved using $ZnFe_2O_4$, $CoFe_2O_4$, and $NiFe_2O_4$-MNPs (10 mg/mL) respectively. Likewise, 10.7, 6.67, and 2.75% removal of 50 ppm 2-CP were achieved with $ZnFe_2O_4$, $CoFe_2O_4$, and $NiFe_2O_4$ (10 mg/mL), respectively. Given these findings, the results showed varying levels of pollutants adsorption, the highest being achieved by $ZnFe_2O_4$, followed by $CoFe_2O_4$, and the lowest removal was observed with $NiFe_2O_4$ for both 4-

CP and 2-CP. The varying removal capabilities can be attributed to the NP size and the type of metal dopant. The smaller the NP size, the larger the surface area, allowing more pollutants/NPs interactions, and hence, better adsorption and higher removal efficiency. As reported earlier in XRD Rietveld analysis, the crystallite sizes were 12.44, 8.33, and 7.313 nm for $NiFe_2O_4$, $CoFe_2O_4$, and $ZnFe_2O_4$, respectively. $NiFe_2O_4$ NPs were the biggest among the others, while $CoFe_2O_4$ was a bit smaller and $ZnFe_2O_4$ being the smallest, which might well explain the observed adsorption capacities.

The oxidative degradation efficiencies of $CoFe_2O_4$, $ZnFe_2O_4$, and $NiFe_2O_4$ NPs towards monochlorophenols in the presence of 1% H_2O_2 are then investigated (**Figure 19b** and **Figure 20b**). The degradation of both mono-chlorophenols, 4-CP and 2-CP was successful and reached 100% with all ferrites, where the highest % degradation for chlorophenols was achieved by $CoFe_2O_4$, followed by $ZnFe_2O_4$, and the lowest for $NiFe_2O_4$ The mechanism behind the degradation reactions is suggested in the **Figure 18**. With 10 mg/mL of $NiFe_2O_4$ catalyst and 1% H_2O_2, 50 ppm of 4-CP degraded completely within 15 minutes, and similarly, at the same conditions, 50 ppm 2-CP degraded completely within 15 minutes as shown in **Figure 19b** and **Figure 20b**, respectively, where the rate of degradation increases with time. Although the $NiFe_2O_4$ NP catalyst load was 10 mg/mL, the time required for complete degradation was slower or similar to the time required to degrade the same pollutants using bare iron oxide Fe_3O_4 NPs. For instance, using 10 mg/mL $NiFe_2O_4$ with 1% H_2O_2, 50 ppm 4-CP degradation was completed within 15 minutes**,** whereas at the same conditions, using 10 mg/mL Fe_3O_4, 50 ppm 4-CP degradation was completed within 13 minutes. Similarly, using 10 mg/mL $NiFe_2O_4$ with 1% H_2O_2, 50 ppm 2-CP degradation was accomplished within 15 minutes, whereas was accomplished within only 5 minutes using Fe_3O_4 NPs. Interestingly, the time required for complete monochlorophenol degradation using $ZnFe_2O_4$ and $CoFe_2O_4$ was very fast. For instance, complete degradation of 50 ppm 4-CP using $ZnFe_2O_4$ (10 mg/mL) was accomplished only within 8 minutes (**Figure 19b**), whereas complete degradation of 50 ppm 2-CP was accomplished within 4 minutes (**Figure 20b**), much faster than bare Fe_3O_4 NPs in both cases.

The improved catalytic performance of the $ZnFe_2O_4$ nanocatalyst can be accredited to the NP size and the specific characteristics of the metal dopant. $ZnFe_2O_4$ have normal spinel structure as mentioned in **Table 1**, where Fenton-like reactions that generate hydroxyl radicals is faster when incorporating Zinc into the magnetite structure, hence, monochlorophenols degradation is enhanced (Aisida et al., 2020). Moreover, the large surface area to volume ratio of $ZnFe_2O_4$ determined by the smaller size of the nanoparticulate crystals (7.313 nm) will enhance the pollutant/catalyst interface which will boost catalytic activity and, hence, increase the rate of monochlorophenols degradation. On the other hand, the reduced catalytic activity of $NiFe_2O_4$ nanocatalyst can be attributed to its different spinel structure orientation as shown in **Table 1**. Because the catalytic activity of spinel ferrites is primarily determined by the redox potential of the octahedral cations, rather than tetrahedral ones, presence of Ni^{2+} ions in the octahedral sites lowers the redox potential of the octahedral pairs since Ni^{2+}/Fe^{3+} pair is not stable, which reduces the catalytic efficiency of the $NiFe_2O_4$ towards the degradation of mono-chlorophenols, 4-CP and 2-CP (Kurian & Nair, 2015; Nair & Kurian, 2017a)).

Costa et al. reported similar results, where the catalytic activity of Fe_3O_4 towards degrading organic compounds was reduced when incorporating Ni^{2+} ions into the magnetite structure ((Costa et al., 2006). It was concluded in their study that Ni^{2+} lowers the redox potential of the octahedral pairs, reduces the prepared catalyst reaction rate with H_2O_2, and minimized hydroxyl radicals' generation. In another study, (Kurian & Nair, 2015)reported an enhancement in the catalytic activity of the Zinc substituted $NiFe_2O_4$, and unsubstituted $ZnFe_2O_4$ for the degradation of 4-CP (Kurian & Nair, 2015; Nair & Kurian, 2017a)). They studied the effect of changing the composition of the spinel ferrite $Ni_xZn_{1-x}Fe_2O_4$ (x = 0.0, 0.25, 0.5, 0.75, 1.0) and reported that the most efficient catalyst composite was found when x=0 (i.e. for $ZnFe_2O_4$). Thus, the catalytic activity of nickel ferrite NPs increases when increasing the amount of zinc substitution, and the unsubstituted $ZnFe_2O_4$ catalyst degrades 4-CP completely within 45 minutes. Similarly, (Nair & Kurian, 2017a) reported an enhancement in the catalytic efficiency

of the $NiFe_2O_4$ when doped with zinc, and found that the zinc rich composite ($Zn_{0.75}Ni_{0.25}Fe_2O_4$) has the highest catalytic activity towards 2,4-dichlorophenol and 2,4-dichlorophenoxy acetic acid degradation, which was completed within 75 and 90 minutes, respectively.

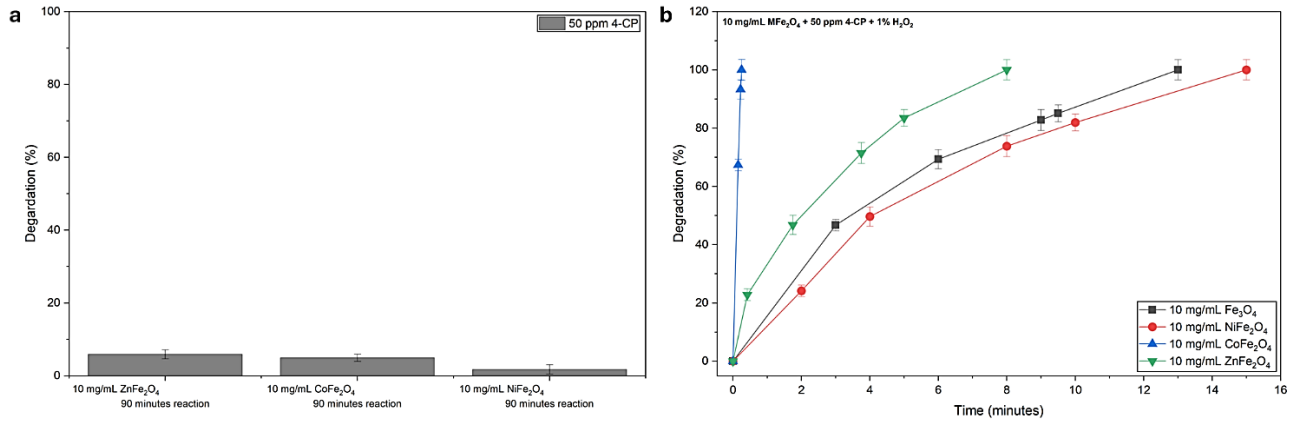


Figure 19. Effect of metal doping on the catalytic degradation of 4-CP for a) 10 mg/mL catalysts dosage + 50 ppm 4-CP (MFe_2O_4 control experiments), and b) 10 mg/mL catalysts dosage + 50 ppm 4-CP + 1% H_2O_2.

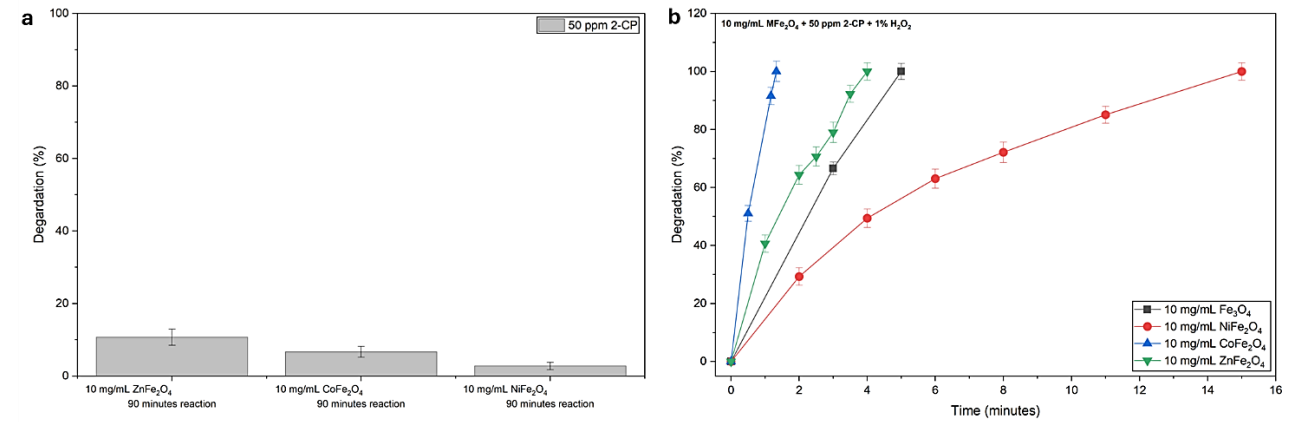


Figure 20. Effect of metal doping on the catalytic degradation of 2-CP for a) 10 mg/mL catalysts dosage + 50 ppm 2-CP + 1% H_2O_2, and b) 10 mg/mL catalysts dosage + 50 ppm 2-CP (MFe_2O_4 control experiment).

Exciting and superior results were obtained using $CoFe_2O_4$ ferrites. The complete degradation of 50 ppm 4-CP and 2-CP was achieved in just 15 seconds and 80 seconds, respectively (**Figure 19b** and **Figure 20b**). This outstanding performance of $CoFe_2O_4$ ferrites can be explained by the high stability of its redox pairs in its inverse spinel structure, Co^{2+}/Co^{3+} and Fe^{2+}/Fe^{3+}, which are located in the octahedral sites that are exposed to the outer surface of the catalysts and are responsible of the catalytic activity of the catalyst (Bhushan Das et al., 2021; Nair & Kurian, 2017a). In addition, the smaller sizes of $CoFe_2O_4$ NPs (8.33 nm) might contribute to these fast degradation times where more active sites are available for the oxidation reactions at the surface of the $CoFe_2O_4$ nanocatalyst. (Costa et al., 2006) reported superior catalytic activity of Co-incorporated magnetite over Ni-incorporated magnetite towards the degradation of methylene blue (MB) and chlorobenzene (CB) due to the surface-initiated reactions involved with Co^{2+} at the octahedral site on the surface of the magnetite catalyst that generates more •OH in Fenton-like reactions due to the stability of the two redox pairs (Costa et al., 2006). Authors showed that in the presence of Co within the magnetite structure, •OH generation in Fenton-like reaction increased, and that increases the MB and CB degradation, however, in presence of Ni within the magnetite structure, •OH generation was inhibited and, hence, that reduced MB and chlorobenzene degradation, in agreement with our findings. They suggested that Ni^{2+} species that replaces Fe^{2+} at the octahedral site are unstable and could not initiate the reactions as in **Equation 1**. Whereas the cobalt redox pair (Co^{2+}/Co^{3+}) is more stable and can produce radicals according to the following reaction:

$$Co^{2+} + H_2O_2 \rightarrow Co^{3+} + HO\bullet + \mathrm{HO}^-$$

Moreover, the reduction of Co^{3+} is thermodynamically favorable as per the following standard reduction potentials:

$$Fe^{3+} + 1e^- \rightarrow Fe^{2+}, \qquad E^0 = 0.77V$$

$$Co^{3+} + 1e^- \rightarrow Co^{2+}, \qquad E^0 = 1.81V$$

$$Fe^{2+} + Co^{3+} \rightarrow Fe^{3+} + Co^{2+}, \qquad E^0 = 1.04V$$

Therefore, electron transfer reactions occurring at the catalyst surface may also contribute to the enhanced catalytic efficiency of $CoFe_2O_4$ in degrading 4-CP and 2-CP. Nair & Kurian reported an improvement in the catalytic activity of Co substituted $ZnFe_2O_4$, and unsubstituted $CoFe_2O_4$ for the degradation of 2,4-dichlorophenol (2,4-DCP) and 2,4-dichlorophenoxy acetic acid (2,4-DCPAA) (Nair & Kurian, 2017b). They studied the effect of changing the composition of the spinel ferrite $Co_xZn_{1-x}Fe_2O_4$ (x = 0.0, 0.25, 0.5, 0.75, 1.0), and reported the most efficient catalyst composite which was found when x=1, that is $CoFe_2O_4$; the catalytic activity of zinc ferrite NPs increases when increasing the amount of cobalt substitution, and the unsubstituted $CoFe_2O_4$ catalyst degrades 2,4-DCP and 2,4-DCPAA completely within 90 minutes, whereas with $ZnFe_2O_4$ catalyst, the degradation efficiency was much less, 54.48% and 84.27% achieved for 2,4-DCP and 2,4-DCPAA, respectively, within 120 minutes. The reasons behind the high catalytic activity observed when Zn in $ZnFe_2O_4$ is substituted by Co are the same as what was mentioned in (Costa et al., 2006) study.

4.2.4 Catalytic Degradation under Various Experimental Conditions

This investigation focuses mainly on examining the influence of NP catalyst dosage and pH on the performance of catalytic degradation. In addition, the effects of H_2O_2 concentration, CP initial concentration, and reaction temperature on the catalytic degradation of CPs using MNPs (i.e. PMNPs and MFe_2O_4) was explored.

4.2.4.1 Effect of Nanocatalyst Dosage

Catalytic oxidation experiments were carried out to investigate the effect of nanocatalyst dosage on the efficiency of CP degradation. As expected, decreasing the dosage of the catalysts to 5 mg/mL increased the time required to reach 100% degradation for 50 ppm 4-CP and 2-CP in the presence 1% H_2O_2. Decreasing the catalyst dosage further to 2 mg/mL resulted in even longer times to fully degrade 4-CP and 2-CP (**Figure 21** and **Figure 22**). The same trend was observed for the metal-doped MFe_2O_4 samples as illustrated in **Figure 23** and **Figure 24**. The fastest rate of degradation was observed when the amount of catalyst used was 10 mg/mL (1% H_2O_2, neutral pH, 50 ppm pollutant concentration). For 2 mg/mL nanocatalyst dosage the rate of reaction decreased and, hence, the degradation rates were found to be slower for all catalysts at this amount. This reduction in degradation efficiency at lower catalyst dosages is likely due to the limited number of active sites available on the catalyst surface. When fewer active sites are present, the interaction between the catalyst and hydrogen peroxide becomes less effective, leading to a decreased production of reactive oxygen species, particularly •OH radicals, which play a key role in the oxidative breakdown of chlorophenols. Consequently, fewer pollutant molecules undergo successful oxidation and degradation. Similar findings have been reported in previous studies, where lower catalyst amounts corresponded to decreased degradation rates, due to both limited production of reactive species and a reduced surface area for pollutant adsorption and subsequent reactions (Han et al., 2018; A. R. Tehrani-Bagha, Gharagozlou, & Emami, 2016).

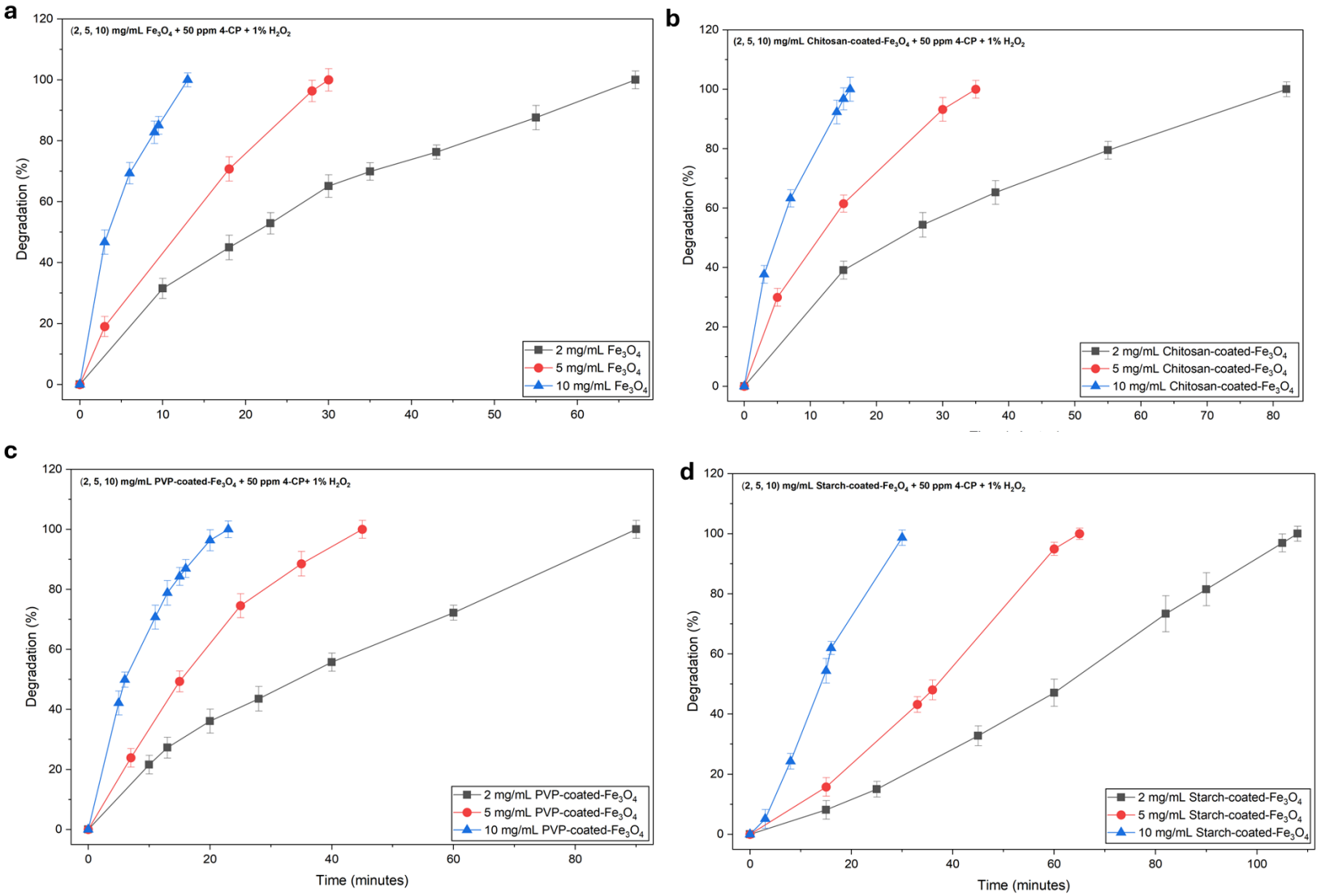


Figure 21. Nanocatalyst dosage effect (2, 5, and 10 mg/mL) on 50 ppm 4-CP degradation in 1% H_2O_2 for a) Fe_3O_4 NPs, b) Chitosan-coated MNPs, c) PVP-coated MNPs, and d) Starch-coated MNPs.

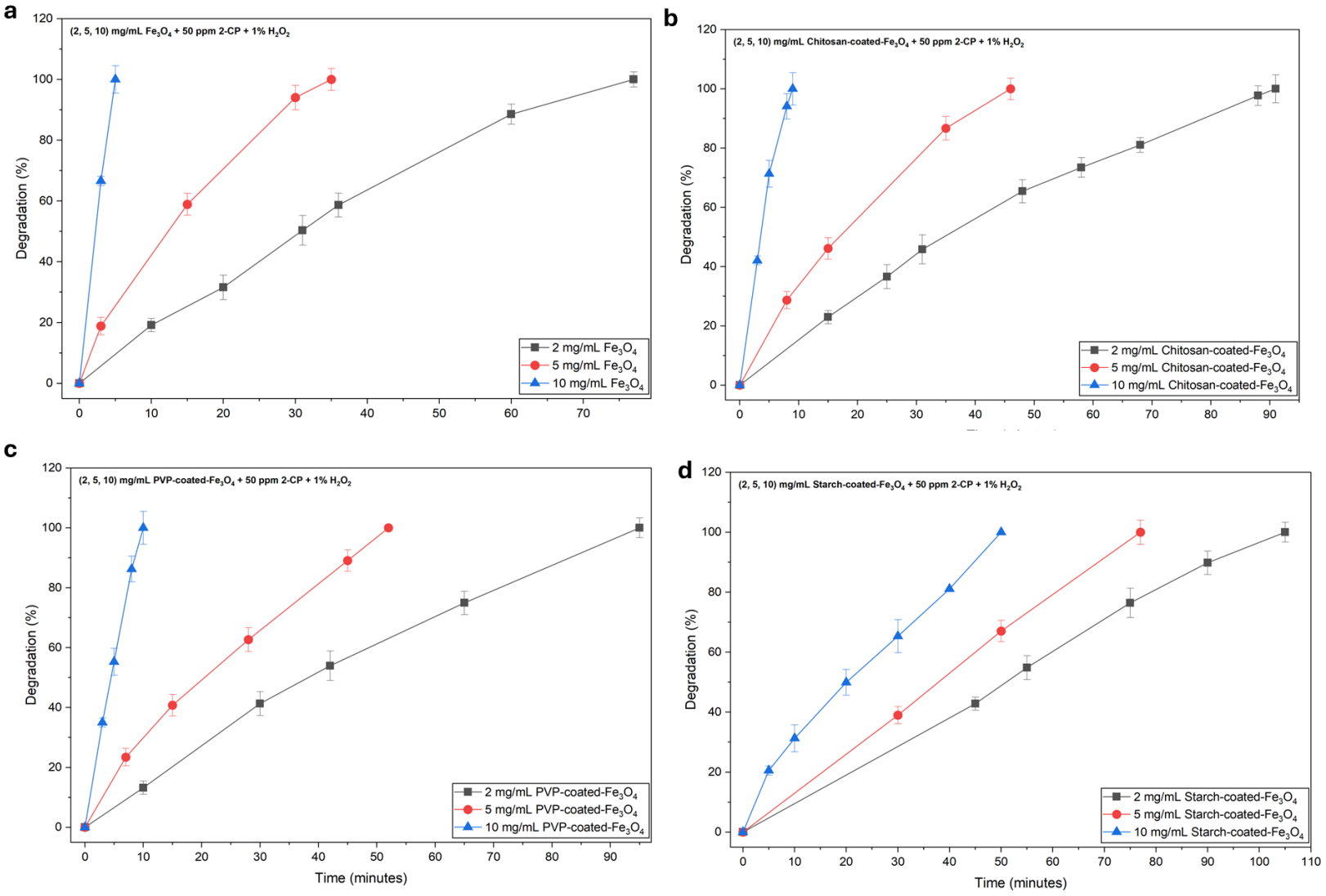


Figure 22. Nanocatalyst dosage effect (2, 5, and 10 mg/mL) on 50 ppm 2-CP degradation in 1% H_2O_2 for a) Fe_3O_4 NPs, b) Chitosan-coated MNPs, c) PVP-coated MNPs, and d) Starch-coated MNPs.

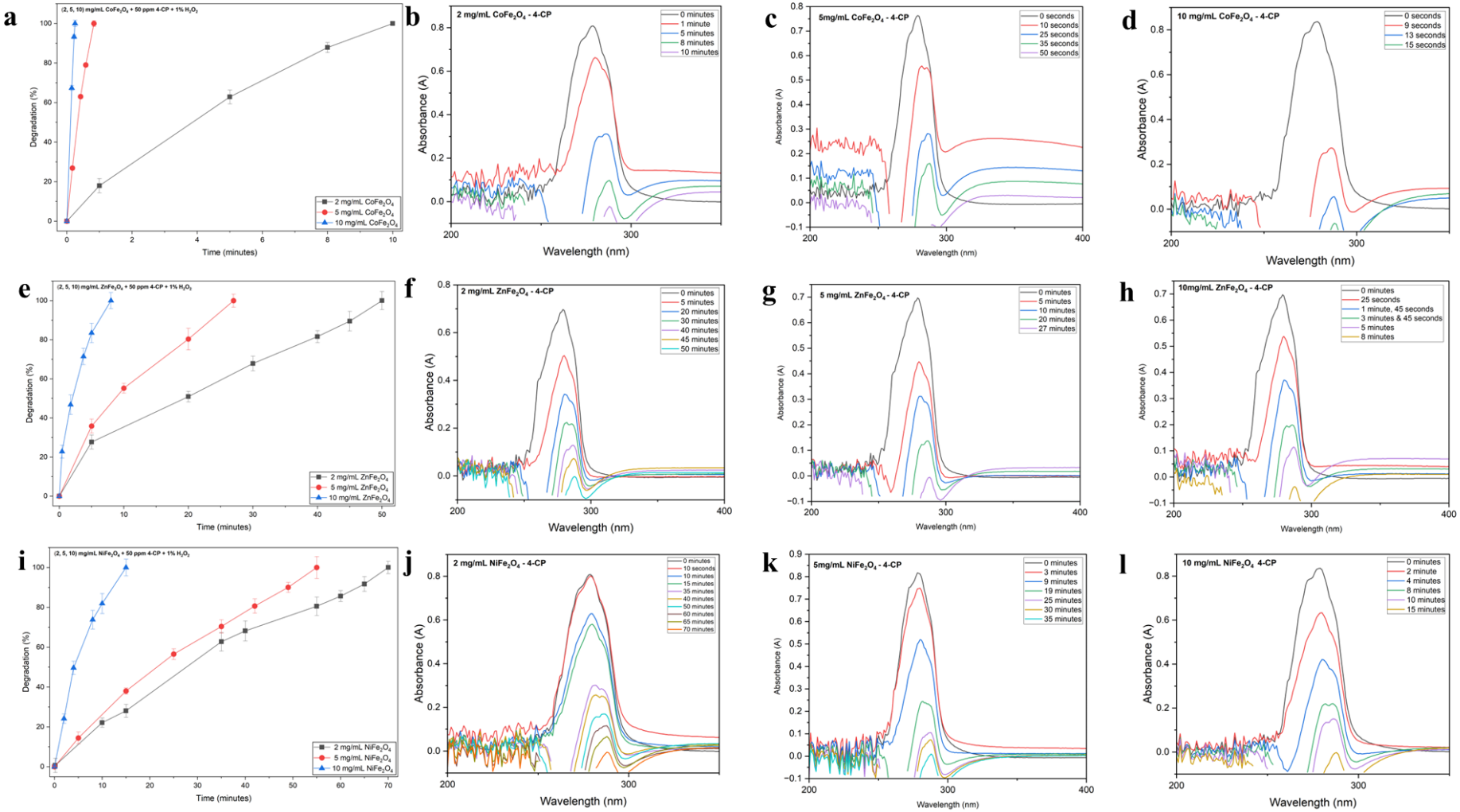


Figure 23. Nanocatalyst dosage effect (2, 5, and 10 mg/mL) on 50 ppm 4-CP degradation in 1% H_2O_2 and their UV-vis absorption spectra for (a-d) $CoFe_2O_4$, (e-h) $ZnFe_2O_4$, and (i-l) $NiFe_2O_4$.

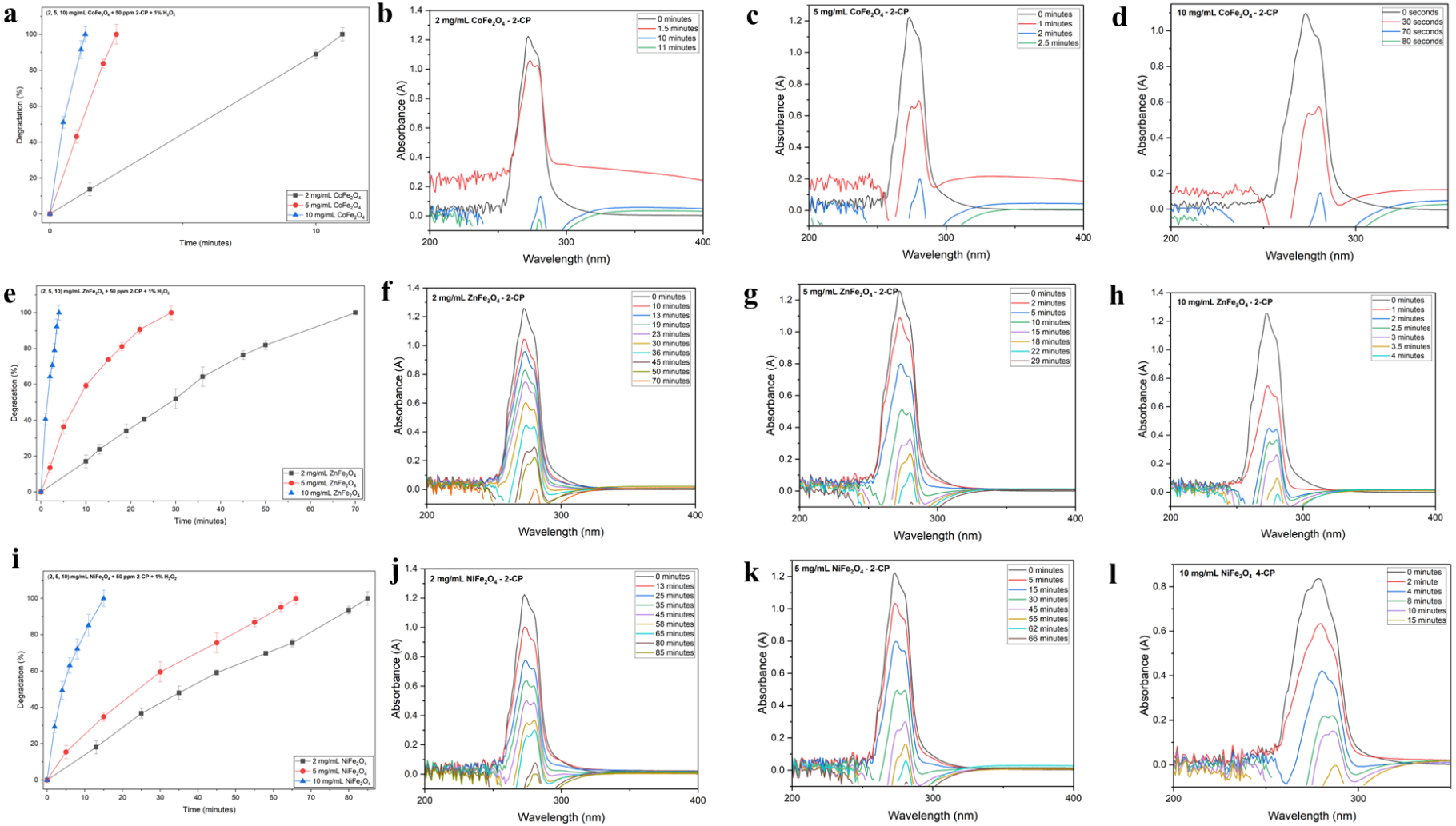


Figure 24. Nanocatalyst dosage effect (2, 5, and 10 mg/mL) on 50 ppm 2-CP degradation in 1% H_2O_2 and their UV-vis absorption spectra for (a-d) $CoFe_2O_4$, (e-h) $ZnFe_2O_4$, and (i-l) $NiFe_2O_4$.

4.2.4.2 Effect of pH

To study the effect of pH on the catalytic oxidation of MNPs (i.e. PMNPs and MFe_2O_4), 4-CP was selected as the model pollutant tested against three different pH conditions (acidic, neutral, and basic at pH = 3.2, 7.0, and 9.9, respectively).

a. Bare Fe_3O_4 NPs

The removal of 4-CP using catalytic degradation was reported to have a higher rate at acidic pH, and a lower rate at neutral and alkaline conditions (Cheng et al., 2015; Lei et al., 2021) . It can be clearly seen from **Figure 25** that pH has a significant influence on the catalytic degradation of 4-CP when the reaction is catalyzed by Fe_3O_4 NPs. Experiments were carried out at different pH values of 3.2, 7.0, and 9.9, and the results well-aligned with those previously reported in the literature. Acidic pH was found to enhance the catalytic degradation of 50 ppm 4-CP, where the time required to reach 100% degradation drops from 13 minutes at pH 7.0 to 9 minutes at pH 3.2, with 30% reduction in time, whereas at basic pH, the time required to reach 100% degradation of 50 ppm 4-CP was found to increase from 13 minutes at pH 7.0, to 56 minutes at pH 9.9. The increased Fe_3O_4 catalytic efficiency towards the degradation of 4-CP at acidic pH can be attributed to the abundance of •OH at acidic pH, which are the key reactive species in Fenton-like reactions. •OH formation can be increased at acidic pH due to the higher solubility and availability of Fe^{2+} ions in the solution, hence facilitating **Equation 1** and producing abundant number of •OH ready to oxidize 4-CP. Whereas at basic pH and with a reaction medium abundant with OH^- ions, Fe^{2+} and Fe^{3+} readily precipitates as $Fe(OH)_2$ or $Fe(OH)_3$, thus, reducing the availability of dissolved Fe^{2+} or Fe^{3+} ions that can participate in Fenton-like reactions (Jung, Lim, Park, & Kim, 2009). Furthermore, H_2O_2 is more stable at acidic conditions than at basic conditions, where H_2O_2 will decompose rapidly at basic pH to H_2O and O_2, a reaction that is catalyzed by the basic OH^- ions, hence, reducing H_2O_2 availability for Fenton-like reactions, which reduces

the Fe_3O_4 catalytic efficiency at basic pH (Cheng et al., 2015; Duan et al., 2020; Kadıoğlu, Atalay Eroğlu, Öztürk, Akbal, & Kuleyin, 2025; L. Xu & Wang, 2012).

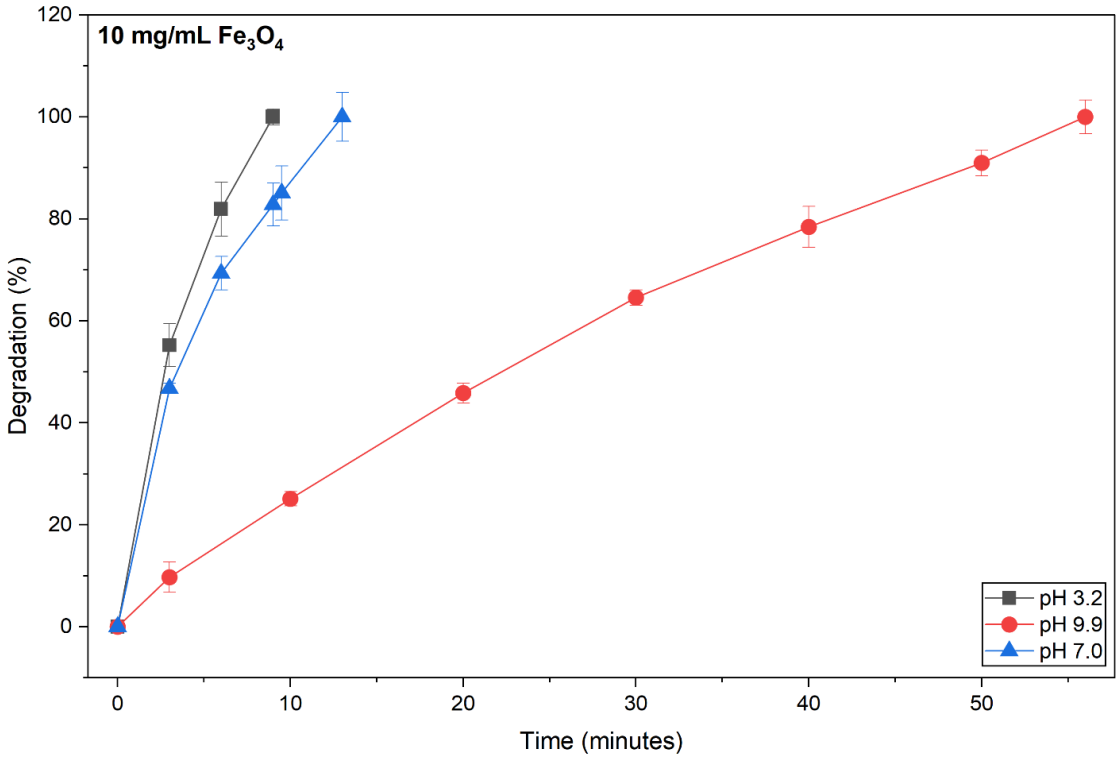


Figure 25. Effect of pH on the degradation of 4-CP using the as-synthesized Fe_3O_4 NPs (10 mg/mL Fe_3O_4 catalyst + 1% H_2O_2 at room temperature).

b. Polymer-coated MNPs

Interestingly, the results of investigating pH influence on the catalytic degradation of 4-CP using PMNPs were unexpected. As discussed earlier, Fenton-like reactions are enhanced at acidic pH and suppressed at basic pH, however, using the as-prepared polymer-coated catalysts, we observed altered results. For instance, for Chitosan-coated and PVP-coated MNPs, the catalytic degradation of 4-CP was enhanced at basic pH of 9.9, and reduced at acidic pH of 3.2. The time required to reach 100% degradation of 4-CP at basic pH of 9.9 in comparison to what was achieved at pH 7.0 reduced by 43.75% when catalyzed by 10 mg/mL Chitosan-coated MNPs (**Figure 26a**), and 56.52% when catalyzed by 10 mg/mL PVP-coated MNPs (**Figure 26b**). For Starch-coated MNPs, the catalytic efficiency under basic conditions remains higher than under acidic conditions

and is comparable to what was achieved at pH 7.0 (**Figure 26c**). This observed enhanced catalytic degradation at basic pH can be ascribed to the surface hydroxyl groups present in the polymers that are deprotonated at basic pH to $-O^-$, thus increasing the availability of reactive sites and generating more •OH when reacting with H_2O_2. Moreover, polymers on the surface of the catalysts may react differently at basic pH where they can form complexes with iron species and change their redox potential by ligand-field effects which increase their solubility and reactivity, hence, promoting their reaction with H_2O_2 and generating more reactive •OH species. Similar results were reported in literature where humic acid modified Fenton reagent was used to degrade organic compounds (phenols, PAHs, BTEX) effectively in the range of pH 5-7, where the rate of degradation increased when the pH increased (Georgi et al., 2007). (Ying Zhang & Zhou, 2019)reviewed the potential of polymers and other chelating agents in enhancing Fenton and Fenton-like reactions at high pH values. Moreover, in an elegant study Ma et al. synthesized a highly efficient and reactive catalyst, Fe-g-C_3N_4/GMC used in Fenton-like reactions at a wide pH range of 4-10 towards the degradation of organic pollutants (RhB, 4-CP, 2,4,6-TCP, BPA, and TCH) ((Ma, Yang, Wen, & Liu, 2017). They found that the chelating agent, g-C_3N_4/GMC, complexed with iron species, reduced the precipitation rate of iron species at higher pH values, and solubilized them in solution. In addition, the chelating agent (i.e. polymer) enhanced the electron transfer between the redox pair Fe^{3+}/Fe^{2+}, which increases the redox potential and hence improved the overall efficiency of the catalyst towards degrading organic pollutants.

c. Metal-doped MFe_2O_4 NPs

As illustrated in **Figure 27**, the catalytic efficiency of the as-synthesized metal-doped ferrites (i.e. $CoFe_2O_4$, $ZnFe_2O_4$, and $NiFe_2O_4$) was enhanced at acidic pH of 3.2, and reduced at basic pH of 9.9. This is expected and is in accordance with bare Fe_3O_4 NPs degradation results. For instance, a reduction of 55%, 25%, and 60% in the time required for complete degradation of 4-CP was observed when using $CoFe_2O_4$, $ZnFe_2O_4$, and $NiFe_2O_4$ at pH 3.2 as illustrated in **Figure 27a**, **Figure 27b**, and **Figure**

27c, respectively, in comparison to the values obtained at pH 7.0 (Note: $CoFe_2O_4$ was studied at dosage of 2 mg/mL instead of 10 mg/mL to observe the reduction in time since the 10 mg/mL $CoFe_2O_4$ dosage at neutral pH was catalyzing complete degradation of 4-CP within 15 seconds only). Whereas at pH 9.9, the time required for degradation was much longer and did not reach complete degradation of 4-CP with 2 mg/mL $CoFe_2O_4$ and 10 mg/mL $NiFe_2O_4$ catalyst, even after 40 minutes reaction. Nevertheless, complete degradation of 4-CP was achieved with 10 mg/mL $ZnFe_2O_4$ at basic pH of 9.9, however with an increment of 62.5% in the time required, compared to what was achieved at pH 7.0. The catalytic enhancement observed for MFe_2O_4 at acidic pH can be also attributed to the same factors mentioned earlier influencing the as-synthesized Fe_3O_4 at acidic pH. Mainly, the acidic pH increases the solubility of metal ions (Co^{2+}, Zn^{2+}, Ni^{2+}, Fe^{2+}, Fe^{3+}), hence facilitating production of an abundant number of •OH ready to oxidize 4-CP. Whereas at basic pH, H_2O_2 readily decompose to H_2O and O_2, thus reducing •OH generation and decreasing the catalytic efficiency of MFe_2O_4 at higher pH values. In addition, metal ions could precipitate as metal hydroxides at basic pH which reduces the availability of metal ions that can participate in Fenton-like reactions. As a result, •OH generation will be less, and hence the degradation rate of 4-CP will be less at higher pH values.

Most of the research reported enhanced catalytic efficiency for spinel ferrites at acidic pH. (Han et al., 2018) synthesized $MgFe_2O_4$ and reported higher RhB degradation rates at acidic pH due to enhanced reactivity of the catalyst to produce •OH at acidic conditions, while at basic conditions, RhB degradation decreased due to the decomposition of H_2O_2. Similarly, (Roshanfekr Rad, Farshi Ghazani, Irani, Sadegh Sayyafan, & Haririan, 2015) synthesized $CoFe_2O_4$ and investigated their catalytic efficiency towards the degradation of phenol at pH range of 2-5, and found the highest degradation rate at pH 3. (Hamdan, Haija, Banat, & Eskhan, 2017) found that acidic condition is the optimum condition to achieve high and efficient degradation rate of phenol when using $CuFe_2O_4$ catalyst.

4.2.4.3 Effect of H_2O_2 Concentration

The degradation of 4-CP with 2 mg/mL $CoFe_2O_4$ at pH 7.0 with two H_2O_2 concentrations were investigated as shown in **Figure 28**. When H_2O_2 initial concentration increased from 1% to 2%, the degradation rate increased significantly and the time required for complete degradation decreased from 10 minutes in 1% H_2O_2 to 4 minutes in 2% H_2O_2, with 60% reduction in degradation time. Our finding agreed with the reported results in literature where a reduction in time was observed when increasing the initial H_2O_2 concentration. The increased catalytic activity at higher H_2O_2 concentration is due to the H_2O_2 dosage effect on Fenton-like reaction, where more •OH would be generated in a solution enriched with H_2O_2 molecules ready for the reaction. Our observed results are in agreement with previously published research. For instance, (Han et al., 2018) catalyzed the degradation of RhB by $MgFe_2O_4$, and reported higher degradation rates when H_2O_2 initial concentration increased from 0.5 to 1%. (A. R. Tehrani-Bagha et al., 2016) studied the effect of H_2O_2 concentration on the catalytic degradation of RR120, and found the degradation rate increased when increasing H_2O_2 concentration from 5 to 20 mM. (L. Xu & Wang, 2012) investigated the degradation rate of 2,4-DCP over Fe_3O_4 under different H_2O_2 concentrations and found the rate is increasing when H_2O_2 concentration increased from 0.6 to 12 mM.

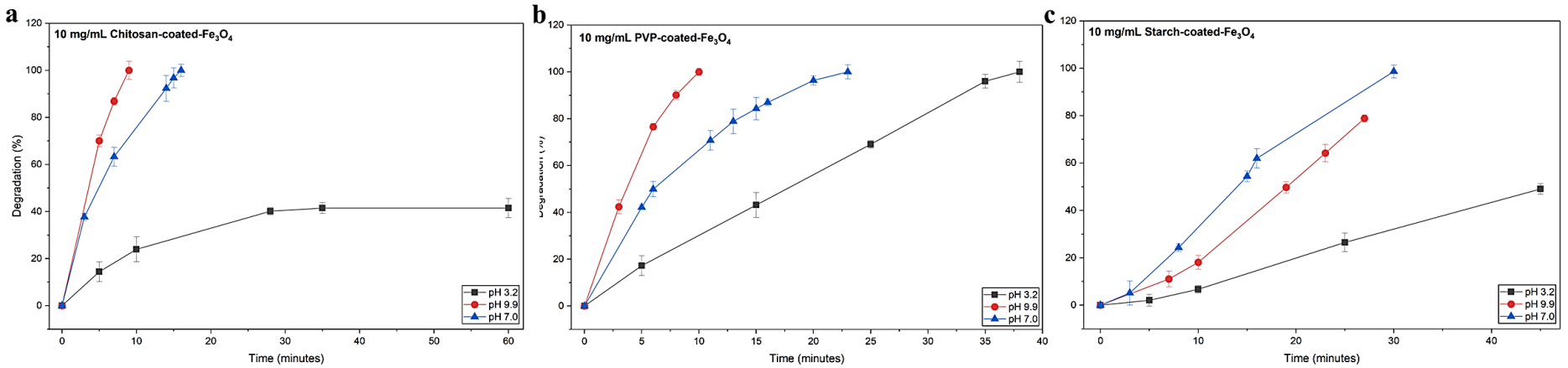


Figure 26. Effect of pH on the degradation of 50 ppm 4-CP using 10 mg/mL catalyst, 1% H_2O_2, room temperature of as-prepared a) Chitosan-coated MNPs, b) PVP-coated MNPs, and c) Starch-coated MNPs.

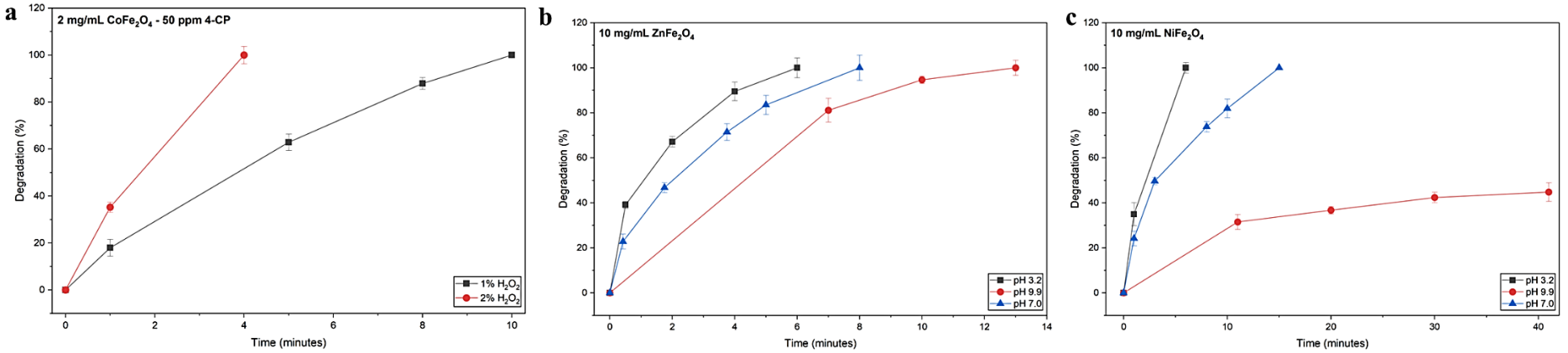


Figure 27. Effect of initial pH on the degradation of 50 ppm 4-CP using 1% H_2O_2 at room temperature of as-prepared a) $CoFe_2O_4$ NPs (2 mg/mL), b) $ZnFe_2O_4$ NPs (10 mg/mL), and c) $NiFe_2O_4$ NPs (10 mg/mL).

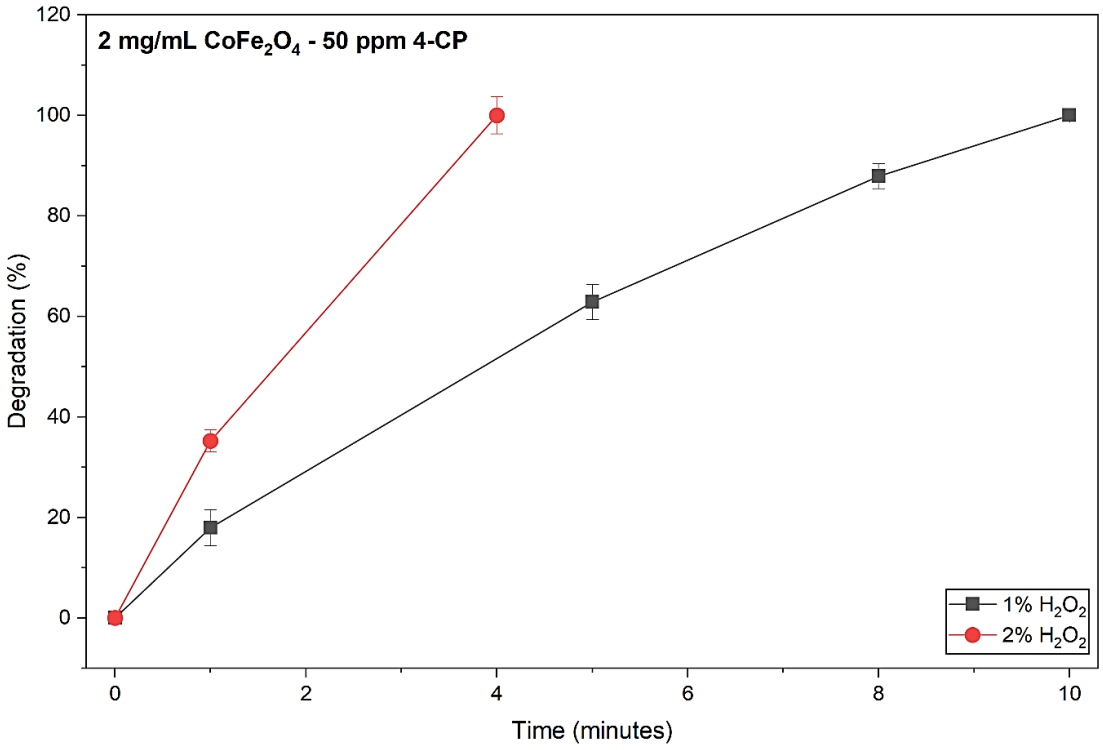


Figure 28. Effect of H_2O_2 concentration on the degradation of 50 ppm 4-CP using $CoFe_2O_4$ nanocatalysts (2 mg/mL).

4.2.4.4 Effect of Chlorophenol Concentration

The effect of CP initial concentration was investigated using 2 mg/mL $CoFe_2O_4$. The reaction conditions were kept at room temperature, pH 7.0 and in the presence of 1% H_2O_2. As shown in **Figure 29**, the time required for complete degradation of 4-CP using 2 mg/mL $CoFe_2O_4$ decreased from 10 minutes to 1.5 minutes when the concentration of 4-CP was reduced from 50 ppm to 10 ppm, respectively. The lower degradation efficiency of 4-CP at higher 4-CP initial concentration can be attributed to the increased availability of 4-CP molecules in the solution at higher 4-CP initial concentration. As the 4-CP initial concentration rises, more 4-CP molecules get adsorbed onto the surface of the $CoFe_2O_4$ catalyst, occupying a larger number of active sites which cause surface saturation. This surface saturation limits the

availability of these active sites for H_2O_2 activation and subsequent •OH radical generation, leading to less reactive radicals formed that can degrade the pollutant 4-CP.

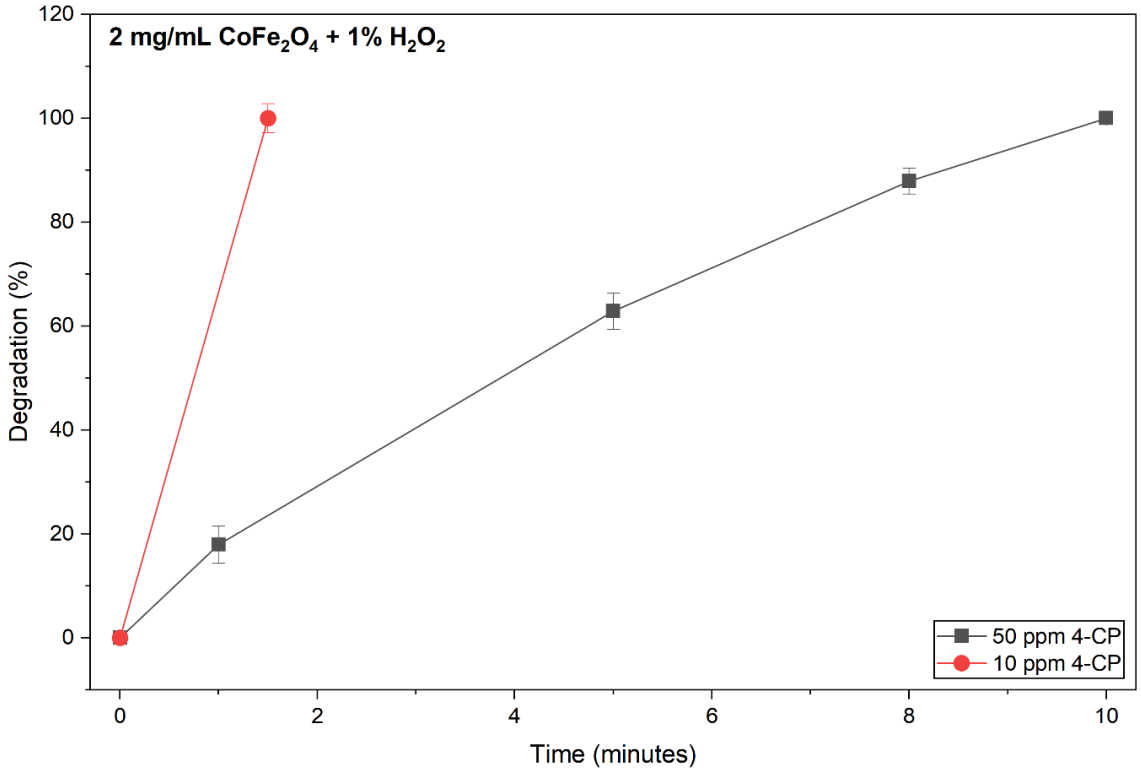


Figure 29. Effect of chlorophenol's concentrations on catalytic degradation at room temperature, 1% H_2O_2 for $CoFe_2O_4$ (2 mg/mL) + 50 & 10 ppm 4-CP.

4.2.4.5 Effect of Temperature

As shown in **Figure 30** the rate of 4-CP degradation increased with increasing temperature. The time required to achieve complete degradation (100%) decreased from 10 minutes at 22 °C to 2 minutes at 35 °C. The enhanced degradation efficiency can be attributed to both kinetic and thermodynamic factors. Thermodynamically, increasing the temperature accelerates of •OH generation at the catalyst's surface-active sites. This trend aligns with the Arrhenius equation, which predicts an

exponential rise in reaction rates with temperature as a larger fraction of molecules attain the activation energy necessary for reaction. In this system, the elevated temperature enhances the decomposition rate of H_2O_2 into highly reactive •OH radicals, thereby increasing their availability for oxidative degradation of 4-CP (Munoz et al., 2014). Furthermore, the increased thermal energy at higher temperatures leads to more collisions between the pollutant molecules, 4-CP, and the reactive radicals, thus increasing the rate of degradation. The overall degradation reaction is thus endothermic in nature, where thermal input favors the reaction progression, enhancing the oxidative degradation efficiency of the $CoFe_2O_4/H_2O_2$ system (A. R. Tehrani-Bagha et al., 2016).

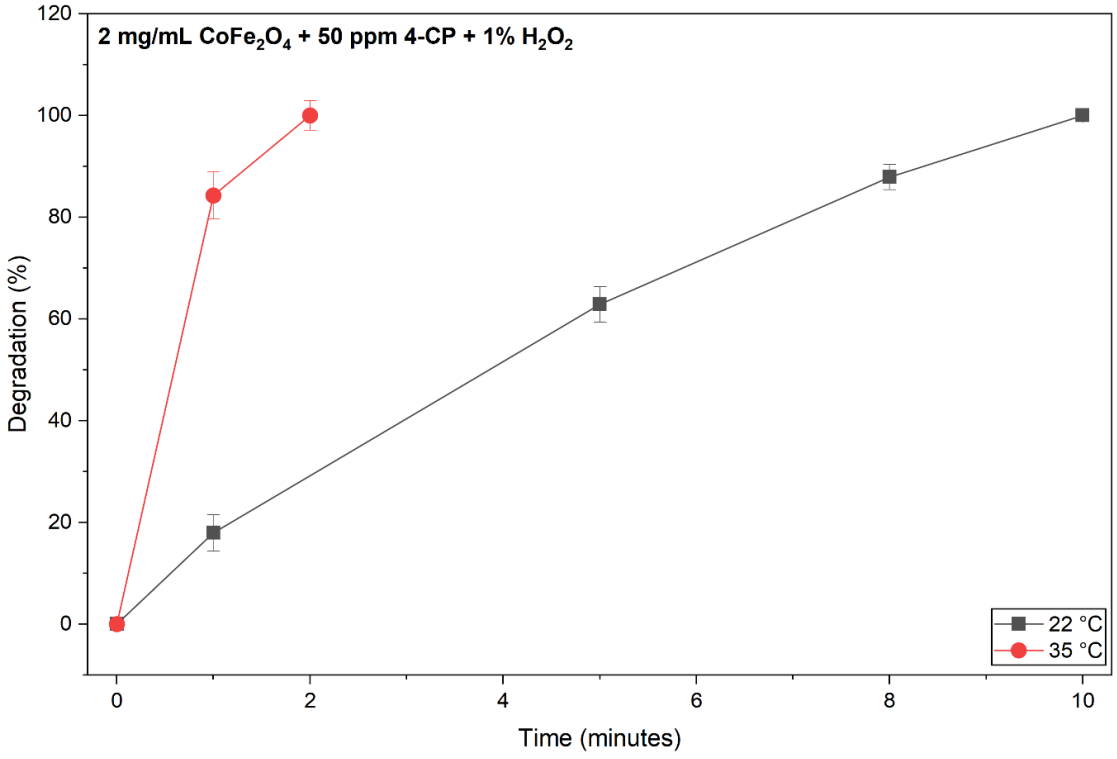


Figure 30. Effect of temperature on 50 ppm 4-CP degradation using $CoFe_2O_4$ NPs (2 mg/mL) at two different temperatures of 22℃ and 35℃.

4.2.5 Dechlorination and TOC Removal

Since CPs consist of chlorinated aromatic rings, their degradation mechanism involves breaking the covalent bonds between the chlorine atoms and the carbon atoms in the benzene ring through hydroxyl radicals generated in the Fenton-like reaction. This will release the chlorine atoms in reaction medium in the form of the dissolved chloride ions, causing an increase in chloride concentration over time (J. Xu et al., 2013; Zhu, Yi, & Zhang, 2011). In addition, while the hydroxyl radicals are effectively degrading 4-CP into smaller intermediate organic by-product, the total organic compounds (TOC) will be high at the beginning, however, over time, further oxidation and degradation of these organic molecules will result in the reduction of TOC. Eventually, when complete degradation of organic molecules is achieved, all organic carbon will be converted to inorganic carbon, CO_2, thus TOC will be minimal, or will reach zero (Rodrigues, Madeira, & Boaventura, 2013). Thus, to better understand the mechanistic degradation, the chloride and TOC concentrations were determined for 4-CP degradation using the most efficient catalyst $CoFe_2O_4$ with a dosage of 2 mg/mL. As illustrated in **Figure 31a**, complete degradation of 50 ppm 4-CP was achieved within 10 minutes, and the chloride concentration increased from 0.105 to 1.377 ppm within 10 minutes (**Figure 31b)**. In addition, within 10 minutes, the TOC concentration dropped from 53 ppm to zero, hence, a complete TOC reduction was reached within 10 minutes (**Figure 31c)**, which is an evidence of the highly efficient as-prepared nanocatalyst.

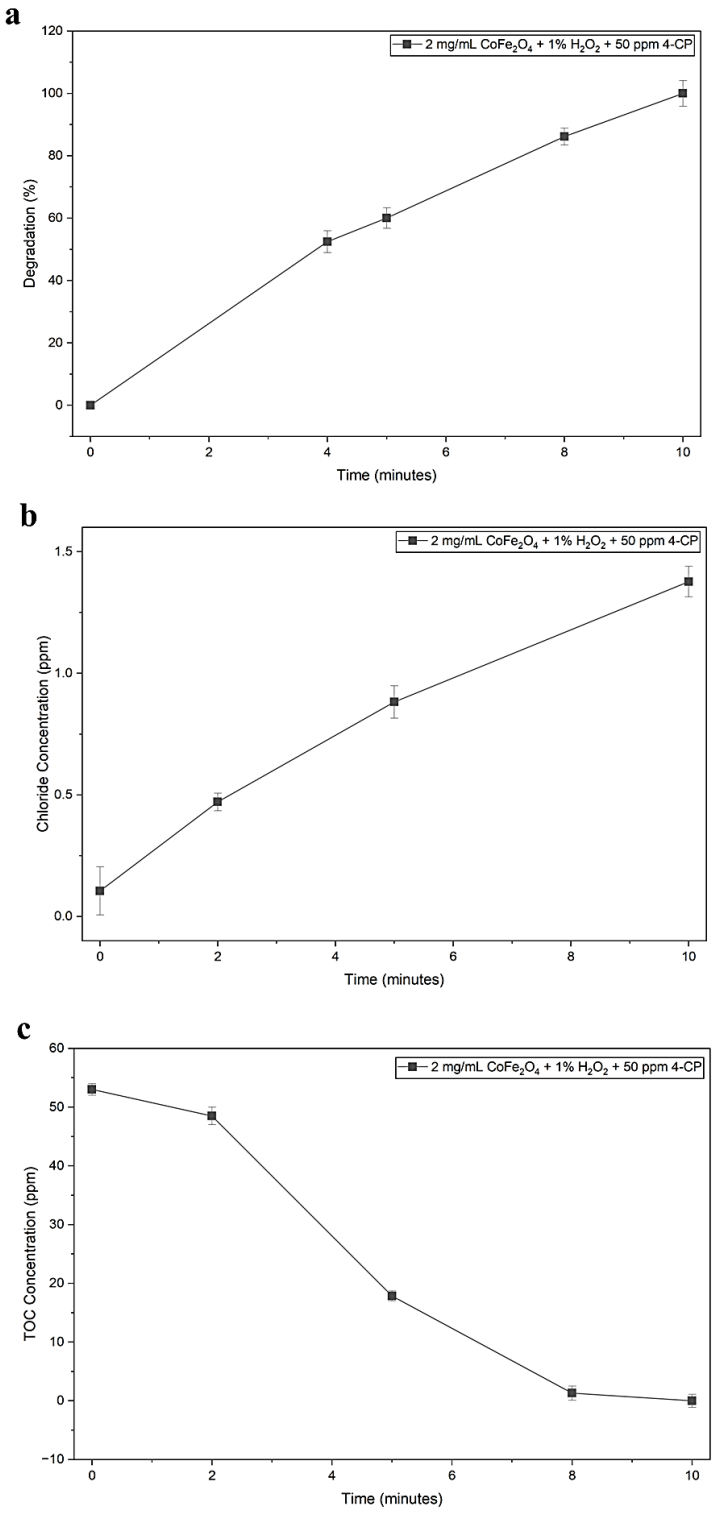


Figure 31. Complete degradation of 50 ppm 4-CP in 1% H_2O_2 and 2 mg/mL $CoFe_2O_4$ nanocatalyst, a) time-based degradation, b) chloride concentration increase over time, and c) TOC reduction over time.

4.2.6 Reusability and Recycling

To evaluate the possibility of reusing the as-prepared nanocatalysts in Fenton-like reactions into chlorophenols degradation, recycling experiments were carried out for different as-prepared nanocatalysts without the use of any desorption agents. As illustrated in **Figure 32a**, even after six cycles, the % degradation of 50 ppm 4-CP remains consistent achieving 100% degradation using $CoFe_2O_4$ NPs (10 mg/mL), demonstrating the superior stability and reusability of the as-prepared $CoFe_2O_4$ nanocatalysts. For bare Fe_3O_4 NPs, the degradation efficiency dropped to 94.90% in the 2nd cycle and to 76.79% in the 6th cycle but still exhibited a good regeneration potential (**Figure 32b**). Finally, PVP-coated MNPs also showed excellent recycling potential, where the % degradation dropped to only 92.86% in the 4th and to 91.10% in the 6th (**Figure 32c**). The slight decrease in degradation efficiency with increasing cycle numbers can be attributed to the deterioration of the nanocatalysts' active sites as reactions continue on the catalyst surface. This is typical as previous studies have also reported a decline in catalytic activity with more cycles, caused by a reduction in available active sites and a decrease in the catalyst's surface area (Nair & Kurian, 2017b; L. Xu & Wang, 2012).

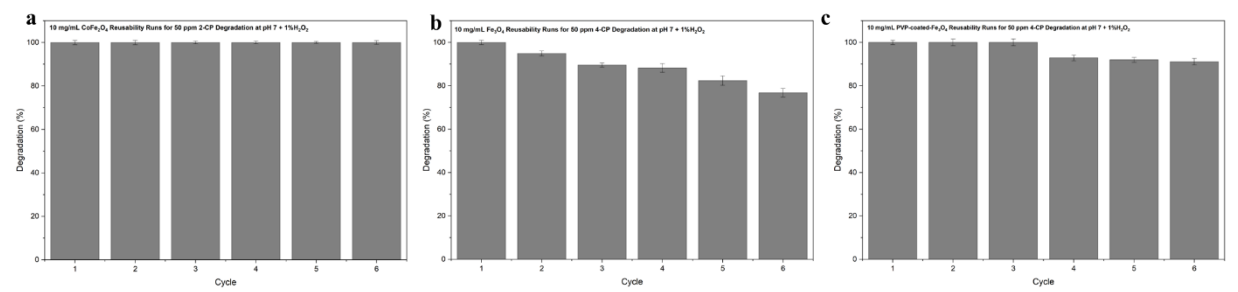


Figure 32. Reusability of the different nanocatalysts at room temperature, in 1% H2O2, and pH 7.0 for a) CoFe2O4 NPs, b) Bare Fe3O4 NPs, and c) PVP-coated MNPs.

4.3 Catalytic Degradation of Chlorophenols under AMF

The degradation efficiency of the two chlorophenols (i.e. 4-CP and 2-CP) using bare Fe_3O_4, PMNPs, and doped MFe_2O_4 under AMF excitation were investigated. The main objective of the study is to assess the influence of AMF on the catalytic degradation of chlorophenols *via* the heat dissipated from MNPs. To our knowledge, this feature has not been previously investigated, making this the first report in the literature.

All utilized MNPs, except starch-coated MNPs, showed enhanced catalytic efficiencies under magnetic excitation relative to their corresponding controls. Notably, PVP-coated MNPs exhibited the highest degradation efficiency, achieving 51.88% and 69.84% degradation for 2-CP and 4-CP, respectively, after 10 minutes compared to only 4.01% and 8.08% without AMF (**Figure 33a-b**). This is even higher than the degradation experiments done at normal shaking conditions in the absence of AMF (i.e. 30% and 26% for 2-CP and 4-CP, respectively). This performance exceeded that of bare Fe_3O_4 NPs and Chitosan-coated MNPs, indicating the significant role of surface functionalization in enhancing thermal catalytic activities. This superior performance of PVP-coated MNPs may be attributed to enhanced colloidal stability and better heat transfer efficiency within the solution. PVP likely improves particle dispersion, resulting in a more homogenous temperature distribution for pollutant interaction during thermal activation. On contrary, starch-coated MNPs showed negligible degradation under AMF for both 2-CP and 4-CP as illustrated in **Figure 33a-b**. This suggests a potential insulation effect of the starch layer or reduced magnetic heating efficiency, leading to ineffective thermal activation.

The same conditions were applied to study the thermal responses for the metal-doped MFe_2O_4 NPs. $CoFe_2O_4$ demonstrated superior performance, achieving complete degradation of both 2-CP and 4-CP as illustrated in **Figure 33c-d**. This indicates exceptional thermal catalytic efficiency and strong magnetic heating capabilities. The effectiveness of $CoFe_2O_4$ in degrading both chlorophenols suggests a highly efficient

thermal activation mechanism driven by its high magnetic saturation and coercivity, which enhanced heat generation under AMF. In contrast, $NiFe_2O_4$ NPs showed lower degradation efficiencies, with 79% for 2-CP and 62% for 4-CP under identical conditions. These findings were much higher than what was observed without AMF as illustrated in **Figure 33c-d**. The lower performance of $NiFe_2O_4$ NPs may be attributed to its lower magnetic heating efficiencies, possibly stemming from lower coercivity and saturation magnetization compared to $CoFe_2O_4$ NPs. Additionally, differences in metal dopant may influence adsorption affinity and catalytic site availability as discussed earlier.

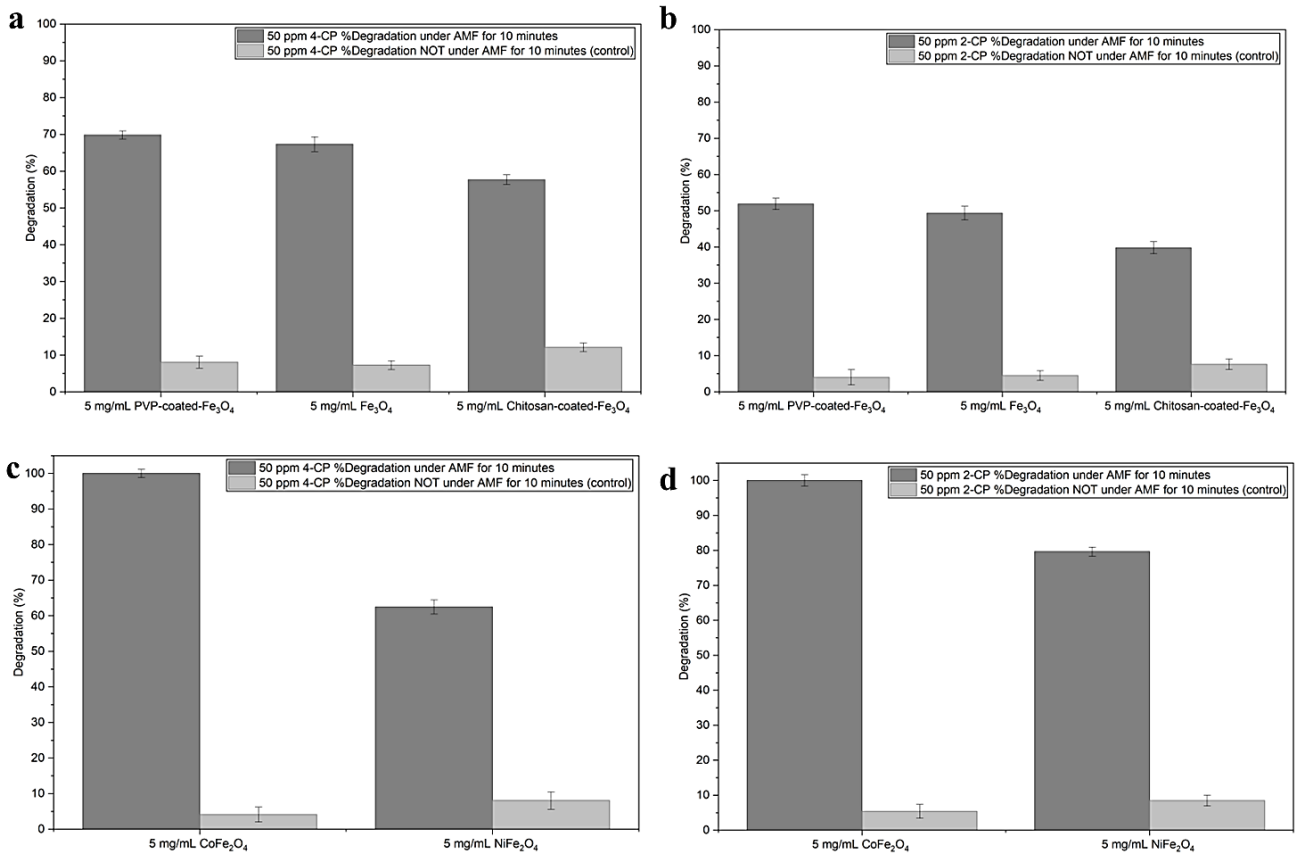


Figure 33. Catalytic degradation of 4-CP and 2-CP using (a-b) PMNPs and (c-d) MFe_2O_4 NPs under the influence of AMF.

Chapter 5. Conclusion and Future Work

5.1. Conclusion

In conclusion, the effective and rapid degradation of hazardous chlorophenol compounds, specifically 4-CP and 2-CP, was successfully achieved using various tailored MNPs, including polymer-coated (PVP, Chitosan, Starch) and metal-doped (Co^{2+}, Ni^{2+}, Zn^{2+}) ferrite nanocatalysts. The as-synthesized MNPs exhibited desirable physicochemical properties, including nanoscale sizes, well-crystallized cubic spinel structures, and strong superparamagnetic behavior, as confirmed through TEM, XRD, FTIR, and VSM analyses. The CPs degradation studies showed that both polymer-coated MNPs and bare-Fe_3O_4 were effective at eliminating CPs albeit at different efficiencies. Interestingly, among the tested catalysts, $CoFe_2O_4$ demonstrated the most outstanding performance, achieving complete degradation of both 4-CP and 2-CP in remarkably short times (15 and 80 seconds, respectively), followed by $ZnFe_2O_4$, which also showed excellent catalytic efficiency, being able to surpass the catalytic behavior of bare-Fe_3O_4, achieving complete degradation for the same within 8 and 4 minutes, respectively. In contrast, $NiFe_2O_4$ displayed the least catalytic efficiency primarily due to the occupancy of octahedral sites by Ni^{2+} ions, which disrupts the redox balance essential for efficient catalytic reaction, leading to slower hydroxyl radical generation and lower overall degradation efficiency. The enhanced catalytic behaviour of Co-doped MNPs is attributed to their spinel structure configuration, smaller particle sizes, and the stability of redox-active cation pairs in octahedral sites that significantly boosted hydroxyl radical generation, accelerating degradation.

Influential operational parameters such as pH, catalyst dosage, pollutant concentration, H_2O_2 levels, and temperature were investigated and found to significantly affect performance. For example, reducing the CPs initial concentration, increasing H_2O_2 concentration, increasing the catalyst dosage, and increasing the reactions' temperature were found to boost the degradation efficiency. While acidic pH enhanced

the catalytic performance of both metal-doped and bare MNPs, interestingly, the polymer-coated MNPs exhibited improved activity under basic conditions. Reusability assessments further confirmed the practical potential of these nanocatalysts, particularly $CoFe_2O_4$, which retained full degradation capacity over six cycles. However, PVP-coated Fe_3O_4 and bare Fe_3O_4 nanoparticles demonstrated good but slightly reduced reusability, maintaining 91.1% and 76.97% degradation efficiency, respectively, by the sixth cycle.

Importantly, the catalytic performance of utilized MNPs was notably improved under AMF, which is a novel thermal activation strategy not previously reported. All MNPs, except starch-coated MNPs, showed enhanced degradation of 4-CP and 2-CP under AMF. This improvement, surpassing conventional stirring and underscores the importance of polymer functionalization in boosting thermal responsiveness and catalytic efficiency.

Overall, the findings of this work highlight the promise of metal-doped and polymer-coated MNPs as highly efficient, reusable, and magnetically-responsive nanocatalysts for the rapid and sustainable treatment of CP-contaminated industrial wastewater. Their strong performance, operational versatility, and regenerative capability make them excellent candidates for scalable environmental remediation applications.

5.2. Future Work

Building upon the promising results demonstrated in this study, several potential directions for future research are proposed to further enhance the catalytic performance and practical applicability of MNPs-based nanocatalysts for CP degradation:

- Functionalization of the promising MFe_2O_4 ferrites with polymers (e.g. PVP and Chitosan). This approach could potentially combine the thermal and colloidal advantages of polymer coatings with the redox enhancing properties of metal dopants, thereby improving catalytic activities under both mechanical stirring and AMF conditions.
- While fixed amount of metal doping was explored in this work, the impact of varying dopant concentrations on catalytic activity remains underexplored. Future studies could systematically investigate how changes in dopant ratios influence the physicochemical properties and degradation efficiency. This would help identify optimal doping levels for maximum performance and stability.
- Future work may also extend this catalytic platform to other persistent organic pollutants, such as other monochlorinated or even multi-chlorinated phenols to validate the versatility of the developed MNPs.
- Scaling-up these experiments to simulate or treat actual industrial wastewater under complex matrices and varying conditions would help evaluate the robustness, selectivity, and environmental impact of the synthesized nanocatalysts in realistic scenarios.
- Better understanding of the underlying mechanisms for CP degradation using MNPs including kinetics, adsorption isotherms, and thermodynamic studies.
- Finally, deeper exploration into the AMF setup itself, including variation of field strength, frequency, exposure time, and NP concentration, could lead to a better understanding of magnetothermal-assisted catalysis and potentially unlock further enhancements in degradation efficiency.

References

Abu-Alsoud, G. F., & Bottaro, C. S. (2021). Porous thin-film molecularly imprinted polymer device for simultaneous determination of phenol, alkylphenol and chlorophenol compounds in water. *Talanta, 223*, 121727. doi:https://doi.org/10.1016/j.talanta.2020.121727

Aisida, S. O., Ahmad, I., & Ezema, F. I. (2020). Effect of calcination on the microstructural and magnetic properties of PVA, PVP and PEG assisted zinc ferrite nanoparticles. *Physica B: Condensed Matter, 579*, 411907. doi:https://doi.org/10.1016/j.physb.2019.411907

Al-Najar, B., Kamel, A. H., Albuflasa, H., & Hankins, N. P. (2023). Spinel ferrite nanoparticles as potential materials in chlorophenol removal from wastewater. *Environmental Science and Pollution Research, 30*(48), 104976-104997. doi:10.1007/s11356-023-29809-7

Al Maashani, M. S., Khalaf, K. A., Gismelseed, A. M., & Al-Omari, I. A. (2020). The structural and magnetic properties of the nano-CoFe2O4 ferrite prepared by sol-gel auto-combustion technique. *Journal of Alloys and Compounds, 817*, 152786. doi:https://doi.org/10.1016/j.jallcom.2019.152786

Aldaoud, A., Lemine, O. M., Ihzaz, N., El Mir, L., Alrub, S. A., & El-Boubbou, K. (2022). Magneto-thermal properties of Co-doped maghemite (γ-Fe2O3) nanoparticles for magnetic hyperthermia applications. *Physica B: Condensed Matter, 639*, 413993. doi:https://doi.org/10.1016/j.physb.2022.413993

Amiri, M., Eskandari, K., & Salavati-Niasari, M. (2019). Magnetically retrievable ferrite nanoparticles in the catalysis application. *Advances in Colloid and Interface Science, 271*, 101982. doi:https://doi.org/10.1016/j.cis.2019.07.003

Ariza-Tarazona, M. C., Villarreal-Chiu, J. F., Hernández-López, J. M., Rivera De la Rosa, J., Barbieri, V., Siligardi, C., & Cedillo-González, E. I. (2020). Microplastic pollution reduction by a carbon and nitrogen-doped TiO2: Effect of pH and temperature in the photocatalytic degradation process. *Journal of Hazardous Materials, 395*, 122632. doi:https://doi.org/10.1016/j.jhazmat.2020.122632

Attallah, A. H., Abdulwahid, F. S., Ali, Y. A., & Haider, A. J. (2024). Enhanced Characteristics of Iron Oxide Nanoparticles for Efficient Pollutant Degradation via Pulsed Laser Ablation in Liquid. *Plasmonics, 19*(5), 2581-2594. doi:10.1007/s11468-024-02192-w

Bakr, E. A., El-Nahass, M. N., Hamada, W. M., & Fayed, T. A. (2021). Facile synthesis of superparamagnetic Fe3O4@noble metal core–shell nanoparticles by thermal decomposition and hydrothermal methods: comparative study and catalytic applications. *RSC Advances, 11*(2), 781-797. doi:10.1039/D0RA08230A

Bhateria, R., & Singh, R. (2019). A review on nanotechnological application of magnetic iron oxides for heavy metal removal. *Journal of Water Process Engineering, 31*, 100845. doi:https://doi.org/10.1016/j.jwpe.2019.100845

Bhushan Das, S., Kumar Singh, R., Kumar, V., Kumar, N., & Kumar, S. (2021). Tailoring the structural, optical and multiferroic properties of low temperature synthesized cobalt ferrite nanomaterials, by citrate precursor method. *Materials Today: Proceedings, 46*, 6527-6533. doi:https://doi.org/10.1016/j.matpr.2021.04.001

Carbajo, J., Silveira, J. E., Pliego, G., Zazo, J. A., & Casas, J. A. (2021). Increasing Photo-Fenton process Efficiency: The effect of high temperatures. *Separation and Purification Technology, 271*, 118876. doi:https://doi.org/10.1016/j.seppur.2021.118876

Chaliha, S., Bhattacharyya, K. G., & Paul, P. (2008). Catalytic Destruction of 4-Chlorophenol in Water. *CLEAN – Soil, Air, Water, 36*(5-6), 488-497. doi:https://doi.org/10.1002/clen.200700180

Chaveanghong, S., Kobkeatthawin, T., Trakulmututa, J., Amornsakchai, T., Kajitvichyanukul, P., & Smith, S. M. (2023). Photocatalytic removal of 2-chlorophenol from water by using waste

eggshell-derived calcium ferrite. *RSC Advances, 13*(26), 17565-17574. doi:10.1039/D3RA01357J

Cheng, R., Li, G.-q., Cheng, C., Shi, L., Zheng, X., & Ma, Z. (2015). Catalytic oxidation of 4-chlorophenol with magnetic Fe3O4 nanoparticles: mechanisms and particle transformation. *RSC Advances, 5*(82), 66927-66933. doi:10.1039/C5RA10433E

Choi, K.-H., Min, J., Park, S.-Y., Park, B. J., & Jung, J.-S. (2019). Enhanced photocatalytic degradation of tri-chlorophenol by Fe3O4@TiO2@Au photocatalyst under visible-light. *Ceramics International, 45*(7, Part B), 9477-9482. doi:https://doi.org/10.1016/j.ceramint.2018.09.104

Costa, R. C. C., Lelis, M. F. F., Oliveira, L. C. A., Fabris, J. D., Ardisson, J. D., Rios, R. R. V. A., . . . Lago, R. M. (2006). Novel active heterogeneous Fenton system based on Fe3−xMxO4 (Fe, Co, Mn, Ni): The role of M2+ species on the reactivity towards H2O2 reactions. *Journal of Hazardous Materials, 129*(1), 171-178. doi:https://doi.org/10.1016/j.jhazmat.2005.08.028

Duan, Z., Zhang, W., Lu, M., Shao, Z., Huang, W., Li, J., . . . Chen, C. (2020). Magnetic Fe3O4/activated carbon for combined adsorption and Fenton oxidation of 4-chlorophenol. *Carbon, 167*, 351-363. doi:https://doi.org/10.1016/j.carbon.2020.05.106

El-Boubbou, K. Acid-stabilized iron-based metal oxide colloidal nanoparticles, and methods thereof. *US Patent, US10629339B2, 2020*.

El-Boubbou, K., Lemine, O. M., Algessair, S., Madkhali, N., Al-Najar, B., AlMatri, E., . . . Henini, M. (2024). Preparation and characterization of various PVPylated divalent metal-doped ferrite nanoparticles for magnetic hyperthermia. *RSC Adv, 14*(22), 15664-15679. doi:10.1039/d4ra01600a

El-Boubbou, K., Lemine, O. M., Ali, R., Huwaizi, S. M., Al-Humaid, S., & AlKushi, A. (2022). Evaluating magnetic and thermal effects of various Polymerylated magnetic iron oxide nanoparticles for combined chemo-hyperthermia. *New Journal of Chemistry, 46*(12), 5489-5504. doi:10.1039/D1NJ05791J

Fathy, M. A., Kamel, A. H., & Hassan, S. S. M. (2022). Novel magnetic nickel ferrite nanoparticles modified with poly(aniline-co-o-toluidine) for the removal of hazardous 2,4-dichlorophenol pollutant from aqueous solutions. *RSC Advances, 12*(12), 7433-7445. doi:10.1039/D2RA00034B

Gallego, A., Laurino Soulé, J., Napolitano, H., Rossi, S. L., Vescina, C., & Korol, S. E. (2018). Biodegradability of Chlorophenols in Surface Waters from the Urban Area of Buenos Aires. *Bulletin of Environmental Contamination and Toxicology, 100*(4), 541-547. doi:10.1007/s00128-018-2300-1

Gangwar, R. K., Dhumale, V. A., Kumari, D., Nakate, U. T., Gosavi, S. W., Sharma, R. B., . . . Datar, S. (2012). Conjugation of curcumin with PVP capped gold nanoparticles for improving bioavailability. *Materials Science and Engineering: C, 32*(8), 2659-2663. doi:https://doi.org/10.1016/j.msec.2012.07.022

Gao, L., Zhuang, J., Nie, L., Zhang, J., Zhang, Y., Gu, N., . . . Yan, X. (2007). Intrinsic peroxidase-like activity of ferromagnetic nanoparticles. *Nature Nanotechnology, 2*(9), 577-583. doi:10.1038/nnano.2007.260

Garba, Z. N., Zhou, W., Lawan, I., Xiao, W., Zhang, M., Wang, L., . . . Yuan, Z. (2019). An overview of chlorophenols as contaminants and their removal from wastewater by adsorption: A review. *Journal of Environmental Management, 241*, 59-75. doi:https://doi.org/10.1016/j.jenvman.2019.04.004

Georgi, A., Schierz, A., Trommler, U., Horwitz, C. P., Collins, T. J., & Kopinke, F. D. (2007). Humic acid modified Fenton reagent for enhancement of the working pH range. *Applied Catalysis B: Environmental, 72*(1), 26-36. doi:https://doi.org/10.1016/j.apcatb.2006.10.009

Giraldo, L., Erto, A., & Moreno-Piraján, J. C. (2013). Magnetite nanoparticles for removal of heavy metals from aqueous solutions: synthesis and characterization. *Adsorption, 19*(2), 465-474. doi:10.1007/s10450-012-9468-1

Granados-Oliveros, G., Gómez-Vidales, V., Nieto-Camacho, A., Morales-Serna, J. A., Cárdenas, J., & Salmón, M. (2013). Photoproduction of H2O2 and hydroxyl radicals catalysed by natural and super acid-modified montmorillonite and its oxidative role in the peroxidation of lipids. *RSC Advances, 3*(3), 937-944. doi:10.1039/C2RA22393G

Hamdan, N., Haija, M. A., Banat, F., & Eskhan, A. (2017). Heterogeneous catalytic degradation of phenol by a Fenton-type reaction using copper ferrites (CuFe2O4). *Desalination and Water Treatment, 69*, 268-283. doi:https://doi.org/10.5004/dwt.2017.0372

Han, X., Zhang, H., Chen, T., Zhang, M., & Guo, M. (2018). Facile synthesis of metal-doped magnesium ferrite from saprolite laterite as an effective heterogeneous Fenton-like catalyst. *Journal of Molecular Liquids, 272*, 43-52. doi:https://doi.org/10.1016/j.molliq.2018.09.045

Hareendran, A., Dais, E., Shinoy, D., Srikripa, S., Shibu, G. M., & Kurian, M. (2022). Nitrogen- and sulfur-doped zinc ferrite nanoparticles as efficient heterogeneous catalysts in advanced oxidation processes. *Journal of Physics and Chemistry of Solids, 161*, 110398. doi:https://doi.org/10.1016/j.jpcs.2021.110398

Hashemi, S. M., Ataollahi, Z., Hasani, S., & Seifoddini, A. (2023). Synthesis of the cobalt ferrite magnetic nanoparticles by sol–gel auto-combustion method in the presence of egg white (albumin). *Journal of Sol-Gel Science and Technology, 106*(1), 23-36. doi:10.1007/s10971-023-06073-2

Hashemian, S. (2013). Fenton-Like Oxidation of Malachite Green Solutions: Kinetic and Thermodynamic Study. *Journal of Chemistry, 2013*(1), 809318. doi:https://doi.org/10.1155/2013/809318

Hazarika, K. P., & Borah, J. P. (2023). Role of site selective substitution, magnetic parameter tuning, and self heating in magnetic hyperthermia application: Eu-doped magnetite nanoparticles. *RSC Advances, 13*(8), 5045-5057. doi:10.1039/D2RA07924K

Hebeish, A., Aly, A., El-Shafei, A., & Zaghloul, S. (2009). Synthesis and characterization of cationized starches for application in flocculation, finishing and sizing. *Egyptian Journal of Chemistry, 52*, 73-89.

Hübner, U., Spahr, S., Lutze, H., Wieland, A., Rüting, S., Gernjak, W., & Wenk, J. (2024). Advanced oxidation processes for water and wastewater treatment – Guidance for systematic future research. *Heliyon, 10*(9), e30402. doi:https://doi.org/10.1016/j.heliyon.2024.e30402

Hwang, J., Choi, M., Shin, H.-S., Ju, B.-K., & Chun, M. (2020). Structural and Magnetic Properties of NiZn Ferrite Nanoparticles Synthesized by a Thermal Decomposition Method. *Applied Sciences, 10*(18), 6279.

Ilosvai, A. M., Dojcsak, D., Váradi, C., Nagy, M., Kristály, F., Fiser, B., . . . Vanyorek, L. (2022). Sonochemical Combined Synthesis of Nickel Ferrite and Cobalt Ferrite Magnetic Nanoparticles and Their Application in Glycan Analysis. *International Journal of Molecular Sciences, 23*(9), 5081.

Jannah, N. R., & Onggo, D. (2019). Synthesis of Fe3O4 nanoparticles for colour removal of printing ink solution. *Journal of Physics: Conference Series, 1245*(1), 012040. doi:10.1088/1742-6596/1245/1/012040

Jiang, H., Zhang, P., Wang, X., & Gong, Y. (2021). Synthesis of magnetic two-dimensional materials by chemical vapor deposition. *Nano Research, 14*(6), 1789-1801. doi:10.1007/s12274-020-3020-5

Jiang, T., Wang, Y., Guo, Z., Luo, H., Zhan, C., Wang, Y., . . . Chen, H. (2022). Bi25FeO40/Bi2O2CO3 piezoelectric catalyst with built-in electric fields that was prepared via photochemical self-etching of Bi25FeO40 for 4-chlorophenol degradation. *Journal of Cleaner Production, 341*, 130908. doi:https://doi.org/10.1016/j.jclepro.2022.130908

Jung, Y. S., Lim, W. T., Park, J. Y., & Kim, Y. H. (2009). Effect of pH on Fenton and Fenton-like oxidation. *Environ Technol, 30*(2), 183-190. doi:10.1080/09593330802468848

Kadıoğlu, E. N., Atalay Eroğlu, H., Öztürk, H., Akbal, F., & Kuleyin, A. (2025). Enhanced degradation of textile wastewater by activated carbon–assisted Fenton oxidation: economic analysis and ANN-based optimization. *Biomass Conversion and Biorefinery*. doi:10.1007/s13399-025-06599-1

Kallawar, G. A., Barai, D. P., & Bhanvase, B. A. (2021). Bismuth titanate based photocatalysts for degradation of persistent organic compounds in wastewater: A comprehensive review on synthesis methods, performance as photocatalyst and challenges. *Journal of Cleaner Production, 318*, 128563. doi:https://doi.org/10.1016/j.jclepro.2021.128563

Kaur, M., Kaur, N., & Vibha. (2016). Ferrites: Synthesis and Applications for Environmental Remediation *Ferrites and Ferrates: Chemistry and Applications in Sustainable Energy and Environmental Remediation* (Vol. 1238, pp. 113-136): American Chemical Society.

Kayan, I., Oz, N. A., & Kantar, C. (2021). Comparison of treatability of four different chlorophenol-containing wastewater by pyrite-Fenton process combined with aerobic biodegradation: Role of sludge acclimation. *Journal of Environmental Management, 279*, 111781. doi:https://doi.org/10.1016/j.jenvman.2020.111781

Kim, S., Nam, S.-N., Jang, A., Jang, M., Park, C. M., Son, A., . . . Yoon, Y. (2022). Review of adsorption–membrane hybrid systems for water and wastewater treatment. *Chemosphere, 286*, 131916. doi:https://doi.org/10.1016/j.chemosphere.2021.131916

Kurian, M., & Nair, D. S. (2015). Heterogeneous Fenton behavior of nano nickel zinc ferrite catalysts in the degradation of 4-chlorophenol from water under neutral conditions. *Journal of Water Process Engineering, 8*, e37-e49. doi:https://doi.org/10.1016/j.jwpe.2014.10.011

Lawrie, G., Keen, I., Drew, B., Chandler-Temple, A., Rintoul, L., Fredericks, P., & Grøndahl, L. (2007). Interactions between Alginate and Chitosan Biopolymers Characterized Using FTIR and XPS. *Biomacromolecules, 8*(8), 2533-2541. doi:10.1021/bm070014y

Lei, M., Gao, Q., Zhou, K., Gogoi, P., Liu, J., Wang, J., . . . Liu, X. (2021). Catalytic degradation and mineralization mechanism of 4-chlorophenol oxidized by phosphomolybdic acid/H2O2. *Separation and Purification Technology, 257*, 117933. doi:https://doi.org/10.1016/j.seppur.2020.117933

Lemine, O. M., Algessair, S., Madkhali, N., Al-Najar, B., & El-Boubbou, K. (2023). Assessing the Heat Generation and Self-Heating Mechanism of Superparamagnetic Fe3O4 Nanoparticles for Magnetic Hyperthermia Application: The Effects of Concentration, Frequency, and Magnetic Field. *Nanomaterials, 13*(3), 453.

Li, W., Wang, Z., Liao, H., Liu, X., Zhou, L., Lan, Y., & Zhang, J. (2021). Enhanced degradation of 2,4,6-trichlorophenol by activated peroxymonosulfate with sulfur doped copper manganese bimetallic oxides. *Chemical Engineering Journal, 417*, 128121. doi:https://doi.org/10.1016/j.cej.2020.128121

Lori, N., Eydokia, P., Vassilis, Z., Anna, P., Eleana, H., & Christos, N. P. (2016). Magnetic Nanoparticles in Medical Diagnostic Applications: Synthesis, Characterization and Proteins Conjugation. *Current Nanoscience, 12*(4), 455-468. doi:http://dx.doi.org/10.2174/1573413712666151210230002

Ma, J., Yang, Q., Wen, Y., & Liu, W. (2017). Fe-g-C3N4/graphitized mesoporous carbon composite as an effective Fenton-like catalyst in a wide pH range. *Applied Catalysis B: Environmental, 201*, 232-240. doi:https://doi.org/10.1016/j.apcatb.2016.08.048

Madannejad, S., Rashidi, A., Sadeghhassani, S., Shemirani, F., & Ghasemy, E. (2018). Removal of 4-chlorophenol from water using different carbon nanostructures: A comparison study. *Journal of Molecular Liquids, 249*, 877-885. doi:https://doi.org/10.1016/j.molliq.2017.11.089

Mesquita, I., Matos, L. C., Duarte, F., Maldonado-Hódar, F. J., Mendes, A., & Madeira, L. M. (2012). Treatment of azo dye-containing wastewater by a Fenton-like process in a continuous

packed-bed reactor filled with activated carbon. *Journal of Hazardous Materials, 237-238*, 30-37. doi:https://doi.org/10.1016/j.jhazmat.2012.07.066

Mohammadi, H., Nekobahr, E., Akhtari, J., Saeedi, M., Akbari, J., & Fathi, F. (2021). Synthesis and characterization of magnetite nanoparticles by co-precipitation method coated with biocompatible compounds and evaluation of in-vitro cytotoxicity. *Toxicology Reports, 8*, 331-336. doi:https://doi.org/10.1016/j.toxrep.2021.01.012

Munoz, M., de Pedro, Z. M., Casas, J. A., & Rodriguez, J. J. (2015). Preparation of magnetite-based catalysts and their application in heterogeneous Fenton oxidation – A review. *Applied Catalysis B: Environmental, 176-177*, 249-265. doi:https://doi.org/10.1016/j.apcatb.2015.04.003

Munoz, M., Pliego, G., de Pedro, Z. M., Casas, J. A., & Rodriguez, J. J. (2014). Application of intensified Fenton oxidation to the treatment of sawmill wastewater. *Chemosphere, 109*, 34-41. doi:https://doi.org/10.1016/j.chemosphere.2014.02.062

Muzenda, C., Nkwachukwu, O. V., Jayeola, K. D., Zinyemba, O., Zhou, M., & Arotiba, O. A. (2023). Heterogenous electro-Fenton degradation of sulfamethoxazole on a polyethylene glycol-coated magnetite nanoparticles catalyst. *Chemosphere, 339*, 139698. doi:https://doi.org/10.1016/j.chemosphere.2023.139698

Nair, D. S., & Kurian, M. (2017a). Catalytic peroxide oxidation of persistent chlorinated organics over nickel-zinc ferrite nanocomposites. *Journal of Water Process Engineering, 16*, 69-80. doi:https://doi.org/10.1016/j.jwpe.2016.12.010

Nair, D. S., & Kurian, M. (2017b). Heterogeneous catalytic oxidation of persistent chlorinated organics over cobalt substituted zinc ferrite nanoparticles at mild conditions: Reaction kinetics and catalyst reusability studies. *Journal of Environmental Chemical Engineering, 5*(1), 964-974. doi:https://doi.org/10.1016/j.jece.2017.01.021

Nakatani, N., Hashimoto, N., Shindo, H., Yamamoto, M., Kikkawa, M., & Sakugawa, H. (2007). Determination of photoformation rates and scavenging rate constants of hydroxyl radicals in natural waters using an automatic light irradiation and injection system. *Analytica Chimica Acta, 581*(2), 260-267. doi:https://doi.org/10.1016/j.aca.2006.08.021

Neyens, E., & Baeyens, J. (2003). A review of classic Fenton's peroxidation as an advanced oxidation technique. *Journal of Hazardous Materials, 98*(1), 33-50. doi:https://doi.org/10.1016/S0304-3894(02)00282-0

Ni, X., Zhang, J., Zhao, L., Wang, F., He, H., & Dramou, P. (2022). Study of the solvothermal method time variation effects on magnetic iron oxide nanoparticles (Fe3O4) features. *Journal of Physics and Chemistry of Solids, 169*, 110855. doi:https://doi.org/10.1016/j.jpcs.2022.110855

Olaniran, A. O., & Igbinosa, E. O. (2011). Chlorophenols and other related derivatives of environmental concern: properties, distribution and microbial degradation processes. *Chemosphere, 83*(10), 1297-1306. doi:10.1016/j.chemosphere.2011.04.009

Oluwasanu, A. A. (2018). *Fate and Toxicity of Chlorinated Phenols of Environmental Implications: A Review*.

Osuna, Y., Gregorio-Jauregui, K. M., Gaona-Lozano, J. G., de la Garza-Rodríguez, I. M., Ilyna, A., Barriga-Castro, E. D., . . . López, R. G. (2012). Chitosan-Coated Magnetic Nanoparticles with Low Chitosan Content Prepared in One-Step. *Journal of Nanomaterials, 2012*(1), 327562. doi:https://doi.org/10.1155/2012/327562

Patil, R. M., Thorat, N. D., Shete, P. B., Bedge, P. A., Gavde, S., Joshi, M. G., . . . Bohara, R. A. (2018). Comprehensive cytotoxicity studies of superparamagnetic iron oxide nanoparticles. *Biochemistry and Biophysics Reports, 13*, 63-72. doi:https://doi.org/10.1016/j.bbrep.2017.12.002

Pera-Titus, M., García-Molina, V., Baños, M. A., Giménez, J., & Esplugas, S. (2004). Degradation of chlorophenols by means of advanced oxidation processes: a general review. *Applied Catalysis B: Environmental, 47*(4), 219-256. doi:https://doi.org/10.1016/j.apcatb.2003.09.010

Petcharoen, K., & Sirivat, A. (2012). Synthesis and characterization of magnetite nanoparticles via the chemical co-precipitation method. *Materials Science and Engineering: B, 177*(5), 421-427. doi:https://doi.org/10.1016/j.mseb.2012.01.003

Porru, M., Morales, M. d. P., Gallo-Cordova, A., Espinosa, A., Moros, M., Brero, F., . . . Ovejero, J. G. (2022). Tailoring the Magnetic and Structural Properties of Manganese/Zinc Doped Iron Oxide Nanoparticles through Microwaves-Assisted Polyol Synthesis. *Nanomaterials, 12*(19), 3304.

Qadri, S., Ganoe, A., & Haik, Y. (2009). Removal and recovery of acridine orange from solutions by use of magnetic nanoparticles. *Journal of Hazardous Materials, 169*(1), 318-323. doi:https://doi.org/10.1016/j.jhazmat.2009.03.103

Radhika, M., & Palanivelu, K. (2006). Adsorptive removal of chlorophenols from aqueous solution by low cost adsorbent—Kinetics and isotherm analysis. *Journal of Hazardous Materials, 138*(1), 116-124. doi:https://doi.org/10.1016/j.jhazmat.2006.05.045

Ramana, P. V., Rao, K. S., Kumar, K. R., Kapusetti, G., Choppadandi, M., Kiran, J. N., & Rao, K. H. (2021). A study of uncoated and coated nickel-zinc ferrite nanoparticles for magnetic hyperthermia. *Materials Chemistry and Physics, 266*, 124546. doi:https://doi.org/10.1016/j.matchemphys.2021.124546

Rangabhashiyam, S., Lins, P. V. d. S., Oliveira, L. M. T. d. M., Sepulveda, P., Ighalo, J. O., Rajapaksha, A. U., & Meili, L. (2022). Sewage sludge-derived biochar for the adsorptive removal of wastewater pollutants: A critical review. *Environmental Pollution, 293*, 118581. doi:https://doi.org/10.1016/j.envpol.2021.118581

Rashid, J., Barakat, M. A., Ruzmanova, Y., & Chianese, A. (2015). Fe3O4/SiO2/TiO2 nanoparticles for photocatalytic degradation of 2-chlorophenol in simulated wastewater. *Environmental Science and Pollution Research, 22*(4), 3149-3157. doi:10.1007/s11356-014-3598-9

Rodrigues, C. S. D., Madeira, L. M., & Boaventura, R. A. R. (2013). Optimization and Economic Analysis of Textile Wastewater Treatment by Photo-Fenton Process under Artificial and Simulated Solar Radiation. *Industrial & Engineering Chemistry Research, 52*(37), 13313-13324. doi:10.1021/ie401301h

Roshanfekr Rad, L., Farshi Ghazani, B., Irani, M., Sadegh Sayyafan, M., & Haririan, I. (2015). Comparison study of phenol degradation using cobalt ferrite nanoparticles synthesized by hydrothermal and microwave methods. *Desalination and Water Treatment, 56*(12), 3393-3402. doi:https://doi.org/10.1080/19443994.2014.977960

Sahni, M., & Locke, B. R. (2006). Quantification of Hydroxyl Radicals Produced in Aqueous Phase Pulsed Electrical Discharge Reactors. *Industrial & Engineering Chemistry Research, 45*(17), 5819-5825. doi:10.1021/ie0601504

Salvador, M., Gutiérrez, G., Noriega, S., Moyano, A., Blanco-López, M. C., & Matos, M. (2021). Microemulsion Synthesis of Superparamagnetic Nanoparticles for Bioapplications. *International Journal of Molecular Sciences, 22*(1), 427.

Samrot, A. V., Sahithya, C. S., Selvarani A, J., Purayil, S. K., & Ponnaiah, P. (2021). A review on synthesis, characterization and potential biological applications of superparamagnetic iron oxide nanoparticles. *Current Research in Green and Sustainable Chemistry, 4*, 100042. doi:https://doi.org/10.1016/j.crgsc.2020.100042

Shen, J., Zhou, Y., Li, S., Gu, P., & Xue, G. (2019). Hydrogel-coated Fe3O4 nanoparticles as an efficient heterogeneous Fenton catalyst for degradation of phenol. *Journal of Materials Science, 54*(15), 10684-10694. doi:10.1007/s10853-019-03661-y

Shin, S., & Jang, J. (2007). Thiol containing polymer encapsulated magnetic nanoparticles as reusable and efficiently separable adsorbent for heavy metal ions. *Chem Commun (Camb)*(41), 4230-4232. doi:10.1039/b707706h

Shin, S., Yoon, H., & Jang, J. (2008). Polymer-encapsulated iron oxide nanoparticles as highly efficient Fenton catalysts. *Catalysis Communications, 10*(2), 178-182. doi:https://doi.org/10.1016/j.catcom.2008.08.027

Srivastava, M., Ojha, A. K., Chaubey, S., & Materny, A. (2009). Synthesis and optical characterization of nanocrystalline NiFe2O4 structures. *Journal of Alloys and Compounds, 481*(1), 515-519. doi:https://doi.org/10.1016/j.jallcom.2009.03.027

Sundaramurthy, J., Kumar, P. S., Kalaivani, M., Thavasi, V., Mhaisalkar, S. G., & Ramakrishna, S. (2012). Superior photocatalytic behaviour of novel 1D nanobraid and nanoporous α-Fe2O3 structures. *RSC Advances, 2*(21), 8201-8208. doi:10.1039/C2RA20608K

Tai, C., Gu, X., Zou, H., & Guo, Q. (2002). A new simple and sensitive fluorometric method for the determination of hydroxyl radical and its application. *Talanta, 58*(4), 661-667. doi:10.1016/s0039-9140(02)00370-3

Tai, C., Peng, J.-F., Liu, J.-F., Jiang, G.-B., & Zou, H. (2004). Determination of hydroxyl radicals in advanced oxidation processes with dimethyl sulfoxide trapping and liquid chromatography. *Analytica Chimica Acta, 527*(1), 73-80. doi:https://doi.org/10.1016/j.aca.2004.08.019

Tehrani-Bagha, A. R., & Balchi, T. (2018). Chapter 12 - Catalytic Wet Peroxide Oxidation. In S. C. Ameta & R. Ameta (Eds.), *Advanced Oxidation Processes for Waste Water Treatment* (pp. 375-402): Academic Press.

Tehrani-Bagha, A. R., Gharagozlou, M., & Emami, F. (2016). Catalytic wet peroxide oxidation of a reactive dye by magnetic copper ferrite nanoparticles. *Journal of Environmental Chemical Engineering, 4*(2), 1530-1536. doi:https://doi.org/10.1016/j.jece.2016.02.014

Tipsawat, P., Wongpratat, U., Phumying, S., Chanlek, N., Chokprasombat, K., & Maensiri, S. (2018). Magnetite (Fe3O4) nanoparticles: Synthesis, characterization and electrochemical properties. *Applied Surface Science, 446*, 287-292. doi:https://doi.org/10.1016/j.apsusc.2017.11.053

Trotsenko, K. E., Shabalkin, I. D., Krivoshapkina, E. F., & Krivoshapkin, P. V. (2026). Alternating magnetic field-enhanced electrocatalysis: Mechanisms, synergistic effects, and future perspectives. *Nano Energy, 147*, 111573. doi:https://doi.org/10.1016/j.nanoen.2025.111573

Tseng, J. M., & Huang, C. P. (1991). Removal of Chlorophenols from Water by Photocatalytic Oxidation. *Water Science and Technology, 23*(1-3), 377-387. doi:10.2166/wst.1991.0436

Tu, Y., Xiong, Y., Tian, S., Kong, L., & Descorme, C. (2014). Catalytic wet air oxidation of 2-chlorophenol over sewage sludge-derived carbon-based catalysts. *Journal of Hazardous Materials, 276*, 88-96. doi:https://doi.org/10.1016/j.jhazmat.2014.05.024

Velásquez, A. A., & Urquijo, J. P. (2021). Synthesis and characterization of magnetite-maghemite nanoparticles in presence of polyethylene glycol obtained by mechanical milling. *Materials Science and Engineering: B, 263*, 114873. doi:https://doi.org/10.1016/j.mseb.2020.114873

Villaseñor, M. J., & Ríos, Á. (2018). Nanomaterials for water cleaning and desalination, energy production, disinfection, agriculture and green chemistry. *Environmental Chemistry Letters, 16*(1), 11-34. doi:10.1007/s10311-017-0656-9

Wang, K., Yang, Q., Zhang, H., Zhang, M., Jiang, H., Zheng, C., & Li, J. (2023). Recent advances in catalyst design and activity enhancement induced by a magnetic field for electrocatalysis. *Journal of Materials Chemistry A, 11*(15), 7802-7832. doi:10.1039/D2TA09276J

Wang, Q., Han, X. H., Sommers, A., Park, Y., T' Joen, C., & Jacobi, A. (2012). A review on application of carbonaceous materials and carbon matrix composites for heat exchangers and heat sinks. *International Journal of Refrigeration, 35*(1), 7-26. doi:https://doi.org/10.1016/j.ijrefrig.2011.09.001

Wang, S. (2008). A Comparative study of Fenton and Fenton-like reaction kinetics in decolourisation of wastewater. *Dyes and Pigments, 76*(3), 714-720. doi:https://doi.org/10.1016/j.dyepig.2007.01.012

Warren, F. J., Gidley, M. J., & Flanagan, B. M. (2016). Infrared spectroscopy as a tool to characterise starch ordered structure—a joint FTIR–ATR, NMR, XRD and DSC study. *Carbohydrate Polymers, 139*, 35-42. doi:https://doi.org/10.1016/j.carbpol.2015.11.066

Xi, G., Yue, B., Cao, J., & Ye, J. (2011). Fe3O4/WO3 hierarchical core-shell structure: high-performance and recyclable visible-light photocatalysis. *Chemistry, 17*(18), 5145-5154. doi:10.1002/chem.201002229

Xu, C., Liu, R., Chen, L., & Tang, J. (2016). Enhanced dechlorination of 2,4-dichlorophenol by recoverable Ni/Fe–Fe3O4 nanocomposites. *Journal of Environmental Sciences, 48*, 92-101. doi:https://doi.org/10.1016/j.jes.2015.10.033

Xu, J., Sheng, T., Hu, Y., Baig, S. A., Lv, X., & Xu, X. (2013). Adsorption–dechlorination of 2,4-dichlorophenol using two specified MWCNTs-stabilized Pd/Fe nanocomposites. *Chemical Engineering Journal, 219*, 162-173. doi:https://doi.org/10.1016/j.cej.2013.01.010

Xu, L., & Wang, J. (2012). Fenton-like degradation of 2,4-dichlorophenol using Fe3O4 magnetic nanoparticles. *Applied Catalysis B: Environmental, 123-124*, 117-126. doi:https://doi.org/10.1016/j.apcatb.2012.04.028

Yamaguchi, M. (2025). Density Functional Theory Calculation of Hydroxyl Radical Formation by Fenton and Fenton-Like Reactions. *International Journal of Quantum Chemistry, 125*(9), e70046. doi:https://doi.org/10.1002/qua.70046

Yan, H., Zhang, J., You, C., Song, Z., Yu, B., & Shen, Y. (2009). Influences of different synthesis conditions on properties of Fe3O4 nanoparticles. *Materials Chemistry and Physics, 113*(1), 46-52. doi:https://doi.org/10.1016/j.matchemphys.2008.06.036

Yang, F., Zhang, R., He, J., & Abliz, Z. (2007). Development of a liquid chromatography/electrospray ionization tandem mass spectrometric method for the determination of hydroxyl radical. *Rapid Commun Mass Spectrom, 21*(2), 107-111. doi:10.1002/rcm.2815

Yew, Y. P., Shameli, K., Miyake, M., Ahmad Khairudin, N. B. B., Mohamad, S. E. B., Naiki, T., & Lee, K. X. (2020). Green biosynthesis of superparamagnetic magnetite Fe3O4 nanoparticles and biomedical applications in targeted anticancer drug delivery system: A review. *Arabian Journal of Chemistry, 13*(1), 2287-2308. doi:https://doi.org/10.1016/j.arabjc.2018.04.013

Zada, A., Khan, M., Khan, M. A., Khan, Q., Habibi-Yangjeh, A., Dang, A., & Maqbool, M. (2021). Review on the hazardous applications and photodegradation mechanisms of chlorophenols over different photocatalysts. *Environmental Research, 195*, 110742. doi:https://doi.org/10.1016/j.envres.2021.110742

Zhang, S., Zhao, X., Niu, H., Shi, Y., Cai, Y., & Jiang, G. (2009). Superparamagnetic Fe3O4 nanoparticles as catalysts for the catalytic oxidation of phenolic and aniline compounds. *Journal of Hazardous Materials, 167*(1), 560-566. doi:https://doi.org/10.1016/j.jhazmat.2009.01.024

Zhang, Y., Cheng, Y., Chen, N., Zhou, Y., Li, B., Gu, W., . . . Xian, Y. (2014). Recyclable removal of bisphenol A from aqueous solution by reduced graphene oxide–magnetic nanoparticles: Adsorption and desorption. *Journal of Colloid and Interface Science, 421*, 85-92. doi:https://doi.org/10.1016/j.jcis.2014.01.022

Zhang, Y., & Zhou, M. (2019). A critical review of the application of chelating agents to enable Fenton and Fenton-like reactions at high pH values. *Journal of Hazardous Materials, 362*, 436-450. doi:https://doi.org/10.1016/j.jhazmat.2018.09.035

Zhu, N.-m., Yi, L., & Zhang, F.-S. (2011). Catalytic dechlorination of polychlorinated biphenyls in subcritical water by Ni/Fe nanoparticles. *Chemical Engineering Journal, 171*(3), 919-925. doi:https://doi.org/10.1016/j.cej.2011.04.041

مُلخص البحث

الكلوروفينول هي مركبات خطرة تُستخدم على نطاق واسع في العديد من الصناعات مثل صناعة البلاستيك والورق والمنسوجات والصلب والأدوية والأصباغ والمبيدات الحشرية ومبيدات الآفات ومبيدات الأعشاب. وبسبب ثباتها العالي في البيئة، فإنها تميل إلى التراكم في التربة والمياه، مما يشكل مخاطر جسيمة على النظم البيئية وصحة الإنسان. في هذا البحث، تم تحضير أنواع مختلفة من الجسيمات النانوية المغناطيسية، سواء كانت مغلفة بالبوليمرات مثل البيروليدون، الشيتوزان، والنشا، أو مشوبة بأيونات معدنية مثل الكوبالت والنيكل والزنك، وتمت دراسة كفاءتها التحفيزية في تحليل مركبين شائعين من الكلوروفينولات هما بارا-كلوروفينول وأورثو-كلوروفينول. تم توصيف الجسيمات النانوية بشكل دقيق باستخدام تقنيات مختلفة مثل المجهر الإلكتروني النافذ، تحليل تشتت الطاقة للأشعة السينية، حيود الأشعة السينية، مطيافية الأشعة تحت الحمراء بتحويل فورييه، وقياس المغناطيسية، وأكدت النتائج أن الجسيمات المحضرة نانوية الحجم، إذ بلغ حجمها بين ٨-١٥ نانومتر، كما أظهرت بنى مكعبة من نوع السبينيل عالية التبلور وخصائص مغناطيسية فائقة. أظهرت دراسات تحليل الكلوروفينولات أن الجسيمات النانوية المغلفة بالبوليمرات أبدت سلوكًا تحفيزيًا أقل من نظيرتها غير المغلفة، بينما أظهرت الجسيمات النانوية المشوبة بالمعادن، وخصوصًا تلك المشوبة بالكوبالت، أداءً مميزًا، حيث تمكنت من تحليل تركيز ٥٠ جزءًا في المليون من بارا-كلوروفينول وأورثو-كلوروفينول بالكامل خلال ١٥ و٨٠ ثانية على التوالي. كما أظهرت الجسيمات المشوبة بالزنك كفاءة عالية أيضًا، حيث حققت تحللاً كاملاً خلال ٨ و٤ دقائق على التوالي لنفس المركبات. ويُعزى هذا الأداء العالي إلى بنية الفيريت من نوع السبينيل، واستقرار أزواج الأكسدة والاختزال في المواقع الثمانية، بالإضافة إلى صغر حجم الجسيمات. كما تبيّن أن عوامل تشغيل إضافية مثل الرقم الهيدروجيني، وكمية المحفز، وتركيز الملوث، ومستوى فوق أكسيد الهيدروجين، ودرجة الحرارة تؤثر أيضًا بشكل كبير على كفاءة التحلل. وأظهرت اختبارات إعادة الاستخدام أن الجسيمات المشوبة بالكوبالت يمكن استخدامها لست دورات دون فقد في النشاط التحفيزي، بينما احتفظت الجسيمات المغلفة بالبيروليدون والجسيمات غير المغلفة (أكسيد الحديد المغناطيسي) بكفاءة تحليلية بلغت ٩١,١٪ و٧٦,٩٧٪ على التوالي في الدورة السادسة. علاوة على ذلك، ساهم تطبيق مجال مغناطيسي متناوب في تسريع عملية التحلل بشكل كبير مقارنة بالتحريك الميكانيكي. وتؤكد هذه النتائج على إمكانات الجسيمات النانوية المشوبة بالمعادن كمحفزات نانوية فعالة وسريعة وقابلة لإعادة الاستخدام لمعالجة مياه الصرف الصناعي الملوثة بمركبات الكلوروفينول.

جامعة البحرين

كلية العلوم **قسم الكيمياء**

تحضير وتحديد خصائص الجسيمات النانو مغناطيسية المغلفة بالبوليمرات وتقييم قدرتها على التسخين وكفاءة معالجة الملوثات

رسالة مقدمة لاستكمال جزئي لمتطلبات درجة الماجستير في الكيمياء البيئية

اسم الطالب

حوراء أحمد محمد

20176829

بإشراف

د. خير الدين البوبو

أستاذ مشارك

جامعة البحرين

نوفمبر 2025